UNIVERSITY OF BIRMINGHAM

DESIGN AND EVALUATION OF AN ENCAPSULATED

ARTIFICIAL DISC

by

Feras Adnan Alnaimat

A thesis submitted to

The University of Birmingham

for the degree of

Doctor of Philosophy

Department of Mechanical Engineering

School of Engineering

University of Birmingham

Sept, 2017

UNIVERSITY^{OF} BIRMINGHAM

University of Birmingham Research Archive

e-theses repository

Abstract

Artificial discs have been developed to replace and restore motion to degenerated intervertebral discs. The most common configuration for these devices include ball and socket articulation surfaces that can induce high frictional torques and wear rates. When these particles interact with the surrounding tissues they can induce inflammations leading to osteolysis, subsidence of the implant and then revision surgery.

A new device has been developed to reduce friction and eliminate wear migration that incorporates an elastomer sheath to encapsulate the disc, retaining debris and an optimised bio-lubricant. The artificial disc has been assessed with an experimental programme that compared the resistive torques of the artificial discs both with and without encapsulation, for a range of motions. Durability tests were also conducted to 2M cycles and gravimetric wear rate was measured in accordance with BS 18192-1: 2011. Encapsulating the articulating surfaces reduced resistive torques and completely eliminated debris migration. Wear rates within the sheath ranged from 10.1 to 11.3 mg/million cycles, well within acceptable levels for this type of device.

The encapsulated discs successfully contained all wear debris and displayed durability in excess of 2M accelerated life cycles. The concept of an encapsulated artificial disc has been shown to be feasible and could replace current technologies.

Acknowledgements

All praise and thanks are due to the Almighty Allah who always guides me to the right path and has helped me to complete this thesis.

I would like to thank my supportive academic supervisors Prof. Duncan Shepherd and Dr Karl Dearn and without their support, guidance and advices this work would not be completed.

 I would like to thank as well other academic and technical staff who supported me in this work and they are: Mr. Carl Hingley, Mr. Lee Gauntlett, Mr. Peter Thornton and Dr. James Bowen.

I would like to thank my parents and siblings who supported me during the PHD.

I would like to thank Tabita Luca for her support during the PHD.

Lastly, many thanks go to the Biomedical research group for their support.

Table of Contents

List of Figures

List of Tables

1 Introduction

Back pain is the main reason for activity limitation and work absence throughout the world (Lidgren, 2003). It is the cause of disabilities for people more than any other disease (Hoy *et al.*, 2014). The most common reason behind neck and back pain is intervertebral disc degeneration (Acton, 2013; Wong *et al.*, 2007). This occurs for a variety of reasons, including ageing, lifestyle and genetics (Buckwalter, 1995; Liuke *et al.*, 2005; Pye *et al.*, 2007; Sambrook *et al.*, 1999). Artificial discs have been developed for pain relief and to restore the motion of the degenerated intervertebral disc (Barberá-Tomás, 2015). The ideal artificial disc should relieve pain and restore the motions of the intervertebral disc without causing any issues during the long years of implantation. However, a variety of developed artificial discs have been found to have drawbacks when they are used *in vivo*. The main reasons for the failure of artificial discs are related to design factors including materials failure as a result of poor choice of bearing surface combinations and poor lubricants which leads to wear (Kurtz, 2006). When the wear particles reach the surrounding tissues it can cause inflammation which leads to a body reaction to foreign bodies, osteolysis and then lead to implant revision surgery (Hallab *et al.*, 2003). There is a need to look for improvements in the design, materials and lubricants that are used in artificial discs to reach an optimum design that can perform for years in patients without failure. A new design idea of encapsulating the artificial disc could help solve the problems related to materials, lubricants and wear. This idea has not been studied previously or applied in any way to lumbar artificial discs.

The main aim of this thesis was to design a synthetically encapsulated ball and socket Total Disc Arthroplasty (TDA). After the new disc was designed, the tribology of the new encapsulated artificial disc was studied under conditions similar to the environmental conditions to the normal disc environment such as the surrounding temperature.

To achieve the aims the following objectives were undertaken:

- A lumbar TDA, was designed and manufactured and containing a lubricant and sealed with a synthetic encapsulation.

- Different bio-lubricants were examined and tested tribologically.

- A range of biomedical encapsulation materials to be used as a synthetic capsule were examined.

- The manufactured encapsulated artificial disc was tested in vitro and compared it with artificial discs without encapsulation.

1.1 Structure of the thesis

Chapter 2 presents the background related to the spine and treatment of neck and back pain. The first section describes the anatomy of the different components and the mechanics of the spine. The second part of it describes spinal pain and the different treatments available. The chapter then discusses the different types of artificial discs that have been used to replace the intervertebral disc. The chapter concludes with the encapsulation of the artificial disc which contains the idea, its origin and how it will be implemented in this thesis.

Chapter 3 describes the design process of the encapsulated ball and socket artificial disc. This chapter firstly describes the required product design specifications for designing an encapsulated artificial disc. The second part of the chapter covers the conceptual drawings meeting the requirements of the product design specifications. The third part of the chapter makes a detailed design after evaluating the different conceptual designs through an evaluation process. Finally the chapter discusses the different stages of the design process and chooses the final design to be manufactured and tested.

Chapter 4 presents the effect of biomedical lubricants on friction between common arthroplasty bearing biomaterials for the encapsulated artificial disc. It presents the different synthetic lubricants that have been tested, that are to be potentially used inside the encapsulated artificial disc. In addition, different biomaterial combinations using the synthetic lubricants were tested using a tribometer. Chapter 4 contributed to choosing the material combinations and lubricants that can be used in the encapsulated artificial disc.

Chapter 5 investigates the material used for the encapsulation sheath. In the chapter the crack nucleation and growth in medical-grade silicone and polyurethane ether elastomers is presented. It discusses the biocompatibility of the different elastomers that can be implanted inside the human body. In addition, it describes tests for the sterilization and ageing effects on crack nucleation and growth of silicone and polyurethane materials. Chapter 5 helped in choosing the correct elastomer that can be used as an encapsulation material for the artificial disc.

Chapter 6 presents the development and evaluation of the encapsulated artificial disc design. It describes the different methods of assembly used. In addition, different assembly configurations

were tested to choose the assembly configuration that can perform to the required level for years inside the human body without failure.

Chapter 7 draws all of the previous chapters together and describes the result of the tests to determine the effect of encapsulating the ball and socket artificial disc on the resistive torque and wear. It is the second stage of evaluation where tribological tests were applied on the different configurations assemblies of the encapsulated artificial discs that have passed the evaluation in chapter 6.

Finally, chapter 8 includes the general discussion and conclusions drawn from the whole thesis. The thesis outline is shown in Figure 1.1.
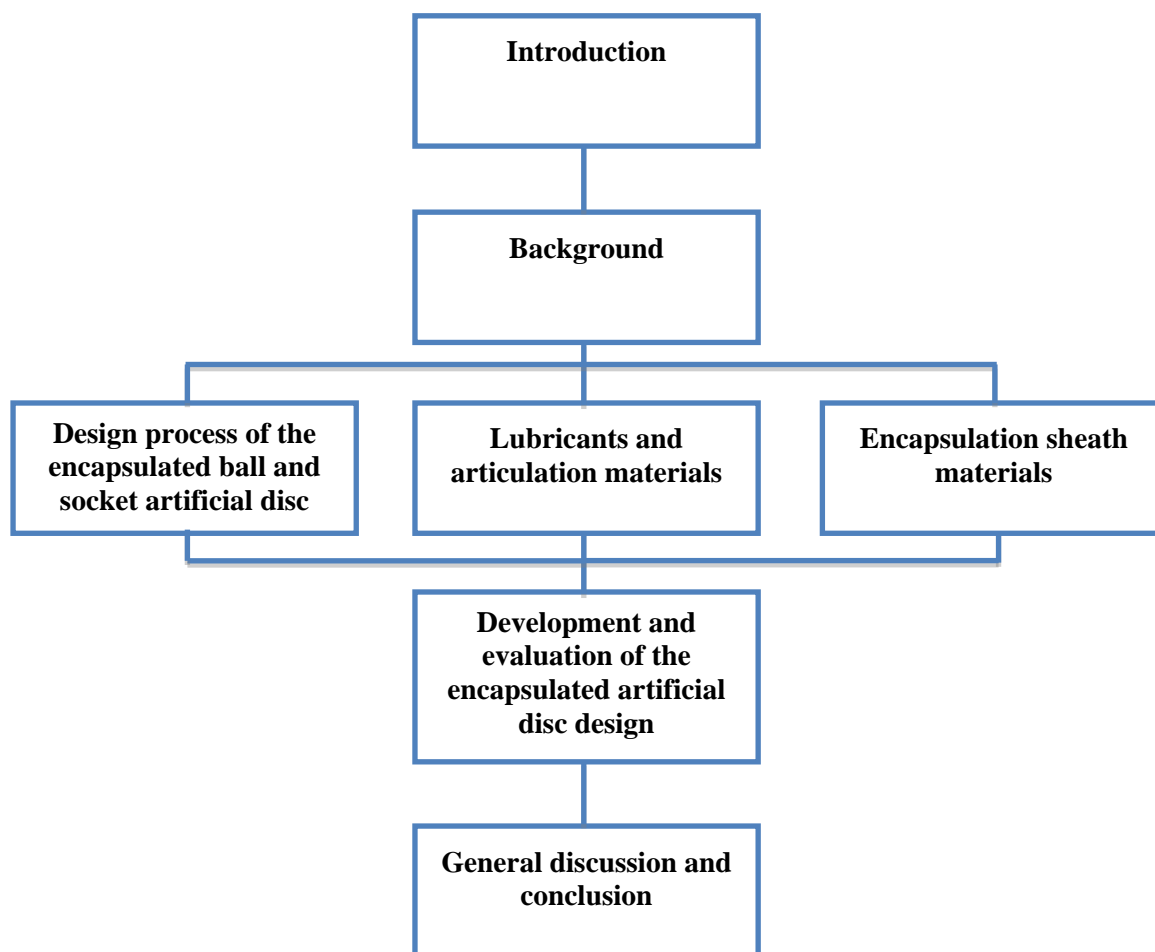
Figure 1.1: Thesis outline.

2 Background

2.1 Overview

This chapter presents the background necessary to understand the research presented in the thesis. Section 2.2 and 2.3 will explain the regions and motions of the spine. Section 2.4 will explain the anatomy and mechanics of the spine. After that section 2.5 describes neck and back pain and the different treatments that are used, including artificial discs. In section 2.6, the reasons behind the failure of the different types of artificial discs are discussed. After this, the concept of how artificial discs can be enhanced through encapsulation is introduced in section 2.7. The last section is a summary of the chapter.

2.2 Regions of the spine

There are five regions in the spine: cervical, thoracic, lumbar, sacral and the coccyx, as shown in Figure 2.1. The cervical region of the spine contains seven vertebrae (C1-C7). The function of the cervical intervertebral discs is to provide flexibility and transfer load for the neck and head. The next region, which is the thoracic region, contains twelve vertebrae (T1-T12). This is followed by the lumbar spine region which contains five vertebrae (L1-L5) (Herwig *et al.*, 2007). The next region is the sacrum, which consist of five vertebrae (S1-S5). The sacrum attaches the spine with the iliac bones of the pelvis through the sacroiliac joint (Kurtz and Edidin, 2006). Finally, there is the coccyx (tail bone) region which four fused vertebrae (Kurtz and Edidin, 2006).
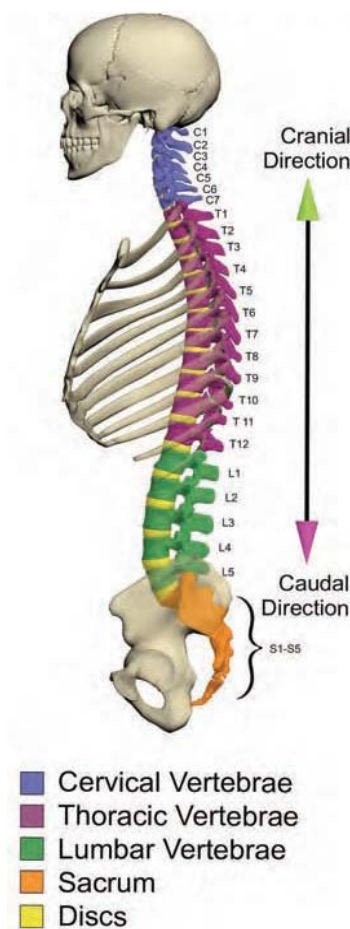
Figure 2.1: The different regions of the spine (Kurtz and Edidin, 2006). Reprinted with

permission from Elsevier.

2.3 Motions of the spine

The directions of the body have different terminology in medicine. The front and back of the

human body are called anterior and posterior, respectively. The upper vertical direction is called

superior and the downward direction is called inferior. The left and right of the human body are

called lateral and the middle of the body is called medial. The vertebral column allows motion for

the spine in different directions. Flexion is the bending anteriorly to the front direction of the body. Extension is bending posteriorly towards the back direction of the body. Lateral bending is bending towards the left and the right sides of the body. Axial rotation is the axial rotation on the vertical axis of the body, as shown in Figure 2.2 (Kurtz and Edidin, 2006).
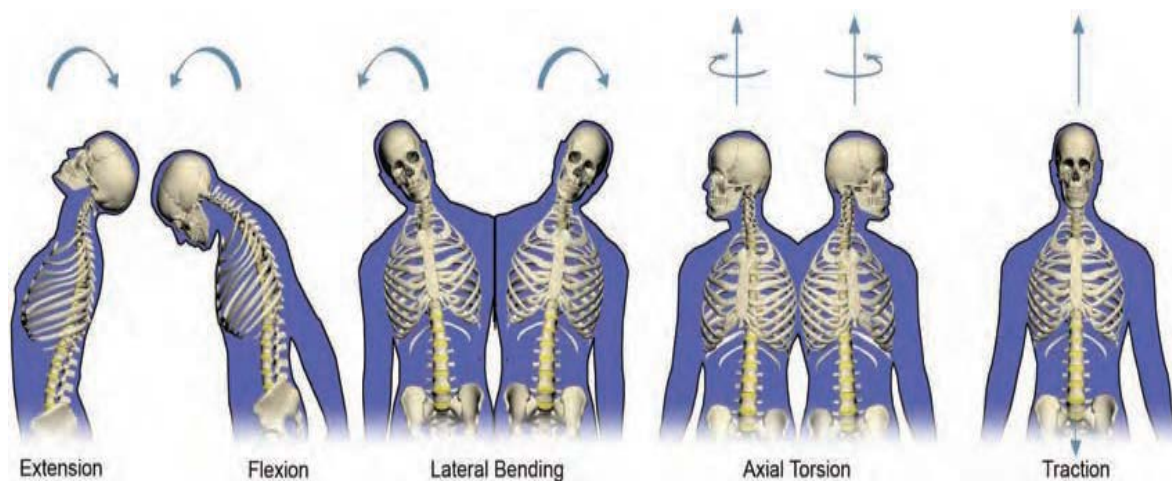
Figure 2.2: Motion of the spine (Kurtz and Edidin, 2006). Reprinted with permission from Elsevier.

2.4 The anatomy and mechanics of the spine

The spine contains hard tissue which comprises vertebra and soft tissue which is the intervertebral disc, ligaments, and the spinal cord (Cramer, 2014). The hard tissue such as vertebrae protects the spinal cord and cauda equina and branching nerves. Between the vertebral bodies there are the intervertebral discs which provide the spine with flexibility and attenuate, and distributes the forces applied by the body (Kurtz and Edidin, 2006).

2.4.1 The vertebrae

The vertebral body helps in supporting the weight of the human body and providing protection for the spinal cord and transferring the loads along the whole vertebral column. Each vertebra contains two main regions which are the vertebral body and the vertebral arch, which is the posterior part of the vertebra. The vertebra comprises trabecular and cancellous bone types, which are spongy and porous bone surrounded by a cortical rim (Cramer, 2014). The vertebral arch which is in the posterior contains different structures which are the laminae, pedicles, superior and inferior articular, transverse and spinous processes (Cramer, 2014), as shown in Figure 2.3. The pedicles are the only connection between the vertebral body and the vertebral arch. The intervertebral discs connect the vertebral bodies through the vertebral column (Cramer, 2014).
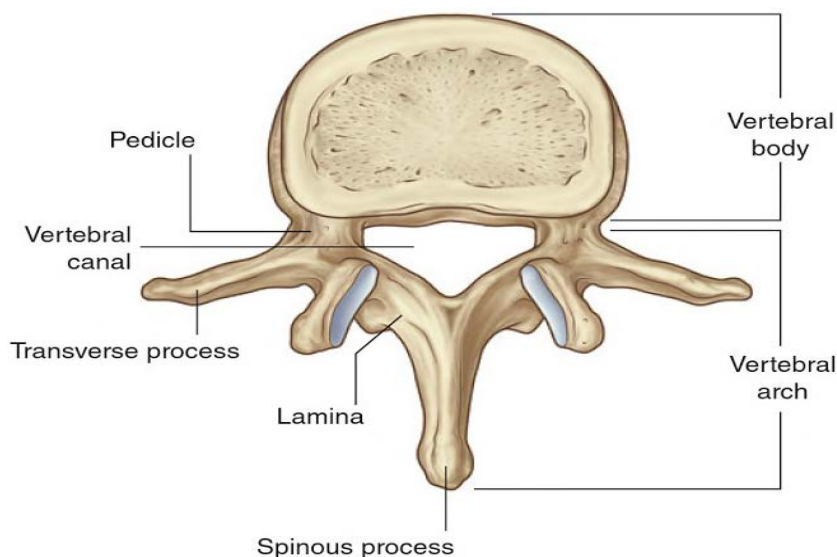
Figure 2.3: Typical vertebral body (Salvo, 2015). Reprinted with permission from Elsevier Health Sciences.

2.4.2 The intervertebral disc

The intervertebral disc is a soft tissue structure positioned between all the vertebral bodies located along the whole vertebral column (Guerin and Elliott, 2006). Six discs are located in the cervical region, twelve in the thoracic, five in the lumber and one between the sacrum and coccyx; therefore, there are twenty four intervertebral discs located in the intervertebral column (Cramer, 2014; Guerin and Elliott, 2006). In addition, the nerves do not reach the inner parts of the disc while it does reach the periphery of the tissue (Guerin and Elliott, 2006). The intervertebral discs are slightly populated with cells and it is thought that poor blood supply and the low cellularity might be a predisposition of disc degeneration (Guerin and Elliott, 2006). They vary in shape and size through the entire vertebral column. They start as a small and round cross-sectional shape in the upper part of the vertebral column and then get larger in size and have a kidney cross-sectional shape through the lower part of the vertebral column (Guerin and Elliott, 2006). Providing support to maintain the loads is one of the main functions of the intervertebral disc (Guerin and Elliott, 2006). At the same time it should be soft enough to provide mobility and flexibility and allow the full motion spine (Guerin and Elliott, 2006).

The intervertebral disc is one of the components which is responsible for the flexibility of the spine while allowing motions to occur between spinal segments (Cramer, 2014). The intervertebral discs vary in shape and size; however, the composition does not change for all the discs along the vertebral column (Guerin and Elliott, 2006). Each intervertebral disc structure contains three main components which are the annulus fibrosus, the nucleus pulposus and the end plates (Cramer, 2014; Guerin and Elliott, 2006), as shown in Figure 2.4. The nucleus pulposus is a semi-solid structure which contains a meshwork of distributed collagen fibres (Guerin and

Elliott, 2006). Water is the major composition of the nucleus pulposus in which it is about 70-80% of the weight of the nucleus pulposus. The dry weight of a healthy nucleus pulposus tissue contains approximately 20% of collagen. From 30 – 50% of the dry weight consists of proteoglycans and the rest of the weight is non-collagenous proteins (Cortes and Elliott, 2014; Guerin and Elliott, 2006). The major proteoglycans in the nucleus pulposus is aggrecan that has a brush like shape structure connecting many glycosaminoglycan molecules with a core protein (Guerin and Elliott, 2006). These glycosaminoglycan molecules have negative charges that attract positive ion charges to reach electroneutrality inside the nucleus pulposus. After the electroneutrality is reached inside, the ion concentration will be higher than the surrounding tissues and this will lead to cause osmotic pressure which attracts water ions inside the nucleus pulposus to balance the ion concentration with the surrounding tissues (annulus fibrosus and end plates) (Guerin and Elliott, 2006). This gel like substance makes the intervertebral disc stiff in compression because of the internal pressure that it provides, acting against the walls of the annulus fibrosus (Cortes and Elliott, 2014). The annulus fibrosus consists of a series of fibrocartilage rings organized to surround the nucleus pulposus. The composition of the annulus fibrsosus is 50% water, 70% collagen approximately of the dry weight and 10% proteoglycans of the dry weight approximately (Eyre and Muir, 1976). It is subjected to compressive and tensile stresses during the physiological motion (Cortes and Elliott, 2014). The collagen fibre layers are arranged in alternating orientations as concentric layers. These arrangements in the layers make the annulus fibrosus to have superior mechanical properties to withstand mechanical loads in different directions (Cortes and Elliott, 2014; Guerin and Elliott, 2006; Middleditch and Oliver, 2005). The cartilaginous endplate is the interface between the vertebral bodies from one side and

the nucleus pulposus and inner layers of annulus fibrosus. The thickness of the endplate is in the range of ~0.2 mm to ~0.9 mm from the centre to the periphery region of the endplate (Moon *et al.*, 2013). It does play a major role in the transport of the nutrients and other metabolites to the inner layers of the annulus fibrosus and nucleus pulposus (Cortes and Elliott, 2014).
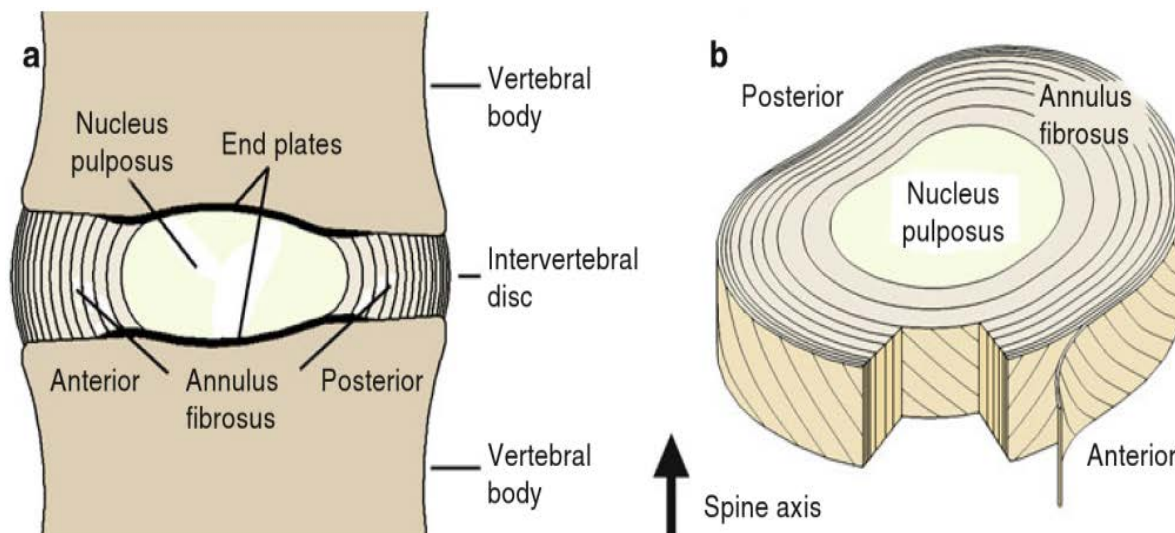
Figure 2.4: a) the intervertebral disc between two vertebrae. b) The components of the intervertebral disc (Cortes and Elliott, 2014). Reprinted with permission from Springer.

2.4.3 The ligaments

The ligaments are responsible for holding the vertebrae together and providing support for the whole vertebral column including the intervertebral discs and vertebrae (Faiz *et al.*, 2011). One of their functions is to limit any excessive motions applied through the spine (Wells, 2010). Type I collagen fibers are the main composition of the ligaments embedded in a hydrated extracellular matrix. There are two main ligaments in the spine: posterior and anterior longitudinal ligaments,

each continuous along the whole vertebral column. However, the anterior ligament is wider and much stronger than the posterior one (Guerin and Elliott, 2006). The anterior ligament is stretched during the extension movement, while the posterior ligament is stretched during the flexion movements (Middleditch and Oliver, 2005). The ligamenta flava are other small ligaments that connect the lamina of the vertebrae from behind. They are stretched during the flexion of the spine similar to the posterior ligaments. However, they are stretched more than the posterior ligaments due their distance from the centre of rotation, and more than the posterior ligaments which cause a higher strain for them. The interspinous ligaments connect the spinous processes between the adjacent vertebrae (Bogduk, 2012). They consist of collagen fibers arranged in fan-like shape (Guerin and Elliott, 2006). The supraspinous ligament connects the posterior part of the spinous processes and it extends from the top of the spine to the third or fifth lumbar vertebrae (Bogduk, 2012; Guerin and Elliott, 2006).

2.4.4 Load and motion mechanism within the intervertebral disc

The load is spread along the spine through any two vertebrae through the intervertebral disc. The only force on the spine during daily activities is compression, as shown in Figure 2.5 (Cripton *et al.*, 2006). When a compressive force is applied to an intervertebral disc an intradiscal pressure (pressure inside the intervertebral disc) will start to appear in the nucleus pulposus to resist the vertical compression force, as shown in Figure 2.5. The nucleus pulposus is a semi-solid structure and contains mostly water, as mentioned earlier. This will result in the expansion of the annulus fibrosus and will result in tensile forces in the walls of the annulus fibrosus. At the same time

during the compression force on the artificial disc there will be a tension force in the surrounding ligaments and muscles. The intradiscal pressure will vary from disc to disc along the spine and will vary with different motions, such as standing, walking and lifting loads (Guehring *et al.*, 2006; Wilke *et al.*, 1999). A three-dimensional coordinate system which was described first by White and Panjabi (1990) and clarified in more detail by Wilke *et al.* (1998) is shown in Figure 2.6. This coordinate system contains three transitional motions x, y, z and three rotational motions α, β and γ, as shown in Figure 2.6. The load will vary between the cervical region and the lumbar region in which it will increase in the lower regions like the lumbar more than the cervical. The load range, defined by ISO 18192-1:2008 standard for testing the cervical artificial and lumbar discs, is between 50 to 150 N and from 600 to 2000 N, respectively (BS ISO 18192-1, 2011). L5/L4 has nearly 60% of the body weight applied on them (Middleditch and Oliver, 2005).
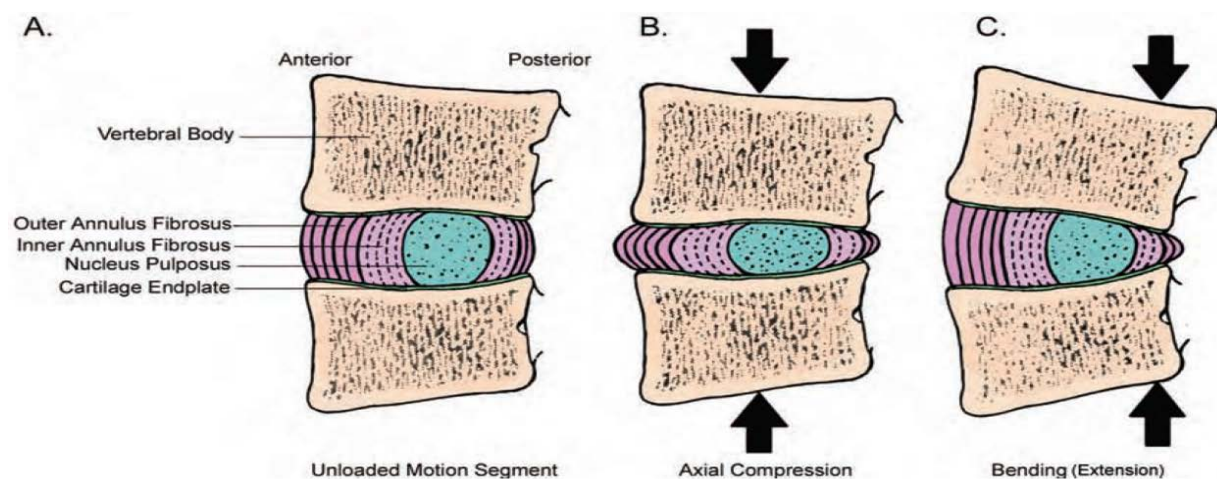
Figure 2.5: The intervertebral disc with different loads: A) Unloaded. B)The axial compression force on the intervertebral disc. C) Bending load (Guerin and Elliott, 2006). Reprinted with permission from Elsevier.
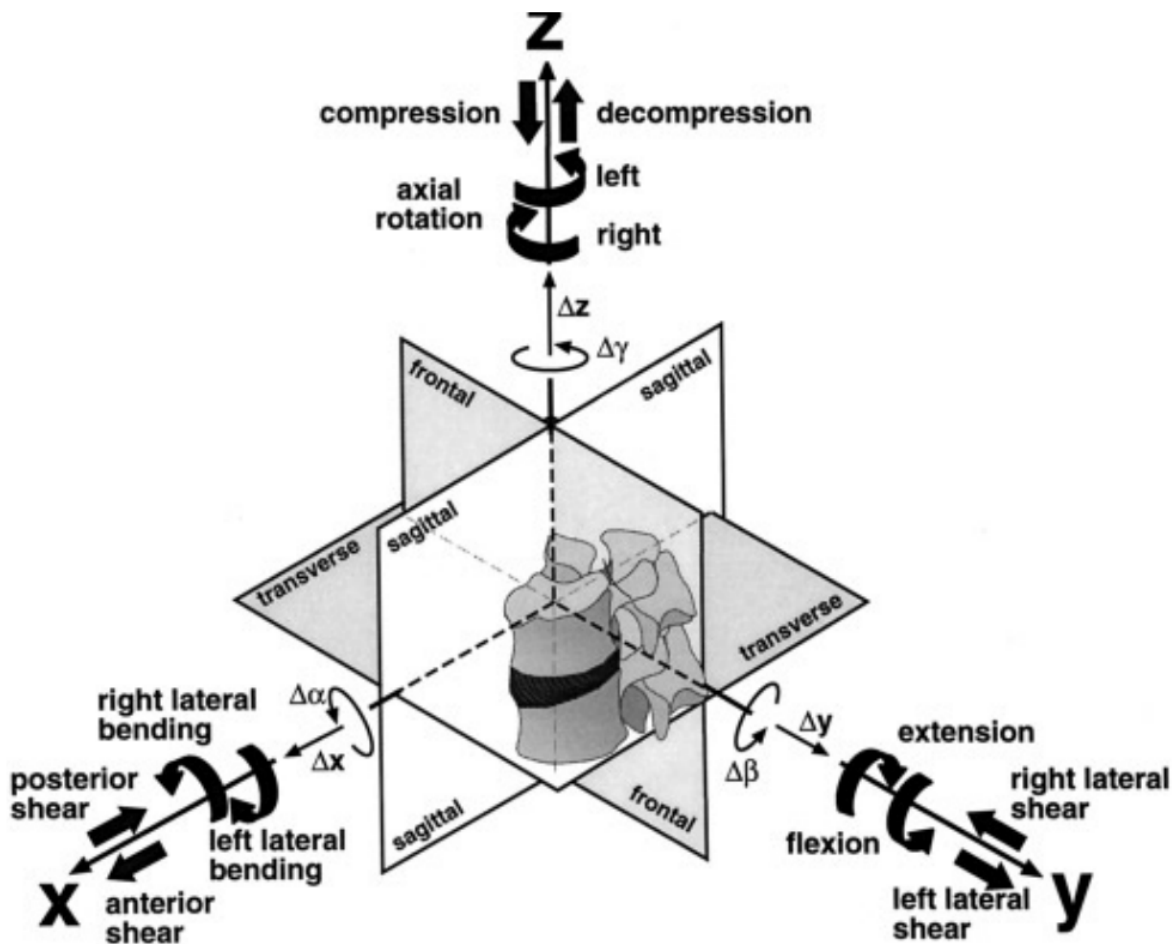
Figure 2.6: The three-dimensional coordinate system for the spine (Wilke *et al.*, 1998). Reprinted with permission from Springer.

2.5 Spinal pain and treatment

One of the most common medical problems is spinal chronic pain. It affects 80% of people at some point during their lives (Medline Plus; Sharon and Fernando, 2012). About one third of the UK adult population have lower back pain every year and around 20% of them consult their GP about the pain (National Institute for Health and Clinical Excellence, 2009). The direct health

care cost estimation in the UK for back pain in 1998 was £1632 million (Maniadakis and Gray, 2000). It was estimated in 2004 that the annual cost of treating back pain in the USA was 193.9 billion dollars (McCarberg *et al.*, 2012). It is also a common reason of chronic disability and it is the cause of a great proportion of work absenteeism and lower productivity (Johnson *et al.*, 1998; Mäkela *et al.*, 1991). Neck and back pain will have an effect on the treatment cost and industry. Intervertebral disc degeneration is one of the common reasons of neck and back pain and it should be fully understood to find the suitable solution for it (Acton, 2013; Wong *et al.*, 2007).

2.5.1 Degeneration of the intervertebral disc

The intervertebral discs can have major negative changes in their composition, structure and mechanical properties with age (Ferguson and Steffen, 2005; Guerin and Elliott, 2006). Different causes lead to intervertebral disc degeneration including genetic inheritance and loading history, all of them weakening the disc and potentially leading to failure during normal activities (Adams and Roughley, 2006). The progression of disc degeneration can be influenced by genetics or environmental influences such as lifestyle or working conditions (Chan *et al.*, 2006; Matsui *et al.*, 1998). In addition, the composition, structure and mechanical properties change with age for the intervertebral disc throughout life (Adams and Roughley, 2006; McKay *et al.*, 2006). The degeneration of the intervertebral disc will affect the nucleus pulposus, annulus fibrosus and endplates (Guerin and Elliott, 2006). In the nucleus pulposus there are matrix metalloproteinases (MMPs) which is the enzyme responsible on the degradation of proteins such as collagen and proteoglycans. In a healthy intervertebral disc, there is a balance between the production of

proteoglycan and the degeneration process of it. In the degenerated nucleus pulposus, the matrix metalloproteinases (MMPs) enzyme will have a higher level which will lead to more degeneration of collagen and proteoglycans and disrupt the osmotic pressure which will lead to dehydration of the nucleus pulposus and it becomes more solid instead of a gel-like phase (Guerin and Elliott, 2006). The dehydration of the nucleus pulposus affects the tissue from pressurizing and this will affect the ability to absorb and transmit the compressive loads through the spine. The mechanical properties change due to ageing for the nucleus pulposus in which the shear modulus increases from 5 to 60 kPa and the compressive modulus decreases from 1 MPa to 0.4 MPa (Iatridis *et al.*, 1997; Johannessen and Elliott, 2005). These changes might be the reasons behind the degeneration of the nucleus pulposus which will affect the whole of the intervertebral disc. Thus, the compressive loads will be directly transmitted to the annulus fibrosus. When the mechanical properties of the nucleus pulposus affect the inner layers of the annulus fibrosus, they may swell inwards because of compressive forces or outwards because of tensile forces (Seroussi *et al.*, 1989). With time the degeneration becomes worse and the mechanical loading increases on the annulus fibrosus which might lead to cracks or tears in the tissue (Iatridis and ap Gwynn, 2004).

2.5.2 Treatment of neck and back pain

Chronic neck and back pain can be treated by conservative or surgical treatments (Adams *et al.*, 2006). The conservative treatment comes in the early stages for patients and it covers rest, medication, certain exercises, physiotherapy and rehabilitation (Adams *et al.*, 2006). Patients that

have conservative treatment are expected to recover after a few weeks from the start of the treatment. But in some cases the patients do not fully recover or when they are in the advanced stage of disc degeneration then a surgical treatment might be needed (Goel *et al.*, 2006). The most common surgical treatments are discectomy and spinal fusion which help reduce pain but do not restore the movement of the treated section (Marcolongo *et al.*, 2006). In spinal fusion, the degenerated intervertebral disc is removed and a fusion cage and bone graft replace it to fuse the two adjacent vertebrae (Kurtz and Edidin, 2006). Fusion treatment can help in removing the pain and restoring the height between the two adjacent vertebrae. However, it eliminates the movement in that part of the spine; in addition, it can affect the adjacent intervertebral discs and cause accelerated damage to them with time (Hilibrand and Robbins, 2004; Park *et al.*, 2004).

Nucleus replacement is another treatment for degenerated disc disease in which the nucleus will be the only part replaced. This would offer a less invasive surgical technique, restoring the biomechanical function of the disc and will lead to pain relief. This surgical treatment might be effective in the early stages of disc degeneration before the annulus fibrosus reaches a significant level of degeneration (Marcolongo *et al.*, 2006).

Another treatment is total disc arthroplasty (TDA) in which the degenerated disc is removed completely and an artificial disc replaces the degenerated one. Artificial disc replacement is able to restore the height of the degenerated disc and restore the movements in that section which fusion procedures cannot do (Goel *et al.*, 2003; Sasso *et al.*, 2007).

2.5.3 Total Disc Arthroplasty (TDA)

Total disc arthroplasty is a surgical treatment for advance cases of degenerated disc disease unlike nucleus replacement which is for the early stage of the disease (Kurtz, 2006). The main aim of the artificial disc device is to restore the motion to the affected area of the spine and to remove pain. Most artificial discs are either flexible elastomer cores mimicking the natural disc or articulating, such as the ball and socket artificial disc (Kurtz, 2006). The first mimicking artificial disc was the Acroflex (Depuy-AcroMed Inc., Massachusetts, USA). It was developed in the early 1970s. It contains a hyperelastic polymer in between a two titanium plates, as shown in Figure 2.7. This polymer layer allows flexible motion for the implanted part. Three generations of Acroflex artificial disc were invented, the first and the third generation used a polyolefin (high density polyethylene) rubber core and the second generation used a silicone elastomer (Fraser *et al.*, 2004; Kurtz, 2006). The most recent designs of the mimicking artificial discs such as the M6 (Spinal Kinetics Inc., California, USA), Freedom disc (AxioMed Spine Corp, OH, USA) and Cadisc-L (Ranier Technology Limited, Cambridge, UK) have not yet been proven to be sufficient to survive for long-term implantation without tearing of the flexible core, as there are no long-term published clinical case studies on them.

Figure 2.7: Acroflex artificial disc (Fraser *et al.*, 2004). Reprinted with permission from Elsevier.

The second group of artificial discs is the ball and socket design which is based on the designs of the hip artificial joint where a socket is used to roll and slide against a ball (Bao and Yuan, 2000). Ball and socket artificial discs are the most commonly used artificial discs; however, they do not mimic the kinematics of natural intervertebral discs (Lee and Goel, 2004), except Charité artificial disc replicated natural kinematics fairly well (O'Leary *et al.*, 2005). Ball and socket artificial discs consist of two parts: the ball which is a convex shape and the socket which is a concave shape. One of the most common examples on the ball and socket artificial discs is the Prodisc artificial disc (DePuy Synthes Spine Inc., Massachusetts, USA), as shown in Figure 2.8. Table 2.1 describes the different artificial discs.

Figure 2.8: Prodisc artificial disc (Kurtz, 2006). Reprinted with permission from Elsevier.

Table 2.1: The different artificial discs with elastomeric components, ball and socket and encapsulated artificial discs (Blumenthal *et al.*, 2005; Fraser *et al.*, 2004; Hou *et al.*, 2014; John, 2014; Kurtz, 2006; Mathews *et al.*, 2004; McNally *et al.*, 2012; Moghadas *et al.*, 2015; Reyes-Sa´nchez *et al.*, 2008; Reyes-Sanchez *et al.*, 2010; Vaccaro *et al.*, 2013; Vicars *et al.*, 2010; Vicars *et al.*, 2012).

Name	Features	Failure
Acroflex (Fraser *et al.*, 2004). Reprinted with permission from Elsevier.	• Developed in 1970s • One component • Non articulating • Polyolefin (high density polyethylene) between titanium endplates	• Failure of the core • Rubber debris cause granulomatous reaction • Osteolysis
Cadisc – L (McNally *et al.*, 2012). Reprinted with permission from Springer.	• Available since 2009 • One component • Non articulating • polycarbonate polyurethane	• No long clinical trials • The company revised the device from the market

Freedom disc (Axiomed)	• Available since 2009. • One component • Non articulating • Silicone polycarbonate urethane elastomer bonded with titanium endplates	• No long clinical trials • No failure reports
(John, 2014). Reprinted with permission from Elsevier.		
Charite	• Developed in the early 1980s. • Three components. • Articulating • UHMWPE core between two CoCr alloy.	• UHMWPE wear particles • Anterior and posterior migration • Breakage of metal wire. • Subsidence • Osteolysis
(Blumenthal *et al.*, 2005). Reprinted with permission from Wolters Kluwer Health, Inc.		

Prodisc (Kurtz, 2006). Reprinted with permission from Elsevier.	• Developed in the late 1980s • Three components • Articulating (Ball and socket) • UHMWPE core attached to the inferior CoCr endplate articulating against CoCr endplate.	• UHMWPE wear particles • UHMWPE core migration • Subsidence • Ostolysis
Maverick (Mathews *et al.*, 2004). Reprinted with permission from Elsevier.	• Developed in the early 2000s • Two components • Articulating (Ball and socket) • CoCrMo Ball and socket endplates	• Metal wear debris • Inflammatory response • Toxicity • Osteolysis

Bryan	• developed by Bryan et al. in 1993 • Four components • Articulating • Two titanium shells and polyurethane core surrounded by polyurethane sheath.	• One case of sheath tear with no inflammatory response
(John, 2014). Reprinted with permission from Elsevier.		
M6 Disc	• Was founded in 2003 • Five components • Non articulating • Two titanium outer plates • Viscoelastic Polycarbonate urethane core • Polyethylene fibres • Polyurethane outer sheath	• No long clinical trials • No failure reports
(Reyes-Sanchez *et al.*, 2010). Reprinted with permission from Elsevier		
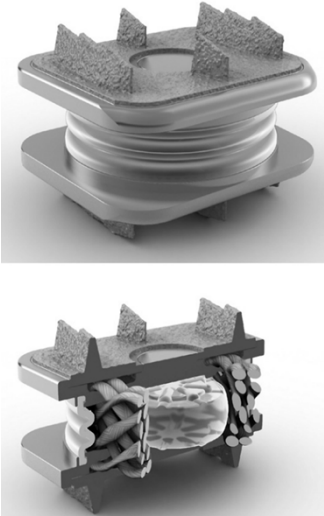
Secure®-C **(Vaccaro *et al.*, 2013).** Reprinted with permission from Wolters Kluwer Health, Inc.	• Was developed in 2006 by Globus Medical (PA, USA) • Was approved by FDA in 2012 • Cervical disc • Three components • Cervical disc • Two cobalt-chrome alloy endplates and an UHMWPE ball core inserted on the bottom plate.	• No revision surgeries or failure • Long-term wear characteristics unknown
Discover **(Hou *et al.*, 2014).** Reprinted with permission from Elsevier	• Developed by Depuy Synthes • Cervical disc • Three components • Articulating device • Titanium alloy endplates articulating against UHMWPE core	• No revision surgeries or failure • Long-term wear characteristics unknown
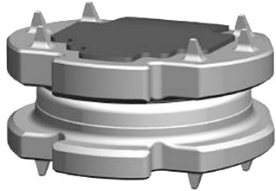
2.6 Total Disc Arthroplasty failure

Different reasons were found for the failure of the artificial discs. For the mimicking artificial discs, such as the Acroflex, the main reason for failure was due to tearing of the elastomer core in between the two titanium endplates. This leads to wear debris reaching the surrounding tissues which can cause osteolysis and then revision surgery (Fraser *et al.*, 2004; Kurtz, 2006). On the other hand, by looking through the history of the ball and socket joints it can be observed that most of them have one major problem that is wear resulting from the sliding of the socket on the ball. It is very common issue in hip artificial joints (Campbell *et al.*, 1996; Ingham and Fisher, 2000; Schmalzried *et al.*, 1996). Although, the highly cross-linked polyethylene artificial hips were having superior wear resisting during the first 10 years but still they show no evidence of improvement in wear and osteolysis after 10 years of implanting (Tsukamoto *et al.*, 2017).

The same problem faced the ball and socket artificial discs when they were implanted (De Kleuver *et al.*, 2003; Hallab *et al.*, 2003; Kurtz, 2006). The wear particles, which are produced from the motion of the ball and socket, cause inflammation in the tissues surrounding the hip joint. The same occurs in the spine with inflammation in the surrounding tissues of the spine around the implanted area (Cunningham *et al.*, 2003). Following the inflammation resulting from the wear and the other body reactions, osteolysis might occurs and affects the fixation between the artificial joint and the bone leading to failure. Sometimes loosening of the implant might occur due to micro-motion between the bone-artificial joint interface, as a biological response resulting from the stress at the bone interface (Burke *et al.*, 1991; Ingham and Fisher, 2000). Hard-on-hard implant bearings, which are metal on metal articulations generally produce smaller fairly round size particles than the soft on hard materials (polymers on metals) which are larger

and have an elongated shape (Hallab, 2009). The particles produced from the testing of the artificial discs in the simulators match the size and type of particles produced *in vivo* (Hallab, 2009). For the artificial hip, there is no doubt in the literature that the wear debris produced by the artificial joint produces an inflammatory response in surrounding tissues of the hip joint and loosening in the implant (Konttinen *et al.*, 1997). For spinal implant devices it was found that their particles activate osteoclastic activity which is known to be the number one cause of failure in the other artificial joint implants as well (Cunningham *et al.*, 2003).

Osteolysis of the artificial disc has been reported previously (Devin *et al.*, 2008; Kurtz *et al.*, 2009; Punt *et al.*, 2011; Punt *et al.*, 2009; van Ooij *et al.*, 2007). It might not cause implant loosening in the artificial disc between the two vertebrae due to the compression force applied by the spine; however, it might lead to subside of the whole implant or part of it in some cases as happened previously which will affect the functioning of the artificial disc (Kurtz, 2006; van Ooij *et al.*, 2007; Van Ooij *et al.*, 2003).

All the previous cases and many other cases support the idea that wear resulting from the spinal implants can cause problems in the surrounding tissues such as osteolysis, subsidence, chronic inflammations, granulomatous masses growth which can cause spinal stenosis, occlusion or stenosis in the surrounding arteries and veins (Devin *et al.*, 2008; Kurtz *et al.*, 2009; Papageorgiou *et al.*, 2014; Punt *et al.*, 2011; Punt *et al.*, 2009; van Ooij *et al.*, 2007).

2.7 Encapsulation of the ball and socket TDR

2.7.1 The clinical case for a new encapsulated TDA device

It is well known from the previous literature in section 2.6 that wear particles resulted from the articulating of the ball and socket artificial disc led to chronic inflammations, osteolysis, subsidence of the implant and then revision surgery (Devin *et al.*, 2008; Kurtz *et al.*, 2009; Punt *et al.*, 2011; Punt *et al.*, 2009; van Ooij *et al.*, 2007). Osteolysis has been observed in many cases in the literature as mentioned previously in section 2.6 and it could be a big issue in the near future. Encapsulating the ball and socket artificial disc could help in preventing this problem by preventing the wear particles from migrating to the surrounding tissues and cause inflammations which might lead to chronic inflammations and osteolysis and then revision surgery. In addition, inserting a lubricant inside the encapsulated sheath might help in producing a better lubrication regime and reducing the wear resulted from the articulating of the socket against the ball which might increase the life of the implant.

2.7.2 Sealing idea

Encapsulation might be a solution for preventing the wear particles from migrating to the surrounding tissue of an implant. By applying a sealing technique, it could help in holding a synthetic lubricant inside the capsule and preventing wear debris from migrating away from the implant to the surrounding tissues. The reduction of the produced wear from the artificial disc might improve the implant by reducing the chances of implant revision and increase the life of

the artificial disc. The idea of encapsulation for artificial joints in general was first suggested by Derbyshire *et al.* (1980) in which they tested the fatigue life, with and without a lubricant, of silicone rubber, segmented polyurethane, avcothane (silicone-polyurethane) and Bion (polyolefin rubber) (Mcmillin, 1987; West *et al.*, 2000). They used polyglycols, glycerine and chlorotrifluoroethylene polymers as lubricants. However, they did not test any attachment methods or the tribology of the encapsulated artificial joint. The idea of encapsulating the artificial joints was then developed and investigated further in the 1980s by Yao and Skorecki (1985) on an artificial shoulder joint. They used a Bion elastomer (stereoregular polyolefin rubber), polyethylene glycol 600 M_n (PEG) as a synthetic lubricant and tested adhesive bonding using silicone adhesive type A and Chemlok 205 and 252. They tested the lubricant from the sheath and the strength of the method of attachments; however, they did not test the tribological performance of the encapsulated artificial joint. A study of encapsulating artificial joints was undertaken using a silicone elastomer (MED-4950) as an outer sheath and different lubricants such as deionized water, bovine serum, hyaluronic acid, therapeutic fluid (alendronic acid sodium, γ-globulin, bisphosphonates and hyaluronic acid) was used inside the capsule (Zhang *et al.*, 2009). They found that the wear volume was reduced after using their therapeutic fluid lubricant in comparison with the other lubricants (Zhang *et al.*, 2009). Finally, the encapsulation of the artificial disc was applied commercially in the Bryan cervical disc, which is a one piece and bi-articulating artificial disc and, has led to a great clinical success (Lauryssen *et al.*, 2012; McKay *et al.*, 2006). Saline was used as the lubricant in the Bryan disc between the articulation surfaces (Fong *et al.*, 2006). In addition, a polyurethane sheath elastomer was used as the material for encapsulation (Fong *et al.*, 2006). In this thesis, encapsulation has been introduced to the ball

and socket artificial disc that is designed in the Biomedical Research Group at the University of Birmingham.

2.7.3 The encapsulated artificial disc design

The design of the encapsulated artificial disc has different stages during the design process. The design of the encapsulated artificial disc will face many challenges. The first challenge will be choosing the articulation materials and the lubricant that will be used inside the encapsulation to reduce the friction and wear. The second challenge is choosing the material of the capsule that will surround the artificial disc. The material has to be biocompatible and should survive for millions of cycles without any fractures. The third challenge is the sealing, or attachment method, of the capsule sheath to the artificial disc in which it should keep the lubricant and wear particles inside the encapsulation. The capsule sheath material should be biocompatible and tear resistance. To measure the ability of the capsule material to apply these kinds of movements during the implant life without tearing would be by measuring the fatigue life of the material. Studying different types of biomedical elastomers in the literature which can be used to produce the capsule sheath, it can be noticed that few types of elastomers can be used as long-term implantation in the human body (Yoda, 1998).

2.7.4 Ball and socket tribology and lubricant choice

Lubrication is an important factor in reducing the friction and thus reducing wear. Friction can be affected by different factors such as surface roughness, implant geometry, load, relative velocity of the bearings and viscosity of the lubricant (Kretzer, 2013). A Stribeck curve can be used to investigate the different lubrication regimes with different frictions and film thicknesses, as shown in Figure 2.9. There are four lubrication regimes that can be found between the articulation surfaces and they are dependent on the lubricant film between the articulating surfaces. The first lubrication regime is the boundary lubrication regime where there is a thin film of lubricant covering the surface asperities. During the articulation, there is direct contact between the asperities of each articulating material. The second lubrication regime is the mixed lubrication regime in which the cavity between the contact surfaces are somewhat covered with a layer of lubricant which partially separates them. The load is carried by the lubricant layer and the asperities of the surfaces. The third lubrication regime is the elastohydrodynamic where there will be an elastic deformation (elastic deformation of contact surface asperities) between articulating materials also an uninterrupted lubricating film will be maintained (Kretzer, 2013). The final lubrication regime is hydrodynamic where there will be an uninterrupted thick lubricating film and elastic deformations will not be taken in consideration in this regime. In both elastohydrodynamic and hydrodynamic there should be no wear (Kretzer, 2013).
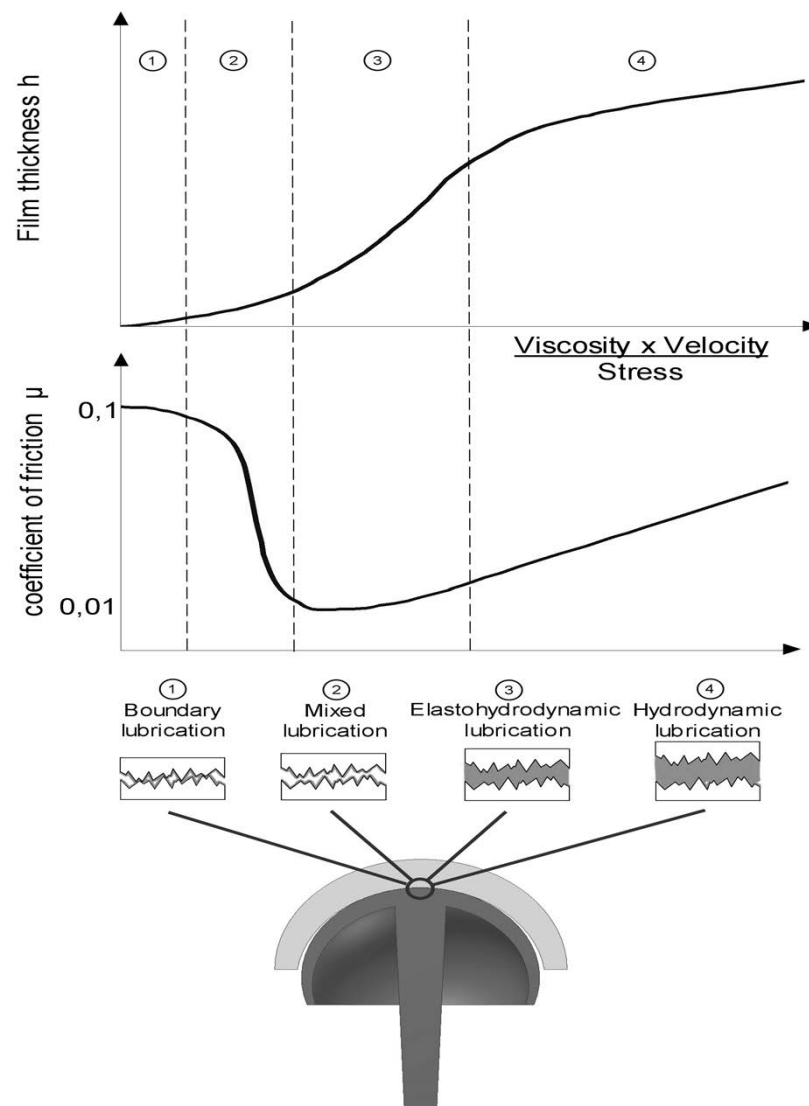
Figure 2.9: Boundary, mixed, elastohydrodynamic and hydrodynamic lubrication regimes

(Kretzer, 2013). Reprinted with permission from John Wiley and Sons.

The choice of the synthetic lubricant is a major challenge in biomedical implants. The lubricant should be biocompatible to be inserted in the body and used between the articulation surfaces. In addition, the lubricant should be capable of reducing the friction between the articulation surfaces and help to reduce wear and increase the life of the implant. Cooke *et al.* (1978) studied different

synthetic lubricants to help reduce the friction in the degenerated synovial joints. They found that polyvinyl alcohol had similar rheological characteristics to silicone oil, but both had different viscosity characteristics to synovial fluid. Synovial fluid is suitable for the natural joints; however, it shows poor lubrication with artificial joints (Derbyshire *et al.*, 1980).

2.7.5 Capsule sheath choice

Elastomers have been classified according to the exposure time by the human body into three categories: Limited exposure which is less than 24 hours, prolonged exsposure which is from 24 hours to 30 days and permenant exposure which is more than 30 days (Chauvel-Lebret *et al.*, 2001). Most elastomers are considered as a foreign body when they are implanted in the human body which leads to an acute inflammatory response and phagocytes existance. It is difficult to understand why they are detected by the immune system while they are inert, unreactive and nontoxic (Chauvel-Lebret *et al.*, 2001). However, to understand why some elastomers are biocompatabile when they are implanted, it is helpful to look at the mechanism of interaction between the proteins surrounding the elastomers when they are implanted. Hydrophopic elastomers such as polyurethane, polyethelene, silicones and (polyethylene terephthalate) dacron become coated with host protiens after the absorption of these protiens by the surface of the implanted elastomer (Chauvel-Lebret *et al.*, 2001). Thus, the elastomer will be coated with a layer of protiens from the interstatial fluid; thus, host inflammatory cells and fibroblasts will not have direct contact with the elastomer (Chauvel-Lebret *et al.*, 2001). Among the few elastomers, polyurethane and silicone are the ones which can be implanted and live for long periods of time

in the human body (Pinchuk, 1994). Some others prefer polyurethane over silicone due to the excellent mechanical properies which can be found in polyurethane (Chauvel-Lebret *et al.*, 2001). The fatigue life of the polyurethane and silicone elastomers will be discussed and compared with literature in chapter 5.

2.8 Summary

The following conclusions can be drawn from this chapter:

- Disc degeneration can occur with ageing, lifestyle and genetics.

- Neck and back pain can be treated by conservative or surgical treatments.

- One of the surgical treatments is total disc arthroplasty (artificial disc).

- Artificial discs have either a flexible elastomer core mimicking the natural disc or articulating with a ball and socket artificial disc.

- The major problem with the articulating artificial discs is wear.

- Wear debris produced by the artificial joint can cause an inflammatory response, osteolysis and subsidence of the implant or part of it and then revision surgery.

- Encapsulating the artificial disc might be a solution for preventing the wear particles from migrating to the surrounding tissue around the implant.

The next chapter discusses the procedure and aspects of designing a new encapsulated artificial disc.

3 Design process for the encapsulated ball and socket artificial disc

3.1 Overview

This chapter presents the design process of the ball and socket artificial disc. The first part in section 3.2 will be an introduction about the design process. Then the product design specification will be described and discussed in detail in section 3.3. After that the conceptual designs will be presented and discussed in section 3.4. The detailed design and simulation will be presented in section 3.5. Results of the detailed design simulation are presented in section 3.6. In section 3.7, a discussion and comparison of the results will be discussed. Finally, the chapter is concluded in section 3.8.

3.2 Introduction

Before the design process of the artificial disc begins there should be a complete understanding of the structure and functions of the original intervertebral disc, which the device will replace, as described in Chapter 2. The design process is a decision making process. When there are problems in a certain device, a tool or a machine there should be suggested solutions to solve these problems (Pal, 2013). The main functions of the artificial discs are to restore the motion of the spine without causing pain and whilst also carrying the required loads with different angular motions without losing the height of the disc space or failure of the artificial disc (Kurtz, 2006). The concept of ball and socket artificial discs such as the Prodisc, Maverick and FlexiCore came from the successful artificial hips which were designed to be ball and socket artificial joints (Kurtz, 2006). However, these artificial discs have a common problem which is the wear produced during articulation, as described previously in Chapter 2. The encapsulation idea was proposed to solve two main problems with the current articulating artificial discs. The first problem is the high friction caused by the poor lubricity of the interstitial fluid and the resulting wear and the second problem is the migration of those wear particles to the surrounding tissues, again as described in chapter 2. According to Pugh's model in the steps towards making a new product, design must go through different processes (Pugh, 1991). The first step in Pugh's model is to identify the market or the user needs. This step was discussed in Chapter 2 about the challenges facing ball and socket artificial discs. The second step is to make a product design specification for the product that will be designed. The third step is to have different conceptual designs to fulfil the product design specification requirements. The fourth step is to make a detailed design after evaluating and selecting the most appropriate conceptual design. The fifth

step is to manufacture and the final step is to sell. However, this thesis will not include the last step and will only focus on evaluating the manufactured prototype of the concept. The aim of this chapter is to present the design process of an encapsulated artificial disc.

3.3 Product Design Specification of the encapsulated artificial disc

The product design specification (PDS) is the second stage of the design process which describes the different requirements of the product. It acts as a control document for the whole design process because it places boundaries on the subsequent designs and it can be updated or partially changed during the design (Pugh, 1991). Figure 3.1 shows the different parts of the product design specification for the design of any product. The parameters from product design specifications were applied to the design of the encapsulated artificial disc and each parameter is discussed in detail below.
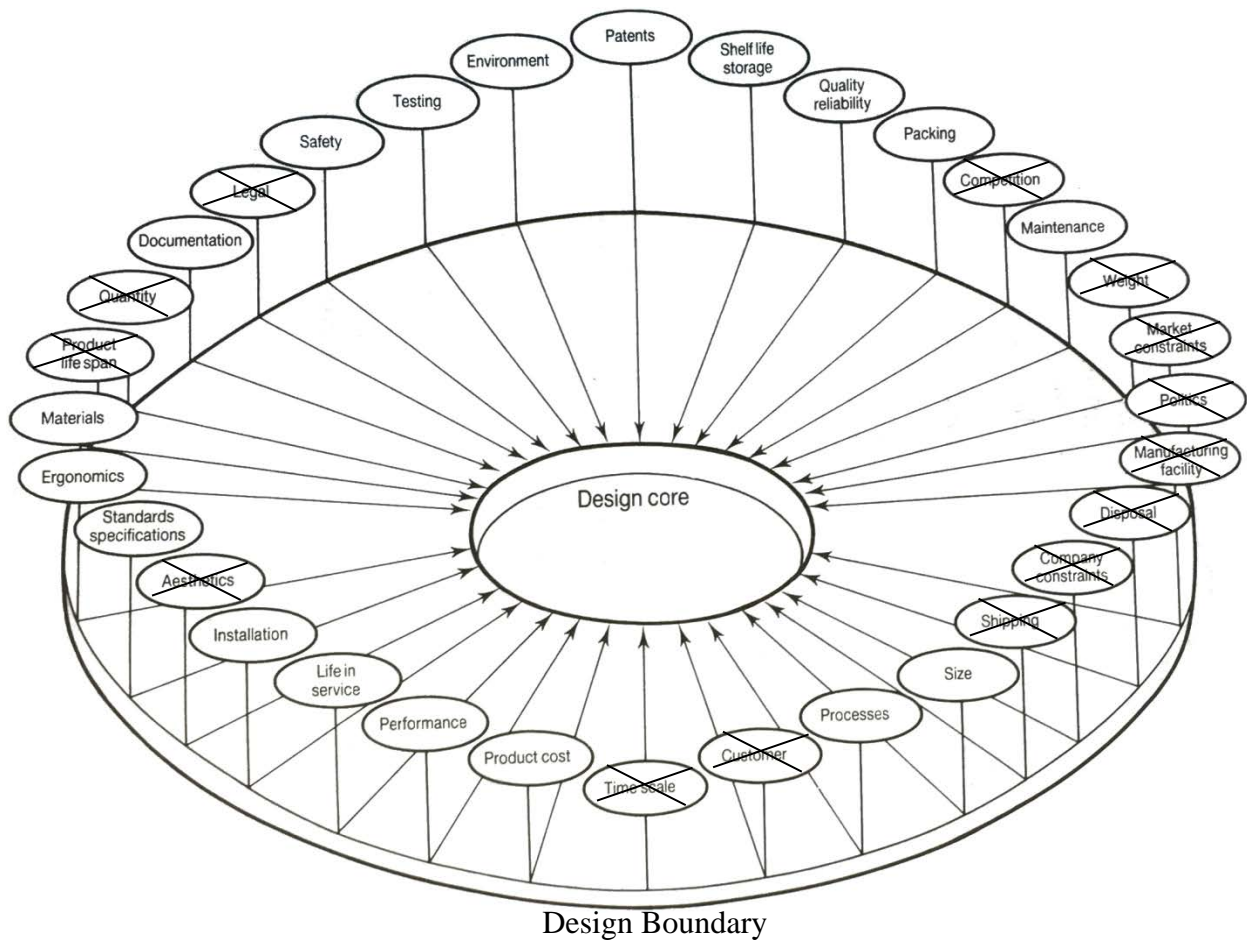
Figure 3.1: Elements of the PDS (Pugh, 1991), crossed elements are elements have not been taken in consideration for the artificial disc.

3.3.1 Performance

A Lumbar TDA should be used inside the human body with an axial load of between 600 and 2000 N according to the standard BS 18192-1:2011 (BS ISO 18192-1, 2011). It should enable an extension angle of -3°, flexion angle of 7°, lateral bending of ±2° and axial rotation of ±2 ° (Berry

et al., 1987; BS ISO 18192-1, 2011; Gilad and Nissan, 1986). In addition, the implant should be stable (no implant loosening) while allowing the required motion in the spine.

The outer sheath, as described in the previous chapter, should seal the artificial TDA, hold the lubricant, keeping it inside the TDA, and prevent any wear particles from migrating to the surrounding tissues. In addition, the outer sheath should not inhibit the required motions. Furthermore, according to the standard BS 18192-1: 2011 (BS ISO 18192-1, 2011), it should be durable enough to exceed at least ten million cycles (ten years) of flexion/extension, lateral bending and axial rotation without having any damage to the sheath, which might lead to lubricant leakage. In addition, the lubricant, contained within the device should be viscous enough to reduce the friction coefficient and reduce the wear produced from the contact of the socket against the ball. The lubricant inside the capsule should be biocompatible as well. The lubricant should be fully sealed and there should be no leakage through the sheath or through the attachment between the sheath and the ball and socket. In addition, it should be used without any refilling for the service life of the artificial disc.

3.3.2 Quality and reliability

For the artificial disc implant, the quality management systems for medical devices, BS EN ISO 13485:2003 (BS EN ISO 13485, 2003) should be followed to achieve the required quality. The risk management and reliability which comes as one of the main approaches of the risk management of the medical device is described in the standard BS EN ISO 14971:2012 (BS EN ISO 14971, 2012).

3.3.3 Environment

The environment that surrounds an intervertebral disc has a temperature of 37 °C. Pressure in the foramen (the space of the spine nerves) is 2.3 kPa for flexion and 4.9 kPa for extension (Morishita *et al.*, 2006). The mean intra-abdominal pressure while standing for adults is about 20 mmHg (Cobb *et al.*, 2005). The surrounding fluid when the TDA is implanted is most likely to be interstitial fluid (Graham, 2006).

3.3.4 Life in service

The TDA should be capable of working for approximate of 10 million cycles *in vivo* according to BS 18192-1: 2011 (BS ISO 18192-1, 2011) standard and not require any replacement when implanted for at least 10 years of continuous use.

3.3.5 Size

The size of the lumbar vertebral discs varies from L1-L5, as shown in Figures 3.2 and 3.3. The size of the vertebrae gives information about the approximate size of the artificial disc that can be implanted and used in the different levels of the lumbar spine. The length of the vertebral body from L1 to L5 is 52 ± 4 mm. The depth of the vertebral body for the same region is 34 ± 3 mm (Berry *et al.*, 1987; Gilad and Nissan, 1986). The height of the vertebral disc is 12 ± 3 mm for the same region (Berry *et al.*, 1987; Gilad and Nissan, 1986). The movement angles of the vertebral column on that region are 7 ± 4 ° (Berry *et al.*, 1987; Gilad and Nissan, 1986). Therefore, the size

of the lumbar artificial disc should be suitable with these dimensions to fit in different lumbar sections. In addition, it should be capable of achieving the sliding angles to give the required motion.
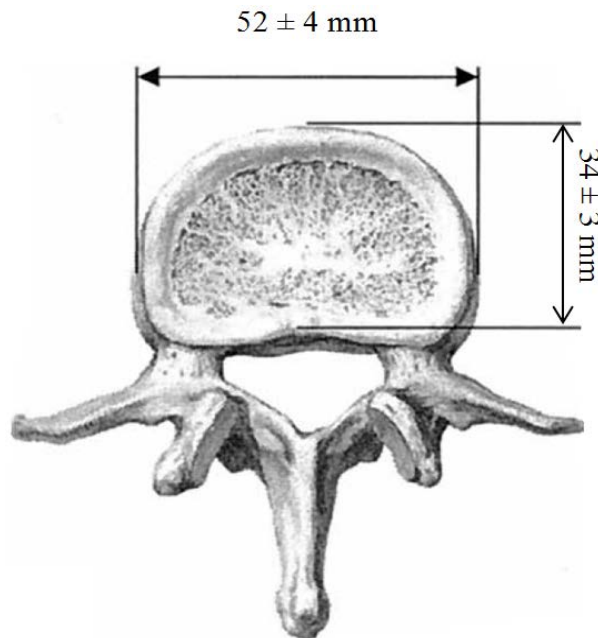
Figure 3.2: Top view and dimensions of lumbar vertebral body (Wolf *et al.*, 2001). Reprinted with permission from Wolters Kluwer Health, Inc.
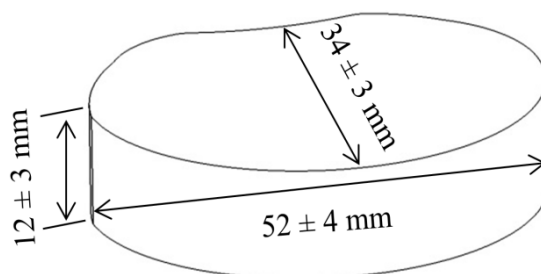
Figure 3.3: Dimensions of lumbar intervertebral space (L1-L5) (author's own drawing, adapted from Berry *et al.* (1987); Gilad and Nissan (1986); Wolf *et al.* (2001) .

3.3.6 Materials

3.3.6.1 Articulation materials

The materials should be chosen from the materials that have met the requirements set out by international standards. BS ISO 21534:2009 (BS EN ISO 21534, 2009) contains a list of the materials that have been proven for the use in artificial hip joints. In addition, the same standard contains a suitable combination of materials and unsuitable combination materials which will be considered. The materials that will be used to manufacture the ball and socket should be capable to maintain a 2000 N axial load; furthermore, they should have a low coefficient of friction when a lubricant in use to reduce the generation of wear particles (Bhushan, 2013).

3.3.6.2 Encapsulation materials

The material to be used in the encapsulation should be biocompatible and suitable for implanting inside the human body for long periods, flexible (i.e. does not inhibit disc motion) and have a long fatigue life. In addition, it should not have any reactions with the surrounding fluids which might lead to encapsulation failure or inflammation in the surrounding tissues. It should be capable of functioning for at least 10 million cycles (10 years) without any failure.

3.3.6.3 Lubricants

The lubricant that will be used inside the capsule should be biocompatible, viscous enough to reduce the friction coefficient to a minimum, which will help in reducing the wear. In addition,

the lubricant should not increase the drag force and lead to difficulty in achieving the required motions (Hamrock *et al.*, 2004).

3.3.6.4 Attachment material

The attachment material and method of attachment should prevent wear particles from migrating to the surrounding tissues between the device and sheath. In addition, it should prevent the lubricant from leaking into the surrounding tissue. It should be capable of sustaining the millions of cycles of movements applied by the artificial disc (flexion/extension, lateral bending and axial rotation). The attachment method should not cause any damage for the sheath or to the surrounding tissues.

3.3.7 Standards and specifications

1. BS EN ISO 21534: 2009 (BS EN ISO 21534, 2009) Non-active surgical implants Joint replacement implants - Particular requirements.

2. BS EN ISO 21535: 2009 (BS EN ISO 21535, 2009) Non-active surgical implants — Joint replacement implants — Specific requirements for hip joint replacement implants.

3. BS EN ISO 21536: 2007 (BS EN ISO 21536, 2007) Non-active surgical implants. Joint replacement implants. Specific requirements for knee-joint replacement implants.

4. BS 18192-1: 2011 (BS ISO 18192-1, 2011) Implants for surgery — wear of total intervertebral spinal disc prostheses.

3.3.8 Testing

The disc replacement implants should be assessed to check if the performance is achieved or not by a preclinical evaluation for:

1. The biocompatibility of all materials, which will be evaluated through the literature.

2. Fatigue testing of the encapsulation sheath should be tested and the effect of sterilization and aging on the fatigue life of the chosen material.

3. The viscosity of the lubricants can be tested by using a viscometer.

4. Friction coefficient of the different material combinations with different lubricants.

5. The resistive torque and wear tests using the BS 18192-1: 2011 (BS ISO 18192-1, 2011) standard applied on the new artificial disc.

3.3.9 Processes

3.3.9.1 Metal surfaces

Metallic components should be polished by using iron-free materials. In addition, surfaces should be free of any cracks, scratches, cavities and other defects (BS EN ISO 21534:2009) (BS EN ISO 21534, 2009).

3.3.9.2 Plastic surfaces

Plastic components of the artificial joint should not be manufactured using a non-removal abrasive or polishing compounds that might stick to the implant. In addition, the components should be free of particulate contamination (BS EN ISO 21534, 2009).

3.3.10 Product cost

The cost of the new artificial disc should be affordable and it should compete with the other artificial discs in the market. The Charité price is about $4,500 to $5,000 in Australia (Arida *et al.*, 2006). Therefore, the price of the encapsulated artifice disc should be around $2500 US dollars.

3.3.11 Documentation

The following documentation should be included with the device:

- Instructions for surgeons on how to prepare the disc before installation inside the human body.
- Instruction manual for the installation procedure and use of the installation tools.
- User manual for the safety and risk management instructions.
- Other quality management system documents as described in BS EN ISO 13485:2003 (BS EN ISO 13485, 2003).

3.3.12   Safety

The implant should not cause any harm such as tissue damage for the patient after implantation. Safety will be evaluated by pre-clinical evaluation including risk assessment at all stages of the life cycle of the implant. In addition, the installation tools should not cause any harm to the surgeons or for the patient during the procedure.

3.3.13   Patents

All patents related to the artificial disc should be investigated and researched to have a better knowledge and understanding of the technological state-of-the-art. A number of previous designs in the literature and patents have been discussed in chapter 2.

3.3.14   Shelf life storage

Shelf life is the factor of the storage on the site of the product, shipping and storing (Pugh, 1991). The mechanical properties of the artificial disc might change when it is stored for a long time. For example, Edidin *et al.* (2000) found that with aging the ductility and toughness decreased for ultra high molecular weight polyethylene, when it was aged using an air circulating oven at 80°C. In Europe and the USA the shelf life of medical implants is about five years to keep the sterility assured (Muratoglu and Kurtz, 2002). Therefore, the shelf life for the artificial disc must be a maximum of five years.

3.3.15   Packaging

3.3.15.1   Protection from damage while in storage and through transport

The packaging for the implant should keep the implant safe from damage when it is stored. In addition, it should be capable of keeping the implant safe while transporting it from the manufacturer to the hospital (Wang and Turndorf, 1983). Furthermore, the implant should be protected from humidity and temperature which might affect the life of the implant when it is stored.

3.3.15.2   Maintaining the sterility

The packaging should be able to keep the sterilization during the transport, storage and handling the implant unless damage has occurred to the packaging of the implant (Levitin *et al.*, 2012).

3.3.16   Installation

Installation of the implant inside the human body needs special tools to control the insertion procedure by surgeons. The project here is focusing on the design and mechanical testing of the encapsulated artificial disc only.

3.3.17   Maintenance

The final product of the disc replacement should be maintenance free. Therefore, it should be able to perform for the full period without any need for maintenance.

3.3.18   Ergonomics

The artificial disc should be easily prepared for installation because surgeons will insert it. It should then be easily installed inside the human body. Furthermore, it should have a description for the surgeons on how to install the device inside the body and how to use the installation tools.

3.4 Conceptual design of the encapsulated artificial disc

The conceptual design stage is where unlimited creative solutions are generated to meet the PDS requirements (Pugh, 1991). The ideas in this stage should be evaluated and improved until a final concept design is selected which is the most suitable for the PDS requirements. Various methods, such as TRIZ, have been used to gain ideas to support this stage and to reach the optimum conceptual design. TRIZ is the Theory of Inventive Problem Solving, invented by the Russian engineer Genrich Altshuller. This theory is a toolkit for problem solving which relies on summarizing the past solutions for a large number of problems to show how the previous techniques can help systematically to solve future problems (Gadd and Goddard, 2011). The general concept of TRIZ can be seen clearly in Figure 3.4. The process of understanding the

problem and trying to find a solution suitable to the problem has different stages which will be described and discussed in this chapter.
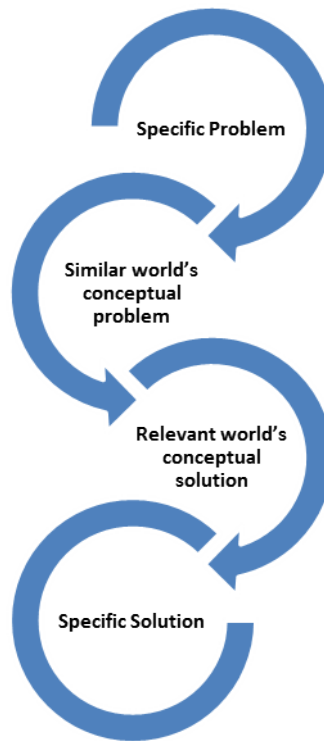
Figure 3.4: The general concept of TRIZ (Gadd and Goddard, 2011).

The golden rule of TRIZ which is fundamental to all methods of problem solving, is the IDEALITY equation shown below. This equation is considered as the starting and the end point of all problem solving and it is focused on three things: achieve more benefits; less harm and less costs.

$$IDEALITY = \frac{\text{all benefits}}{\text{Costs} + \text{Harms}}$$

All TRIZ tools are built to improve the ideality of the solution and one of the most widely used tools is the contradiction matrix.

The first step in TRIZ is to identify the problems that the current ball and socket artificial discs have by developing problem statements. The first problem is the lubricant lubricating the ball and socket artificial discs is interstitial fluid which has low viscosity, as described in chapter 2. Artificial discs with metal against metal or metal against polymer combinations will operate under a boundary or mixed lubrication regime (Shaheen and Shepherd, 2007). This problem might lead to the production of wear particles and then chronic inflammations, osteolysis, subsidence of the whole implant or part of it and then revision surgery, as was described in detail in chapter 2. The second problem is the wear particles that are produced by the articulation between the ball and socket artificial disc. The migration of these wear particles can induce an inflammatory response, causing toxicity, osteolysis and subsidence of the whole implant or part of it, as described in chapter 2. The two problems are listed in Table 3.1.

Table 3.1: Problems bank.

Problems Bank		
No.		Priority
1	Boundary lubrication regime which leads to wear production (volume reduction)	1
2	Migration of wear particles (volume reduction) to the surrounding tissues	2

The second step is to apply the classical TRIZ solutions tools which are based on the study of patents that were used to solve generic problems that have been faced over the history of innovation. In this step the recommended guidelines for choosing the solution tools used as recommended by TRIZ. One of the most powerful tools of TRIZ is the 40 inventive principles. Every engineering problem has at least one or more contradictions. The TRIZ 40 Inventive Principles helps to find different solutions for any contradiction (Gadd and Goddard, 2011). The last step is to implement the solutions that have been suggested by the TRIZ 40 Inventive Principles on the conceptual design of the new artificial disc.

Parameters which are required to be improved are selected from Table 3.1. The first problem which is the high friction coefficient which leads to wear production was solved by the TRIZ 40 Inventive Principles by applying solution No.10 (No.10 is the prior action) and using composite materials (solution No.40 is the composite materials), as shown in Table 3.2. The prior action (No.10) was described by performing changes in the object (material) partially or fully (Gadd and Goddard, 2011). This could be by using different materials combinations to reduce the friction coefficient as much as is practical. The second solution is to use composite materials instead of the materials that are being used (No.40). Composite materials have been used in the hip implant previously (Katoozian *et al.*, 2001; Wang *et al.*, 1998). However, in this chapter we might replace the composite materials with biomedical materials that are well known for their good tribological performance as was recommended by the standard BS ISO 21534:2009 (BS EN ISO 21534, 2009). Some solutions were discarded because they were irrelevant to this kind of problem. The second problem is the migration of the wear particles to the surrounding tissues. The suggested two solutions for this problem are to use No.30 solution (No.30 is the flexible shells and thin

films) to encapsulate the articulation materials to prevent the wear from migrating to the surrounding tissues.

Table 3.2: Contradiction matrix for solving technical contradictions of the encapsulation sheath (Gadd and Goddard, 2011).

Worsening			Parameters that is getting worse						
			1	2	…	7	8	..	39
			Weight of moving object	Weight of stationary object		Volume of moving object	Volume of stationary object		
Improving									
	1								
	⋮								
	13	Stability of the object's composition	21,35,2,39	26,39,1,40		28,10,19,39	34,28,35,40		
	⋮								
	23	Loss of substance	35,6,23,40	35,6,22,32		1,29,30,36	3,39,18,31		
	⋮								
	⋮								
	31	Object-generated harmful factors	19,22,15,39	35,22,1,39		17,2,40	30,18,35,4		
	⋮								
	39								

(Note: left side vertical label "Parameters to be improve")

Applying the suggested solution by TRIZ of encapsulating the ball and socket artificial disc by using thin film or sheath (No.30) will help to prevent the wear from migrating to the surrounding tissues and this solution has helped in developing some conceptual designs related to this idea. The new problem with this idea is the attachment method for this membrane with the ball and socket disc. The attachment method should be biocompatible, strong enough to prevent leakage of the lubricant and prevent detachment of the sheath from the disc. The second problem is the sheath might crack with time when there are applied forces such as tension or compression. The same TRIZ process was applied on these two problems as mentioned earlier to solve the wear problems of the ball and socket artificial disc.

The solution which was suggested using the TRIZ 40 Inventive Principles for the first problem was No.28 (No.28 is to replace mechanical system) or No.24 adding an intermediary (No.24) in which an adhesive can be used to attach the sheath with the artificial disc. In addition, making the surfaces porous or by applying a prior action by roughening the surface (No.31 and No.10) to increase the strength of the attachment between the sheath and the ball and socket disc if an adhesive is used for example, as shown in Table 3.3.

The second problem can be solved by making the sheath curved (No.14 is the spheroidality curvature) instead of straight sheath encapsulating the ball and socket which will reduce the tension applied on the sheath which in turn will increase the lifetime of the sheath.

Table 3.3: Contradiction matrix for solving technical contradictions of the encapsulation sheath (Gadd and Goddard, 2011).

Worsening		Parameters that is getting worse									
		1	2	..	7	…	14	…	36	…	39
					Volume of a moving object		Strength		Device complexity		
Improving	1										
	⋮										
	14	Strength			10,15,14,7		-		2,13,28		
	⋮										
	23	Loss of substance			-		35,28,31,30		35,10,28,24		
	⋮										
	31										
	⋮										
	39										

Parameters to be improved

The new ideas for the conceptual designs, that themselves apply all the ideas that came from TRIZ, incorporated the PDS requirements. Seven sketches of the proposed solutions for the problems highlighted in the product design specification requirements are shown in Table 3.4.

Table 3.4: The different conceptual designs and their specifications for the encapsulated artificial discs.

Concept design	Concept specifications
  Con.1	• Socket against ball. • Straight cylinder sheath as the encapsulation sheath. • Three main parts (ball, socket and sheath). • Adhesive will be used for the attachment method. • Lubricant will be inserted from the upper plate through screw hole.
  Con.2	• Socket against ball. • Curved cylinder sheath as encapsulation sheath. • Three main parts (ball, socket and sheath). • Adhesive will be used for the attachment method. • Lubricant will be inserted from the upper plate through screw hole.
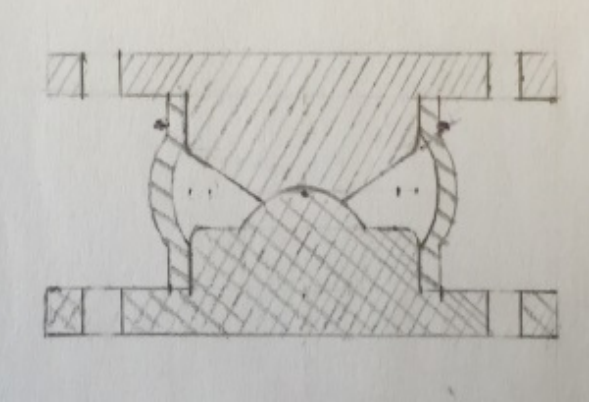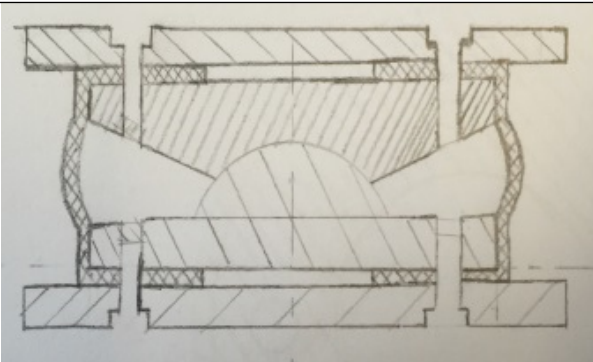
  Con.3	• Socket against ball. • Curved cylinder sheath as encapsulation sheath. • Five main parts (upper plate, Ball, socket, sheath and lower plate). • Mechanical sealing will be used. • Lubricant will be inserted from the upper plate through screw hole.
  Con.4	• Socket against ball. • Curved cylinder sheath as encapsulation sheath. • Three main parts (socket, ball and sheath). • Mechanical sealing will be used. • Lubricant will be inserted from the upper plate through screw hole.
  Con.5	• Mimic intervertebral disc. • Curved cylinder sheath as encapsulation sheath. • Three main parts (upper plate, lower plate, flexible cylinder core, outer sheath). • Adhesive sealing for the sheath. • No lubricant.
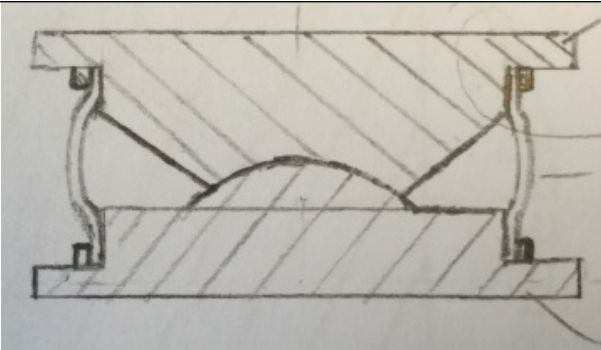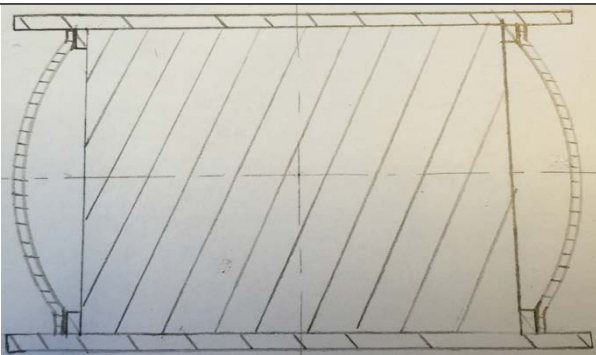
Con.6	• Socket against ball. • Cylinder sheath as encapsulation sheath. • Four main parts (socket, Sphere, socket and sheath). • Adhesive will be used for the attachment method. • Lubricant will be inserted from the upper plate through screw hole.
Con.7	• Socket against ball. • Cylinder sheath as encapsulation sheath. • Four main parts (socket, semi sphere, socket and sheath). • Adhesive will be used for the attachment method. • Lubricant will be inserted from the upper plate through screw hole.
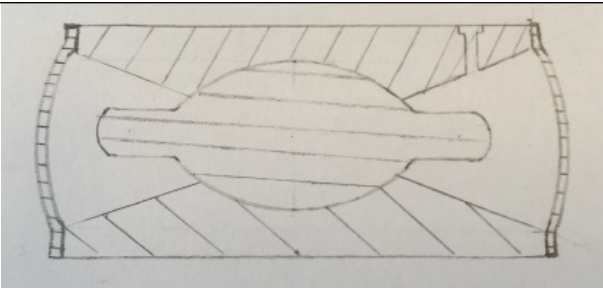
The seven concept designs were evaluated using the evaluation matrix described by Pugh (1991). The new ideas were compared with the Bryan disc, as a benchmark, which has a similar mechanism for encapsulating the device using the evaluation matrix, as shown in Table 3.5. After evaluating the different conceptual designs, the most appropriate concept design (con. 2) was chosen to develop in the detailed design stage.

Table 3.5: Evaluation matrix for the different conceptual designs for the encapsulated artificial disc.

Concept / Criteria	Bryan disc	Con.1	Con.2	Con.3	Con.4	Con.5	Con.6	Con.7
Manufacturing costs		S	S	S	S	S	S	S
Easier assembly		-	-	-	-	-	-	-
More secure locking		+	+	+	-	+	+	+
Stability		+	+	+	+	+	-	+
Sheath strength	D	-	+	+	+	+	+	+
Wear	A	+	+	+	+	+	+	+
lubricant	T	+	+	+	+	-	+	+
Ease of installation	U	S	S	S	S	S	S	S
Complexity	M	S	S	-	S	S	S	S
Mimic the intervertebral disc		S	S	S	S	+	S	S
Number of parts		+	+	-	+	+	S	S
Durability		+	+	+	+	+	+	+
Life in service		+	+	+	+	+	+	+

Limitation of motion		+	+	+	+	-	+	+
size		S	S	S	S	S	S	S
--------------	--------------	-------	---------	---------	-------	-------	-------	-------
Σ+		8	9	8	8	8	7	8
Σ-		2	1	3	2	3	2	1
ΣS		5	5	4	5	4	6	6

3.5 Detailed design of the encapsulated artificial disc

The detailed design of the socket of the artificial disc was undertaken using SolidWorks 2011 (Dassault Systèmes SolidWorks Corp., Massachusetts, USA). The detailed drawing of the encapsulated artificial disc is shown in Figure 3.5.
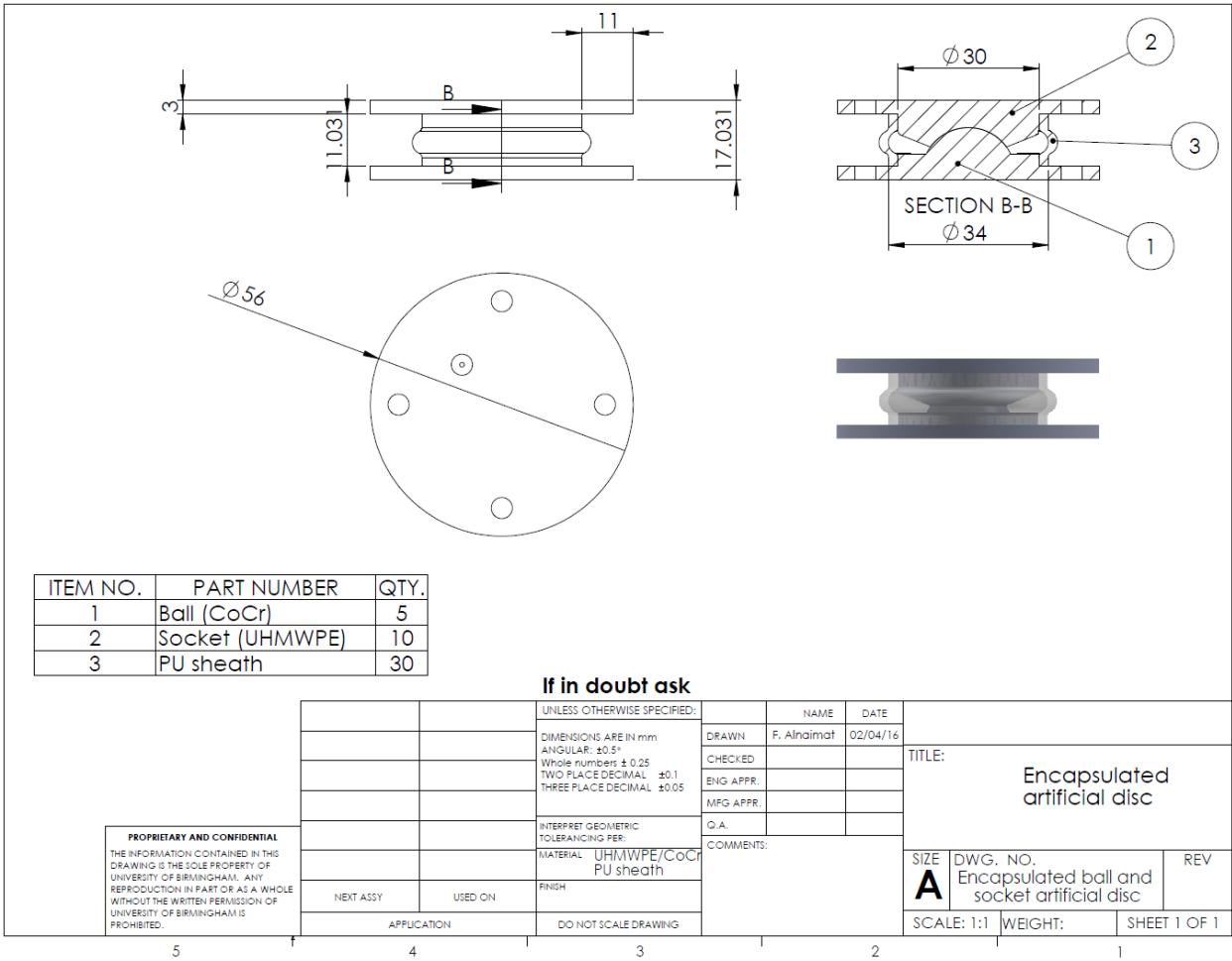
Figure 3.5: SolidWorks drawing of the encapsulated artificial disc. The encapsulated artificial disc contains three parts: 1) Ball. 2) Socket. 3) Encapsulation sheath.

The detailed drawings of the ball and the socket are shown in Figure 3.6 and Figure 3.7.
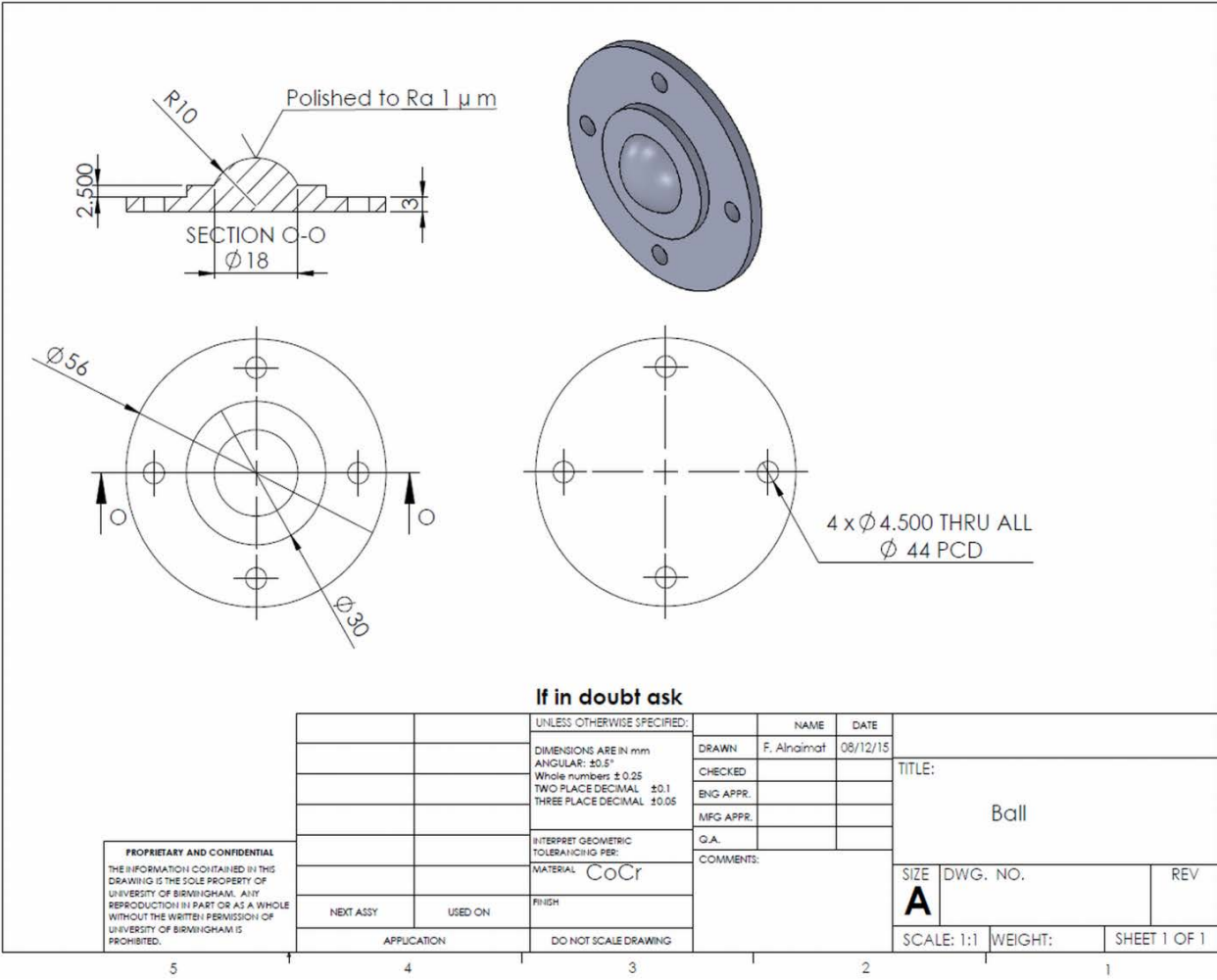
Figure 3.6: SolidWorks drawing of the first part the CoCr ball (Moghadas, 2012).
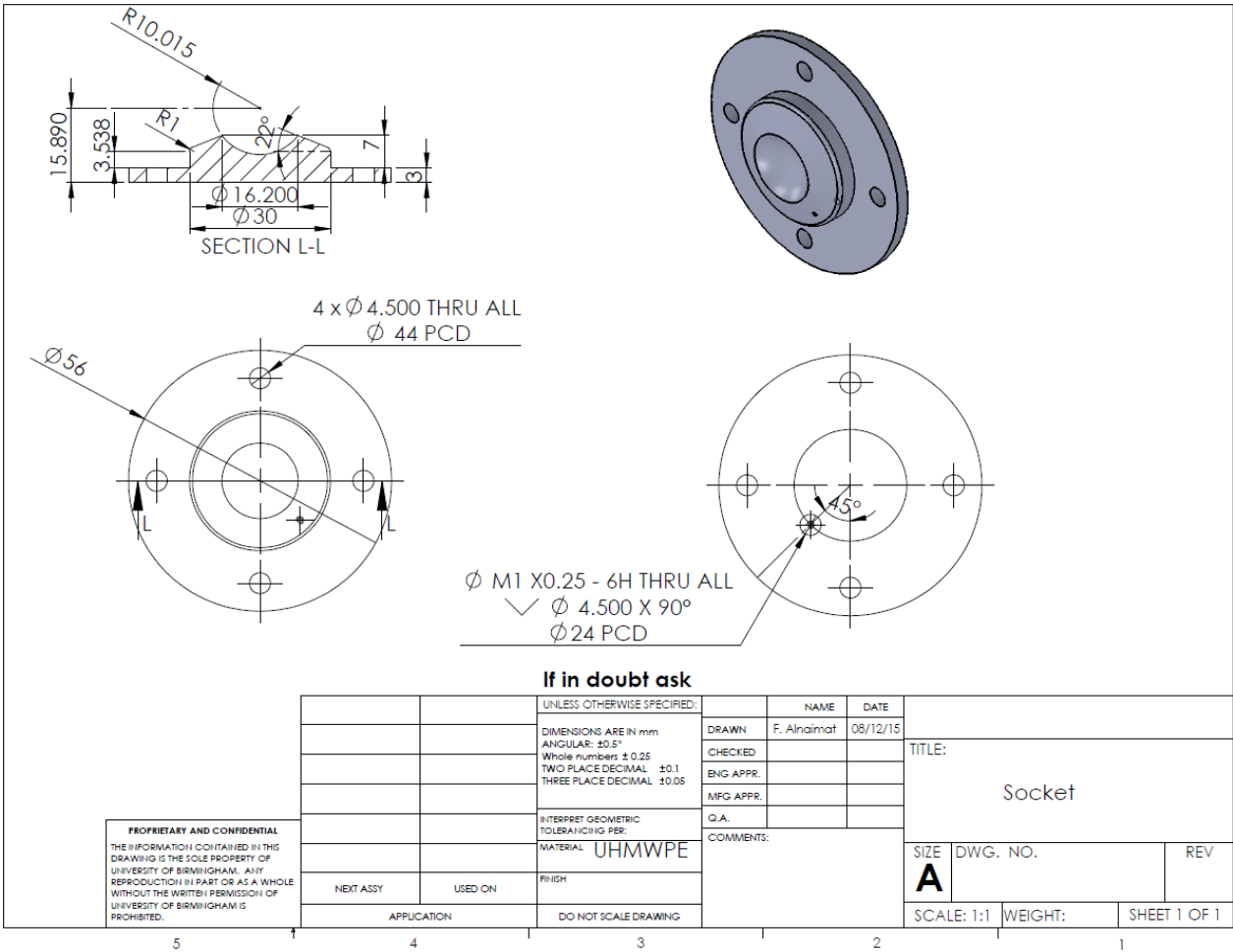
Figure 3.7: SolidWorks drawing of the second part the UHMWPE socket.

The engineering drawings of third part the polyurethane ether sheath used to encapsulate the ball and socket artificial disc, as shown in Figure 3.8. The polyurethane ether sheath was suggested in chapter 5 to be used as an encapsulation material for the artificial disc.
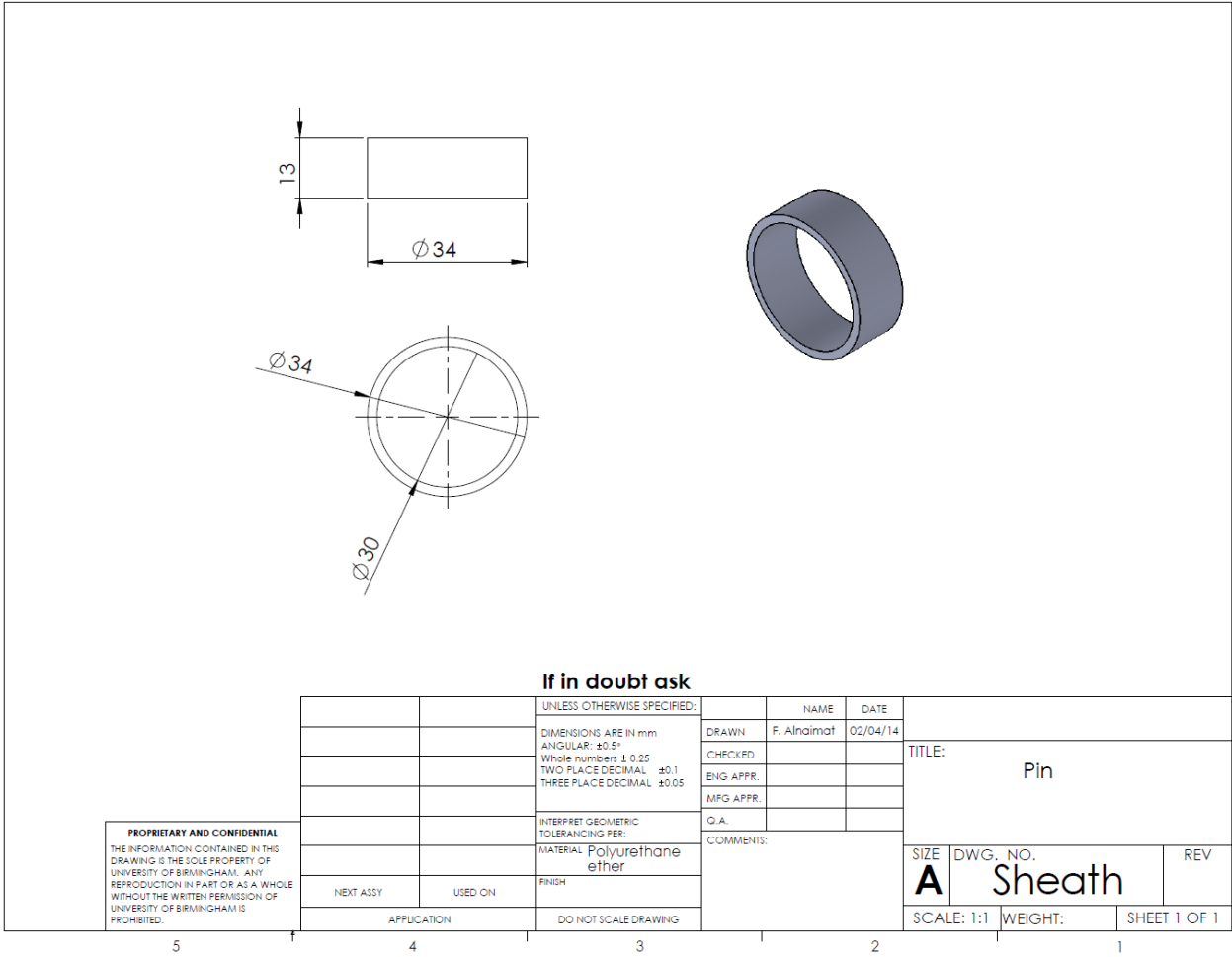
Figure 3.8: SolidWorks drawing for the third part the polyurethane ether encapsulation sheath.

Different designs for the socket, that included changing the position of the lubricant insertion hole were analysed using SolidWorks simulation (Dassault Systèmes SolidWorks Corp., Massachusetts, USA) for optimised stresses. The ball with a 10 mm radius was designed and manufactured previously by Moghadas (2012). The socket was designed with a 10.015 mm radius with a hole for inserting lubricant. Reducing the radial clearance leads to an increase in the lubricant film thickness (Jin *et al.*, 1997; Shaheen and Shepherd, 2007). Choosing a radial clearance to be 0.015 mm was based on a previous study (Moghadas, 2012). Different models with different hole sizes and positions were designed and analysed using the SolidWorks simulation tool. A vertical 2000 N load according to the standard ISO 18192-1:2011 was applied on the different models. Material properties for the ball and socket were set in SolidWorks and the analysis was run for the different ball and socket artificial discs, as shown in Table 3.6. The mesh was chosen to be parabolic tetrahedral with total elements and total nodes varying between the different models, as shown in Table 3.7 and Figure 3.11.

Table 3.6: Materials properties used in the simulation by SolidWorks. The data in this table from (ASTM F75-98, 2001; Jin, 2002; Kurtz, 2004).

Mechanical properties	CoCr Ball	UHMWPE Socket
Tensile strength	235 MPa	53 MPa
Elastic modulus	211 GPa	725 MPa
Yield strength	450 MPa	23 MPa
Poisson's ratio	0.31	0.46
Mass density	8900 kg/m^3	930 kg/m^3
Shear modulus	88 GPa	0.32 GPa

Table 3.7: Different models of the ball and socket artificial discs with different lubricant hole sizes and positions.

Model name	Model 1	Model 2	Model 3	Model 4	Model 5
Lubricant hole size	Centre of the socket	10 mm far from centre	11 mm far from centre	11 mm far from centre	12 mm far from centre
Lubricant hole size	M2	M2	M2	M1	M1
Total elements	51397	51547	51606	51898	51583
Total nodes	77417	77745	77831	78116	77689

Constraints were applied to the model as follows:

- The ball was fixed from the bottom flat plate.

- Contact between the surfaces of the ball and socket was set to no penetration through the bearing surfaces, as shown in Figure 3.9. This prevented the penetration of the socket through the ball during the application of the load. The coefficient of friction value was chosen to be 0.05; however, it will not affect due to the static loading which was applied vertically.
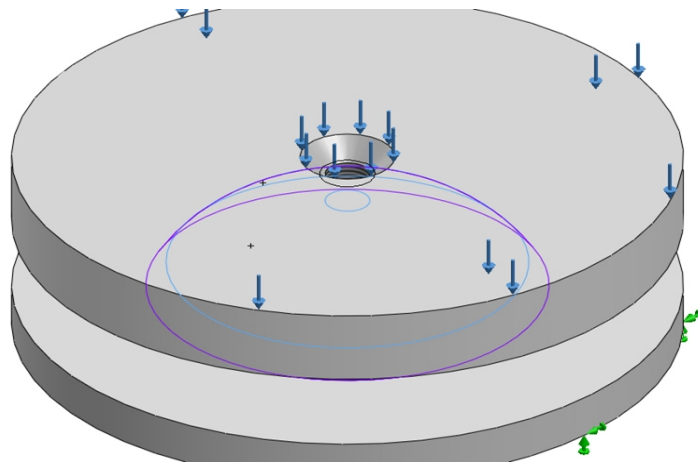
Figure 3.9: Constraints contact set between the ball and socket contact surface. The blue arrows represent the load, the green arrows on the rigid surface which was in the bottom of the ball. The purple and blue surface between ball and socket are the constraints.

- Another constraint was applied to prevent the penetration of the parallel surfaces beside the contact surface of the ball and socket, as shown in Figure 3.10.
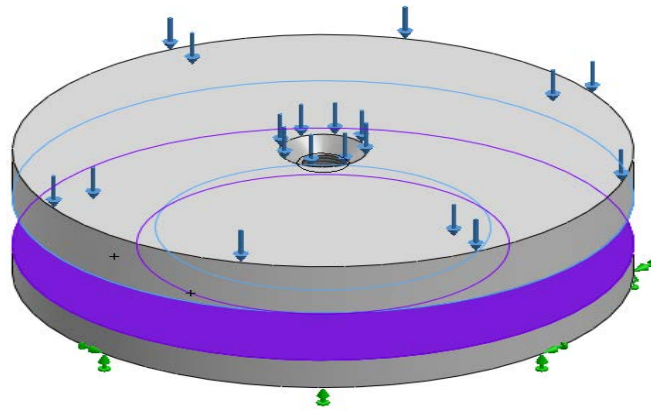
Figure 3.10: Constraints contact set between the parallel surfaces of the ball and socket. The blue arrows represent the load, the green arrows on the rigid surface which is in the bottom of the ball. The purple and blue surface between ball and socket are the constraints.
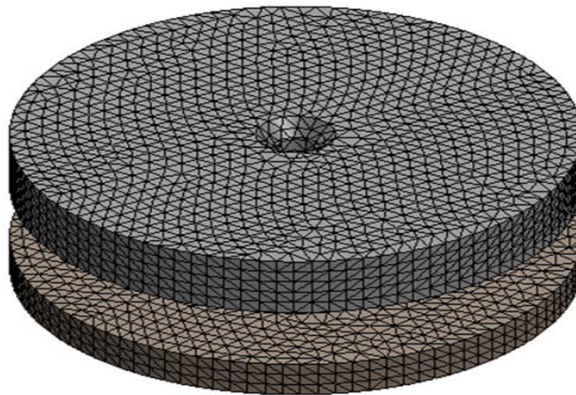
Figure 3.11: Meshed finite element model 1.

3.6 Results of the simulation

Von Mises stress was used as a tool of evaluating stress within implant bearings UHMWPE against metal previously (Enab, 2012; Fouad, 2011; Hua *et al.*, 2012; Korhonen *et al.*, 2005). For

the first model with the lubricant hole in the centre of the socket with an M2 hole, the von Mises stress were the highest at the edges of the lubricant hole where they reached 31 MPa the stresses are much higher than the yield strength of the UHMWPE, as shown in Table 3.6. The von Mises stress then reduced far from the centre, as shown in Figure 3.12. To modify this model, the lubricant hole was positioned far from the centre in the area of low von Mises stress. Therefore, the second model was performed with the lubricant hole 10 mm from the centre with a 45° angle from lateral bending motion (the x axis).
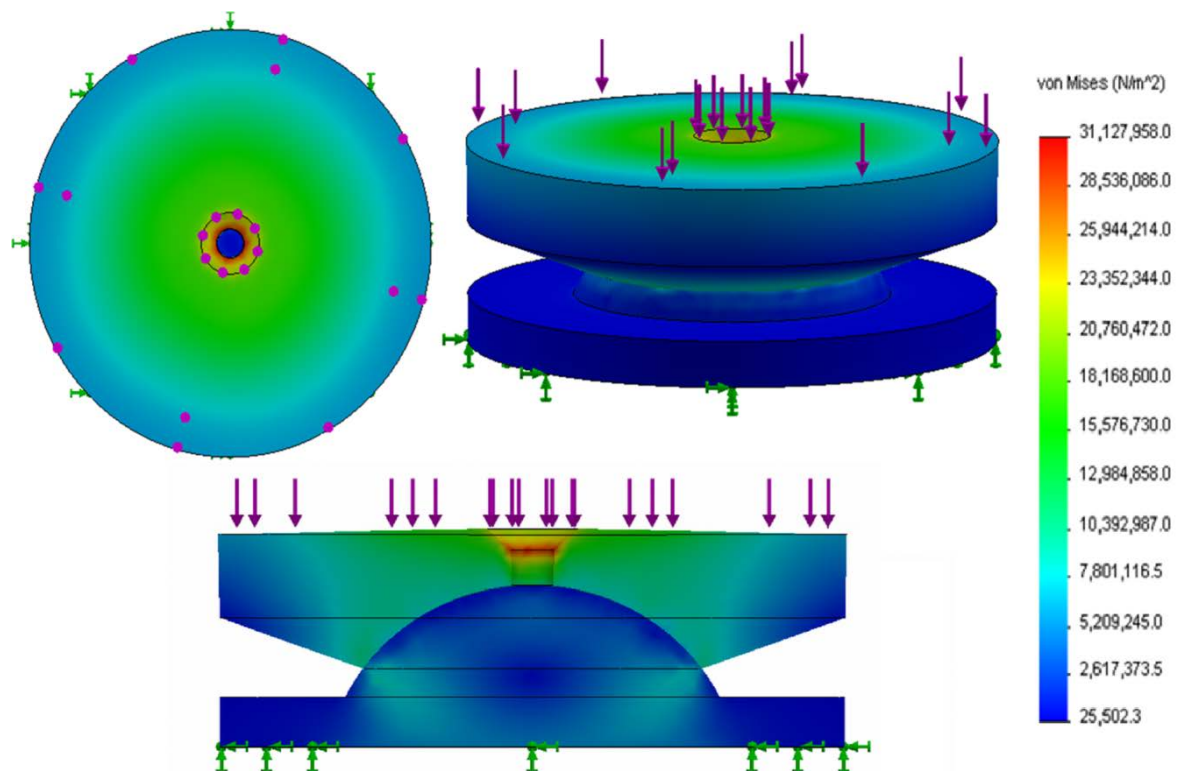
Figure 3.12: Von Mises stress distribution for model 1 with M2 lubricant hole located at the centre of the socket.

The second model showed improvement in reducing the maximum von Mises stress from 31 MPa in model 1 to 27.6 MPa in model 2, as shown in Figure 3.13. The stresses around the lubricant hole were between 18.3 MPa and 23 MPa. The maximum von Mises stress, which was 27.6 MPa located on the contact between the socket and the ball in which this place will be facing articulating between them and will produce wear.
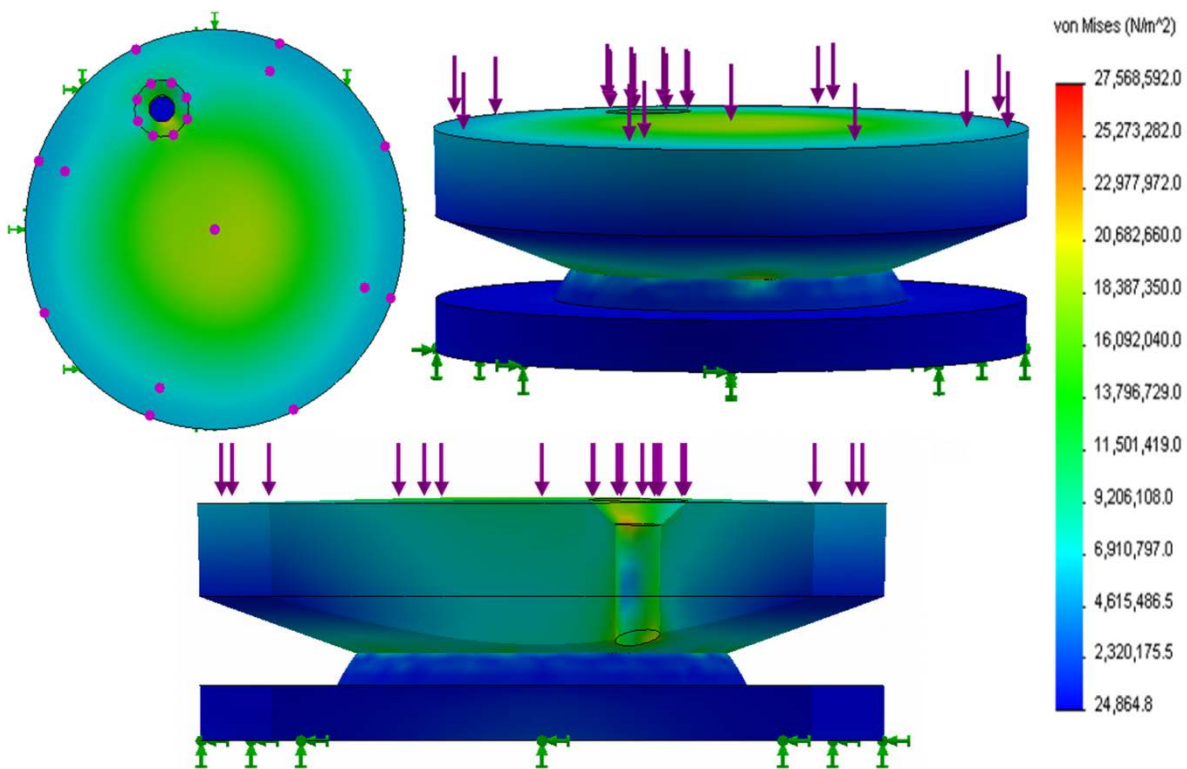
Figure 3.13: Von Mises stress distribution for model 2 with M2 lubricant hole located 10 mm far from the centre of the socket.

The third model moved the lubricant hole further from the socket centre more than the second model. Therefore, the third model had the lubricant hole at 11 mm distance from the centre of the

socket with 45º angle degrees from lateral bending motion (the x axis). The maximum von Mises stress reduced for the whole model to reach 25.5 MPa from 27.6 MPa in the second model, as shown in Figure 3.14. The von Mises stresses on the lubricant hole were in the range 15 to 21.3 MPa. The highest von Mises stresses were around the contact edges of the socket against the ball as mentioned earlier.
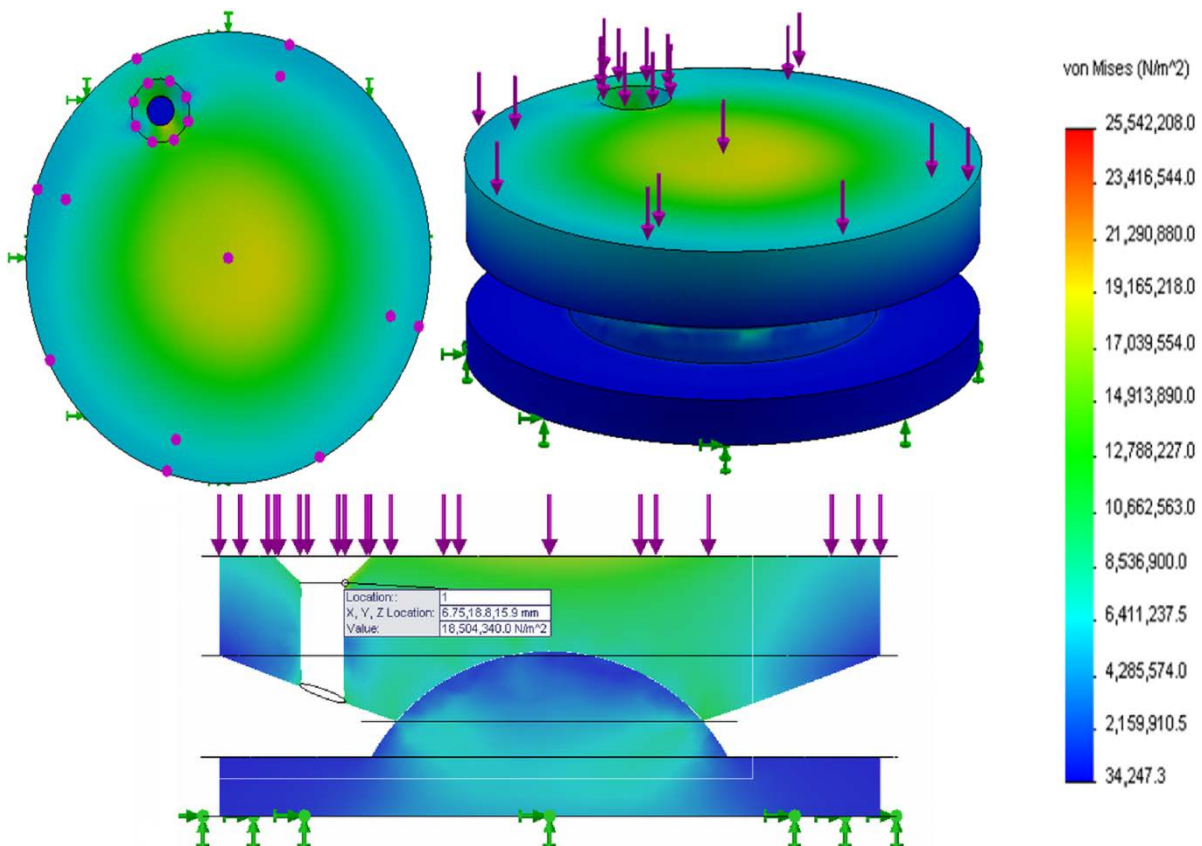
Figure 3.14: Von Mises stress distribution for model 3 with M2 lubricant hole located 11 mm far from the centre of the socket.

The fourth model used the same distance (11 mm) between the lubricant hole and the centre of the socket as the third model. However, the M2 hole was replaced with a M1 hole to reduce the weakness of the socket plate when loaded with a 2000 N force. The highest von Mises stress was located on the edges of the contact surface between the ball and socket where the socket articulates against the disc, as shown in Figure 3.15.
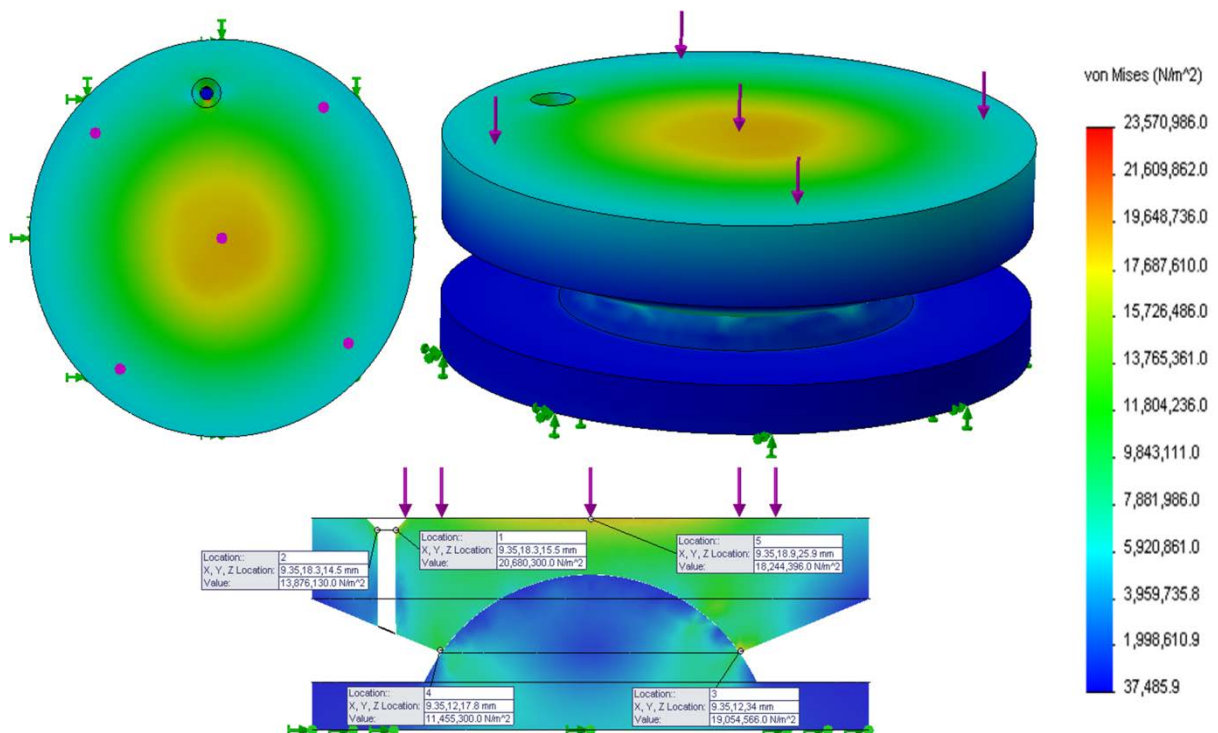
Figure 3.15: Von Mises stress distribution for model 4 with M1 lubricant hole located 11 mm far from the centre of the socket.

In the fifth model, as shown in Figure 3.16, the M1 lubricant hole was moved further to 12 mm from the centre of the socket. In general, the von Mises stress was reduced slightly with this

model than the previous model. The highest von Mises stress was 23.33 MPa located on the edges of the contact surface between the ball and socket where the socket is articulating against the disc, as shown in Figure 3.17.
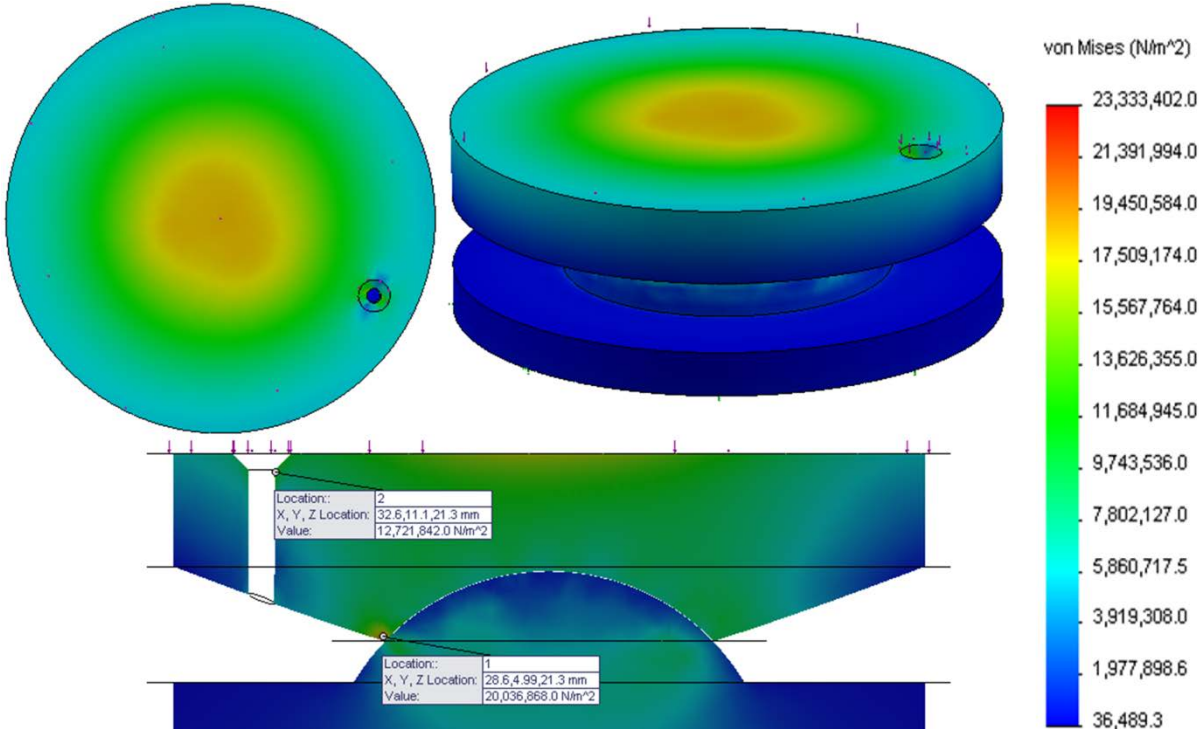
Figure 3.16: Von Mises stress distribution for model 5 with M1 lubricant hole located 12 mm far from the centre of the socket.
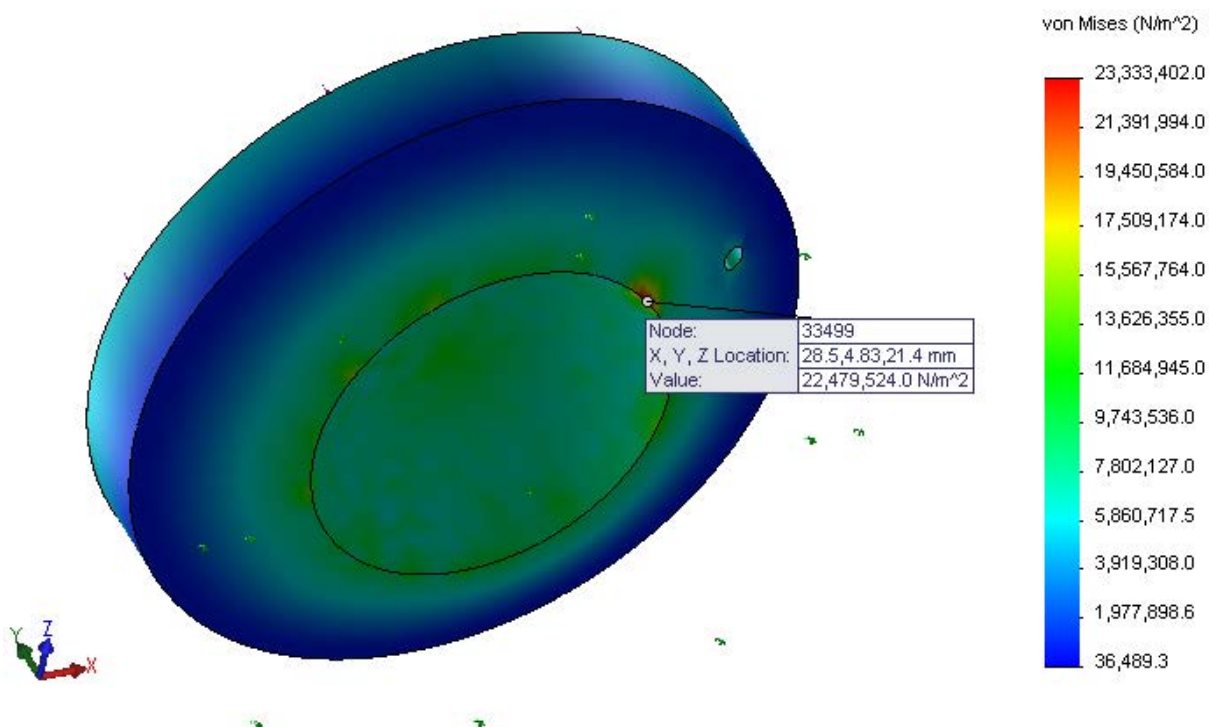
Figure 3.17: Von Mises stress distribution for model 5 with M1 lubricant hole located 12 mm far from the centre of the socket. Maximum stresses on the contact edge on the socket.

3.7 Discussion

The product design specification was developed to satisfy the needs requiring the application of an encapsulated ball and socket artificial disc. Conceptual designs were produced to meet the product design specification needs. By using the TRIZ problem solving methodology seven design concepts were developed. An evaluation matrix was used to test these seven concepts and to evaluate them before proceeding to the concept design with the highest score in the evaluation matrix. Concept design 2 had the highest total score in the evaluation matrix compared with the

other conceptual designs. Therefore, a detailed design was made from this concept. However, during the detailed design the position of the lubricant hole was a challenge facing this design. Therefore, a simulation for this detailed design with different lubricant hole positions was investigated. Five different models were designed using SolidWorks with different lubricant hole positions for each model. The five different models were tested using the SolidWorks simulation tools to evaluate the different detailed designs. All the simulation parameters were the same for all five models; however, the only change was the lubricant hole position. The first model, where the lubricant hole was in the middle, showed the highest von Mises stress between all the models. These high stresses were located on the walls of the lubricant hole itself and on the contact edges between the ball and socket. However, when this lubricant hole was moved to a distance of 10 mm far from the centre it was noticed that it gave lower values of von Mises stress in general for the new model and there was no high von Mises stresses on the wall of the lubricant hole. However, the high stresses were on the contact edges between the ball and socket parts, as shown in Figure 3.17. It was noticed that the further that the lubricant hole is from the socket centre the lower the von Mises stress, as shown in model 3. In model 4 the lubricant hole where chosen to be smaller from M2 to M1 to see the effect of the hole size on the stress in general. This modification helped as well in reducing the von Mises stress in general from 25.5 MPa to 23.5 MPa. The last model where the M1 lubricant hole was moved further to a distance 12 mm far from the socket centre gave a small improvement to the von Mises stress to reach 23.3 MPa. Therefore, after this point it is expected that the changes in the von Mises stress will be small and will not have a huge impact on the whole design. Thus, the last model (model 5) was chosen to be

manufactured and tested using the spine simulators as will be described in chapter 6 and 7 in detail.

3.8 Conclusion

The design process was discussed in this chapter for an encapsulated ball and socket artificial disc. In addition, a simulation for the detailed design was undertaken using SolidWorks simulation tools. This chapter can be concluded by these points:

- The Pugh design model was applied to the encapsulated ball and socket artificial disc and a product design specification was developed to help design an encapsulated artificial disc.

- Different conceptual designs were designed to satisfy the product design specification using the technique of TRIZ.

- Design 2 had the highest score in the evaluation matrix between all the other concepts.

- A detailed design for concept design 2 was undertaken using SolidWorks after evaluating the conceptual designs using the conceptual design evaluation matrix.

- The lowest von Mises stress (23.33 MPa) was found to be in the fifth model where the lubricant hole (M1) was placed 12 mm far from the centre of the socket. This model was selected to be manufactured and tested as an encapsulated artificial disc.

- The highest von Mises stress in all the models was placed on the edges of the contact region between the ball and socket, as shown in Figure 3.17.

The next chapter will investigate the coefficient of friction of the different articulation material combinations with different bio-lubricants that can be used in the encapsulated artificial discs.

4 The effect of biomedical lubricants on friction between common arthroplasty bearing biomaterials for encapsulated spinal implants

4.1 Overview

This chapter presents the effect of the synthetic biomedical lubricants on the friction of the different biomedical materials used in artificial joints. The introduction in section 4.2 discusses synthetic lubricants and how they have been used to solve friction and wear problems. The materials and methods are then described and how they are used when testing the different biomedical materials with the lubricants in section 4.3. The results are presented in section 4.4, followed by the discussion and comparison of the results in section 4.5. The chapter is concluded in section 4.6. The work and the results of this chapter have been published in Alnaimat *et al.* (2016).

4.2   Introduction

In the spine region and around the intervertebral discs it is interstitial fluid rather than synovial fluid that lubricates an artificial disc when it is implanted (Graham, 2006). Interstitial fluid does not have the same lubrication properties as synovial fluid which is found in commonly replaced synovial joints such as the hip and knee (Yao *et al.*, 2003) Instead it has a lower viscosity and a value for lubricity between Ringer's solution and bovine calf serum, both of which are lower than synovial fluid (Shaheen and Shepherd, 2007; Yao *et al.*, 2003). This relatively low viscosity is likely to lead to challenging tribological conditions for any spinal implant device that relies on bearing surfaces. A lubricant's primary function is to reduce both friction and wear between surfaces which are articulating against each other (Furey, 2000). An improved lubrication regime, i.e. a functioning lubricant that prevents surfaces from coming into contact can help to minimise the generation of wear particles, which have been noted to cause a variety of pathologies in the recipient of an implant and performance related issues for the device. It has been proposed that joint replacement implants might benefit from a capsule which can seal an artificial lubricant within the joint to reduce friction and wear, whilst simultaneously preventing wear debris from migrating to surrounding tissues (Derbyshire *et al.*, 1980; Yao and Skorecki, 1985). This study is the first practical part in the development of an encapsulated disc replacement, where the friction of various biomaterials and lubricant combinations was investigated. A commercially available example of such a device is the Bryan disc (Medtronic Sofamor Danek, Inc., Memphis, TN), which relies on the idea of using encapsulation with saline solution as a lubricant. The disc has shown promising clinical results (Anderson *et al.*, 2004; Yanbin *et al.*, 2015; Zhang *et al.*, 2014). It seems reasonable, therefore, that a biocompatible polymer based lubricant could be used with

joint implant replacements because saline would result in higher friction. Synthetic polymer lubricants have been used since the 1960s (Helal and Karadi, 1968). More recently, Kobayashi *et al.* (2014) have used polyethylene glycol (PEG) as a synthetic polymer lubricant with synovial fluid to lubricate knee replacements. In natural synovial joints, the lubricant is synovial fluid and the lubricity of this fluid is similar to water due to the high shear rates inside these prostheses (Jin *et al.*, 1997). In disc replacements, the implants are likely to be lubricated with interstitial fluid, as mentioned earlier, and it has relatively low viscosity which is likely to lead to challenging tribological conditions for any spinal implant device that relies on bearing surfaces. If encapsulation is to be successful in spinal implant devices, there will be a need to be an appropriate synthetic lubricant to reduce friction and wear, and increase implant durability.

Polyvinyl Alcohol (PVA) has been shown to be a promising lubricant because of its physical properties, the lubricity of the solution and its biocompatibility (Baker *et al.*, 2012; Cooke *et al.*, 1978). Hermann and Haehnel prepared polyvinyl alcohol (PVA) in 1924 by hydrolyzing polyvinyl acetate in ethanol with potassium hydroxide (Gajra[*] *et al.*, 2012). The linear formula for the PVA is [-CH2CHOH-]n. The PVA has different degrees of polymerization and degrees of hydrolysis (Toyoshima, 1973). There are two classes of PVA: partially hydrolysed and fully hydrolysed (Toyoshima, 1973). Generally, PVA is a tasteless, odourless and white or creamy colour granular powder. It is highly soluble in polar solvents such as water (Toyoshima, 1973). The solubility of PVA depends on the degree of hydrolysis in water (Hassan *et al.*, 2002). A PVA solution, Polyviol W40/140 (Wacker Chemie AG, Munich, Germany) with 5% and 10%, was studied as a synthetic lubricant for synovial joints. It showed a similar viscosity behaviour to a silicone lubricant, but different viscosity behaviour than synovial fluid (Cooke *et al.*, 1978). PVA

and polyvinylpyrrolidone (PVP) have been used in artificial tear fluids with an appropriate viscosity to lubricate dry eyes (Florence, 2010). PVA hydrogels have been developed as an artificial membrane in contact lenses (Kita *et al.*, 1990). The material has also been used as a hydrogel membrane for the encapsulation of implanted Langerhans islets cells in the pancreas to immunoisolate them from the immune response (Burczak *et al.*, 1996; Young *et al.*, 1996). It has also been used by Jiang *et al.* (2004) as a one piece tricuspid heart valve made entirely from a PVA hydrogel. PVA has also been used as an artificial articular cartilage to repair joint surfaces (Oka, 2001), as well as the film coatings for pharmaceutical and dietary supplement tablets where a barrier is required to protect tablets from moisture and other contaminants. PVA is not considered as carcinogenic and there are no reports related to chronic toxicity or carcinogenicity when it is taken orally (DeMerlis and Schoneker, 2003). It is, therefore, the ideal candidate for the encapsulated joint lubricant, but the ideal composition to produce the required lubricating properties is not clear.

The aim of this chapter was to screen and compare the frictional behaviour of the most widely used materials in artificial discs with potential synthetic lubricants for use in encapsulated implants. PVA of different viscosities, Ringer's solution and bovine calf serum were used as the test fluids.

4.3   Materials and methodology

4.3.1 Tribological specimens

The test samples comprised an upper pin and a lower disc. The upper pin samples were machined to 8 mm diameter and 15 mm length, while the lower disc samples were machined to 79 mm diameter and were 5 mm in thickness, the drawings of the pin and disc are shown in Appendix A. The tested materials were cobalt chrome (CoCr) alloy Haynes 25/L605 (ASTM F90-09, 2009) supplied by (Dynamic Metals Ltd, Hemel Hempstead, UK), ultra high molecular weight polyethylene 1000 (UHMWPE) and unreinforced polyether ether ketone (PEEK) 450G (supplied by Direct Plastics Ltd, Sheffield, UK). These materials have been previously tested for spinal implants (Moghadas *et al.*, 2012b; Xin *et al.*, 2013).

All of the tribological specimens were polished using a Buehler Alpha Grinder Polisher (Buehler Ltd, Illinois, USA). The surface roughness of each pin and disc was measured three times using an Alicona G4 InfiniteFocus (Alicona, Raaba, Austria). The results of the surface roughness measurements are shown in Table 4.1.

Table 4.1: Surface roughness of test specimens.

Material	Mean Ra ± Standard Deviation (µm)
CoCr Disc	0.92±0.05
CoCr Pin	1.11±0.02
UHMWPE Pin	0.82±0.11
PEEK Disc	0.87±0.06
PEEK Pin	1.26±0.04

4.3.2 Lubricants

The Polyvinyl alcohol (PVA) solution was prepared by using different concentrations which led to different viscosities. The more concentrated solution and the higher the molecular weight the more viscous the lubricant. The materials required to prepare the solution were: PVA powder (Sigma-Aldrich, St. Louis, MO, USA), distilled water, a magnetic stirrer and a heater or water bath shaker. To prepare a 4% PVA solution, 96 ml distilled water was heated to 80-90 °C. Once the water reached the required temperature, 4 g of PVA was sprinkled into the water while being stirred continuously to make ensure that the solution was continuously shaking. This procedure took approximately twenty to thirty minutes. The lubricant was ready for use after cooling to room temperature. The solution should be clear and completely homogeneous with no granulose or agglomerated masses after mixing.

Three types of lubricant were used in this study, although it should be noted that several concentrations of polyvinyl alcohol (PVA) were tested. They were:

- Ringer's solution – prepared with a 1.2 g Ringer's solution tablet (Oxoid Ltd., Hampshire, UK) in 500 mL of distilled water.

- Bovine calf serum – prepared by defrosting the serum (SeraLab, West Sussex, UK) over 24 hours at 5 °C before diluting with 20 g/L deionized water and adding 0.3 g of sodium azide powder to minimize bacterial growth (Sigma-Aldrich, MO, USA) .

- PVA – prepared from powder with a molecular weight of 31,000-50,000 g/mol, 98-99% hydrolysis. The PVA was prepared as the procedure above and the concentrations of PVA were:

- PVA A: 4 g per 100 mL of distilled water.

- PVA B: 10 g per 100 mL of distilled water.

- PVA C: 20 g per 100 mL of distilled water.

- PVA D: 30 g per 100 mL of distilled water.

4.3.3 Viscosity measurements

The viscosities of the different PVA lubricants were measured using an AR-G2 cone on plate rheometer (TA Instruments Ltd., West Sussex, UK), as shown in Figure 4.1. A 60 mm diameter standard steel cone with a 2° angle was used to measure the viscosity of the lubricants.

A lubricant volume of 8 ml was placed between the cone and the plate of the rheometer using a plastic pipette. The cone was then lowered until there was direct contact between the cone, plate and lubricant. The cone was positioned with a 54 µm truncation gap as carved (written) in the geometry shaft of the AR-G2 rheometer cone (Mazzeo, 2015).

The experiment was performed at 22°C and 37 °C for shear rates from 0.1 s^{-1} to 1000 s^{-1}. Three tests were undertaken for each lubricant and the mean viscosity with 95% confidence intervals calculated.
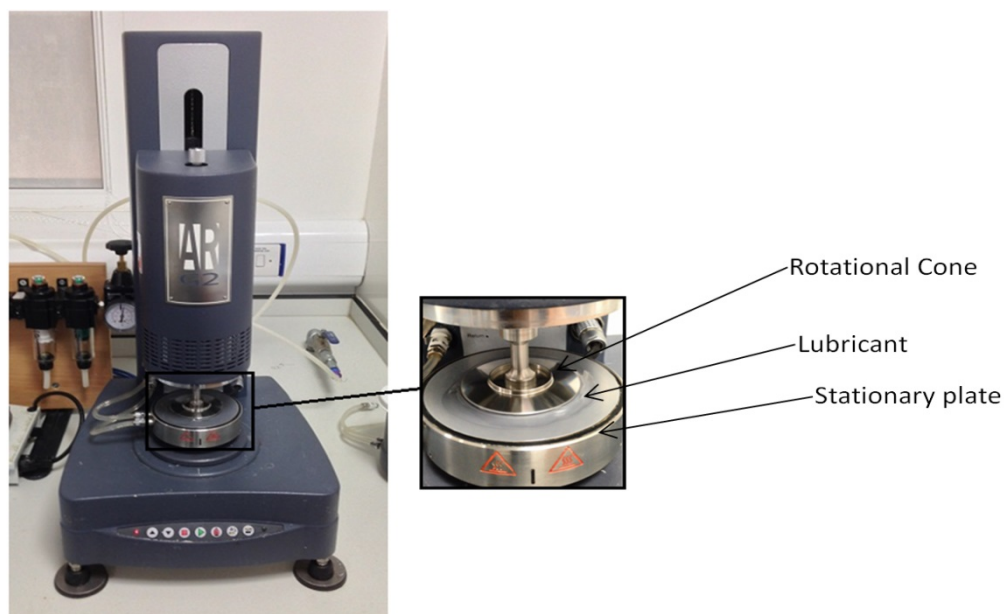
Figure 4.1: The AR-G2 cone-on-plate rheometer.

4.3.4 Tribological experiments

Tribological tests were conducted using a bespoke pin on disc tribometer as used in previous studies for biomedical materials for implants (Alnaimat *et al.*, 2016; Chand *et al.*, 2007; Gispert *et al.*, 2006; Unal and Mimaroglu, 2003; Wang *et al.*, 2005), shown in Figure 4.2, according to the standard ASTM G99-05 (ASTM G99-05, 2010) at room temperature. The apparatus was calibrated against a variety of reference materials including steel against steel and steel against ceramic, both dry and lubricated. The rotational speed of the disc, as recommended by the standard, was 60 RPM (6.3 rad/s) and the tangential velocity was 160 mm/s. The normal force was 29.4 N (0.15 MPa stress) applied vertically on the pin similar to previous studies (Chand *et*

al., 2007; Gispert *et al.*, 2006; Unal and Mimaroglu, 2003; Wang *et al.*, 2005). Each experiment was run for 60 minutes, which corresponded to a total sliding distance of 560 m.
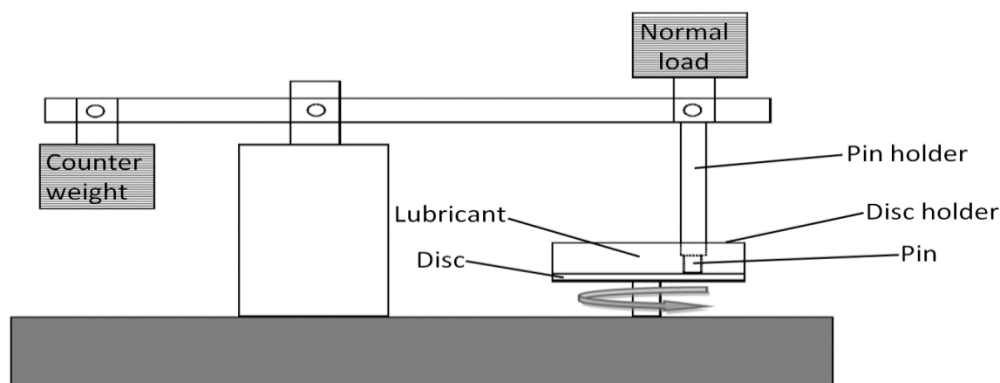
Figure 4.2: A schematic representation of the pin on disc tribometer.

Friction force data was acquired using a SoMat eDAQ mobile data acquisition system (Hottinger Baldwin Messtechnik GmbH, Germany) at a rate of 1 Hz. For each experiment 10 ml of lubricant was added to the disc holder. The mean steady-state friction coefficient and standard error of repeatability, as described in section 4.3.5, were calculated from the last ten values of each experiment. Table 4.2 lists the materials and lubricants used in each test. A moving average trendline with a period of 25 readings was used to smooth out fluctuations in the friction coefficient data. The friction force was calculated from the strain gauge by measuring the strain from standard weights according to the calibration method described in the Somat edaq manual (HBM Inc., Marlborough, USA). A half bridge circuit was used comprising two stain gauges each of them with a gauge factor of $2.05 \pm 1\%$ and resistance of $120.4\Omega \pm 0.35\%$ (Omega, Cheltenham, UK). The procedure used to calibrate the gauges is fully described in the Somat

edaq manual (HBM Inc., Marlborough, USA), but is summarised below. The summary for computing the strains from gauge and bridge factors using Somat edaq, comprises a tool that defines the calibration using selected shunt resistors for the Somat edaq software along with a corresponding equivalent strain based on gauge and bridge factors of the bridge configuration. Using the Somat software the strain was calculated from Eq. [1]:

$$E_S = \frac{1000000 \times R_g}{B_F \times G_F (R_g + R_s)} \tag{1}$$

where E_s is the equivalent strain, R_g is the nominal gauge resistance, R_s is the shunt resistance, G_F is the gauge factor and B_F is the bridge factor. Standard masses were added and the strain recorded.

This process was repeated six times for each standard mass. The friction coefficient was calculated from Eq. [2]:

$$\mu = \frac{F}{N} \tag{2}$$

where F is the friction force and N is the normal force.

The friction force was calculated from the strain gauge by measuring the strain from standard weight and measuring the gauge factor.

Table 4.2: Materials and lubricants used in each test.

Experiment	Pin	Disc	Lubricants
CoCr/CoCr	Cobalt chrome alloy	Cobalt chrome alloy	Ringer's solution, calf serum and PVA A, B, C and D
CoCr/PEEK	Cobalt chrome alloy	PEEK	Ringer's solution, calf serum and PVA A, B, C and D
PEEK/PEEK	PEEK	PEEK	Ringer's solution, calf serum and PVA A, B, C and D
UHMWPE/PEEK	UHMWPE	PEEK	Ringer's solution, calf serum and PVA A, B, C and D
UHMWPE/CoCr	UHMWPE	Cobalt chrome alloy	Ringer's solution, calf serum and PVA A, B, C and D

4.3.5 Standard error

Standard error of the mean is the measure of the accuracy with which a sample represents a population. It is the standard deviation divided by the square root of the number of observations in that sample (Logan, 2011).

$$Standard\ error = \frac{\sigma}{\sqrt{n}} \qquad\qquad [1]$$

Where σ is the standard deviation and n is the sample size.

4.4   Results

4.4.1 Viscosity results

Results were taken at a shear rate of 1000 s^{-1} which was judged to be the point at which the measured viscosity became stable. The viscosity of Ringer's solution was $2.25 \times 10^{-3} \pm 1.3 \times 10^{-5}$ Pa.s which was the lowest viscosity for all of the tested lubricants. Bovine calf serum followed with a viscosity of $2.35 \times 10^{-3} \pm 1.14 \times 10^{-4}$ Pa.s. The viscosity of PVA A was $2.53 \times 10^{-3} \pm 0.23 \times 10^{-3}$ Pa.s, PVA B was 0.094 ± 0.01 Pa.s, PVA C was 1.65 ± 0.01 Pa.s and the viscosity of PVA D was 2.08 ± 0.077 Pa.s. All viscosity measurements are shown in Figure 4.3. The graph of the different lubricants viscosities at 37 ^{o}C is shown in Appendix B.
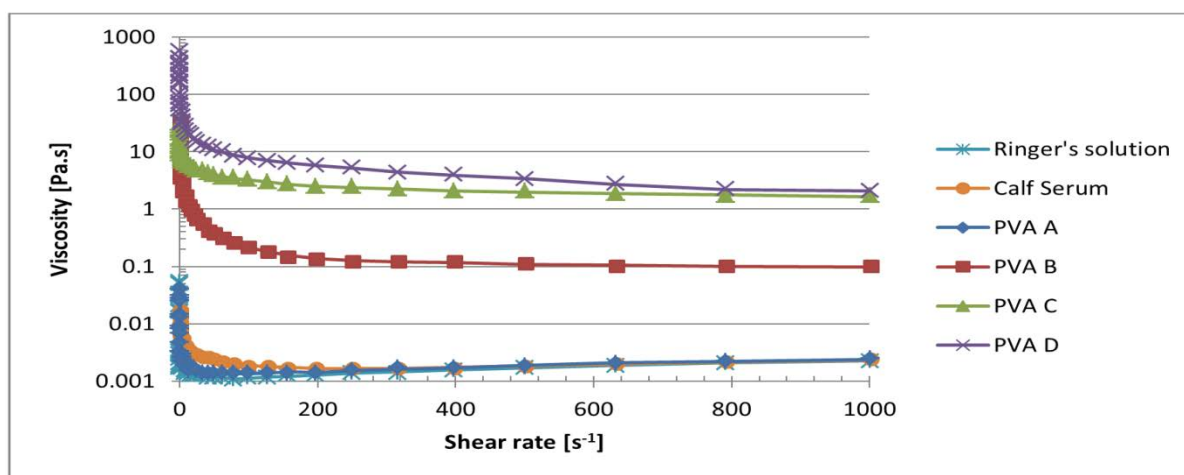
Figure 4.3: The viscosity of tested lubricants against shear rate at 22 ^{o}C; note that the viscosity axis is on a logarithmic scale, base 10.

4.4.2 Tribological results

Figure 4.4 shows the friction coefficient for cobalt alloy sliding against cobalt alloy. The friction coefficient reached 0.33 on average when Ringer's solution was used to lubricate this combination. The protein content of the calf serum might be the reason behind reducing the friction coefficient, where it reached 0.3 on average for this combination. PVA A showed a lower average friction coefficient, 0.27, than ringer's solution and calf serum. The viscosity of the solution increased with the increment of the concentration of the PVA, while the friction coefficient decreased. Thus a lower average friction coefficient 0.17 was shown for the cobalt against cobalt with the PVA B. However, it does not show the lowest friction coefficient for this material combination. PVA C led to the lowest friction coefficient for Co against Co and gave a friction coefficient 0.09 on average. However, when the viscosity increased by more than 1.650 ± 0.01 Pa.s it was observed that the mean friction coefficient for metal against metal started to increase instead of decreasing. This can be seen with PVA D where the mean friction coefficient was 0.1. The reason for this increase was likely to be due to an increase in frictional forces caused by high viscosity shear loss. It could also be affected by a change in the flow properties of the lubricant, meaning that it acts more like a foam, as described by Thong *et al.* (2014).
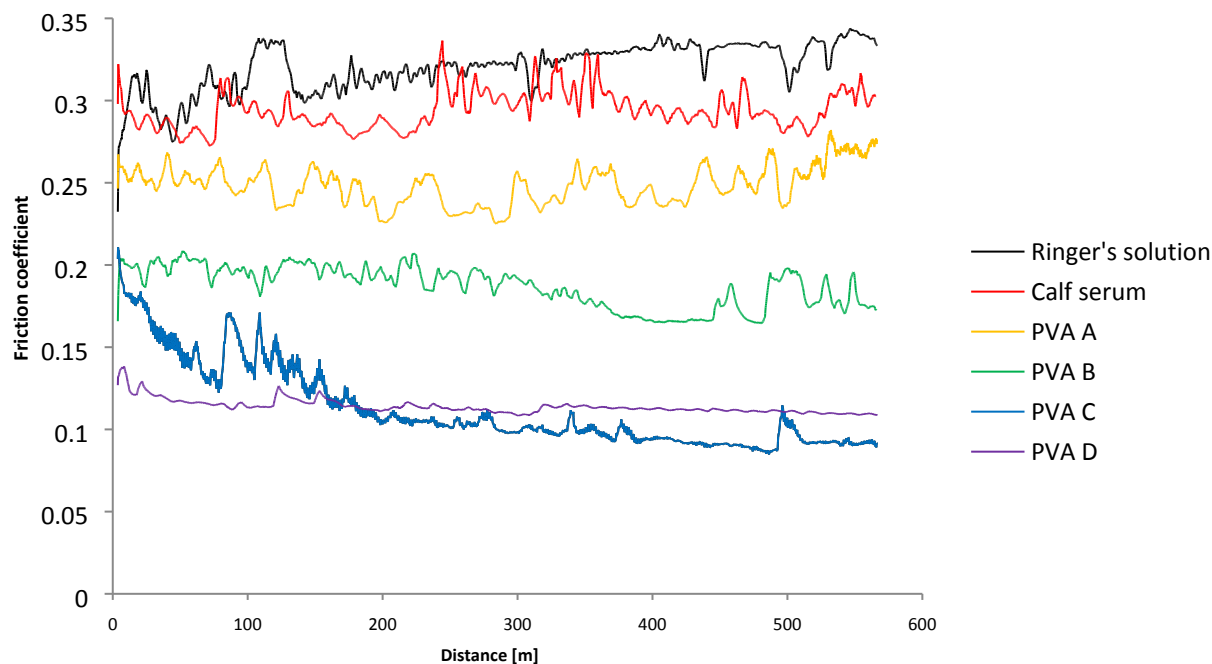
Figure 4.4: Cobalt alloy against cobalt alloy friction coefficient experiment using different

lubricants.

The friction coefficient for the combination of cobalt alloy against PEEK can be seen in Figure

4.5, in which the highest mean friction coefficient was 0.2 for Ringer's solution. This is followed

by a lower mean friction coefficient of 0.198 for calf serum. When the polymer lubricant PVA

was used the friction coefficient was smoother and lower in all cases. The friction coefficient for

PVA A was 0.176 and for PVA B it was 0.16 on average. The lowest mean friction coefficient

was 0.05 for PVA C. The friction coefficient increased for PVA D and it was 0.07 on average.

This followed the same trend as described for the CoCr experiments described above.
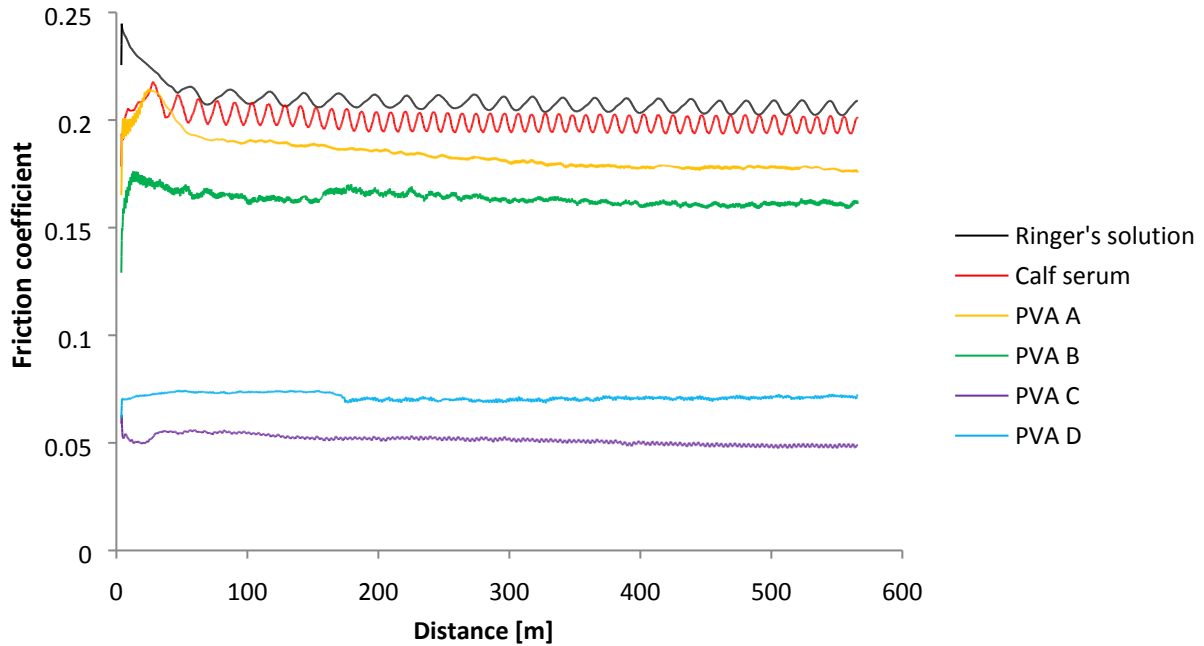
Figure 4.5: Cobalt alloy against PEEK friction coefficient experiment using different lubricants.

Figure 4.6 shows the PEEK against PEEK results. The highest friction coefficient was nearly 0.34 on average for PEEK against PEEK with Ringer's solution. The friction coefficient was reduced when calf serum was used, being 0.26 on average. The friction coefficient became much smoother and lower again when PVA was used as a lubricant. For PVA A the mean friction coefficient was 0.15. The lowest friction coefficient was 0.037 on average for PVA C. Using PVA B with this material combination gave a mean friction coefficient 0.07 and the mean friction coefficient increased when the PVA D was used and reached 0.055 which was higher than the friction coefficient for PVA B.
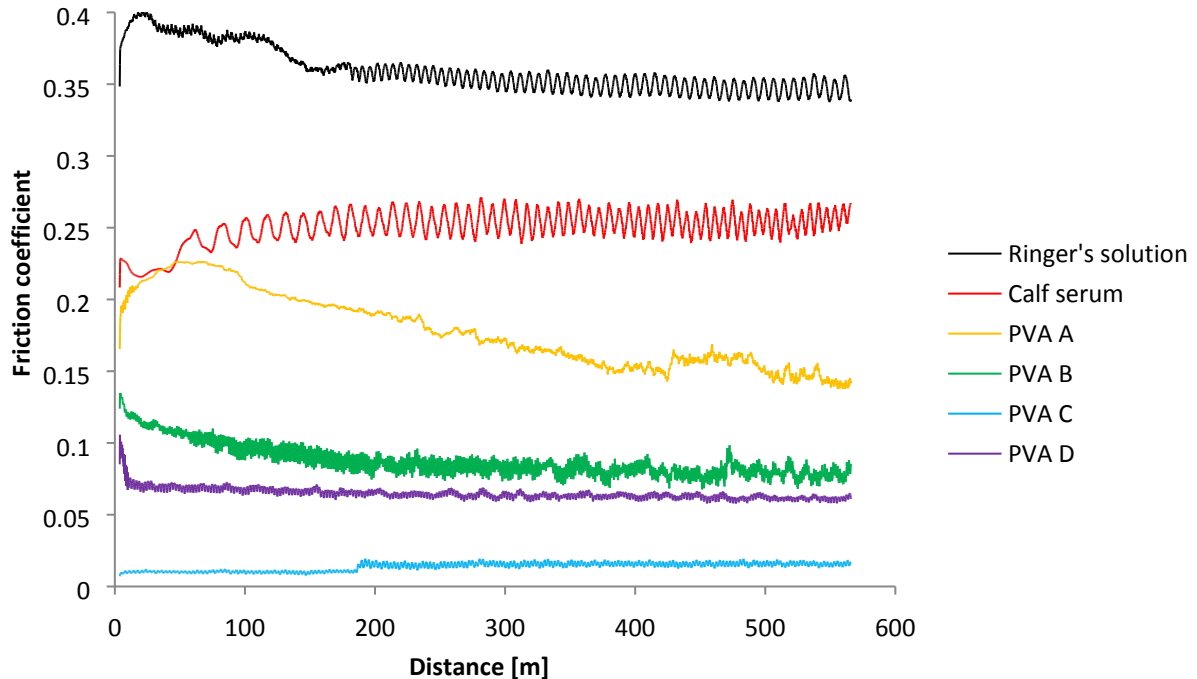
Figure 4.6: PEEK against PEEK friction coefficient experiment using different lubricants.

The UHMWPE/PEEK friction coefficient results are shown in Figure 4.7, as an example of the friction coefficient against sliding distance data. The mean friction coefficient for Ringer's solution was 0.2 and for bovine calf serum it was 0.19. With this combination the difference between the Ringer's solution and calf serum was small. The mean friction coefficient for the PVA A was 0.14 and decreased for PVA B to become 0.079 and reached the lowest value of 0.02 for the PVA C for this material combination. The value of the mean friction coefficient for this material combination increased to a value of 0.04 when PVA D was used.
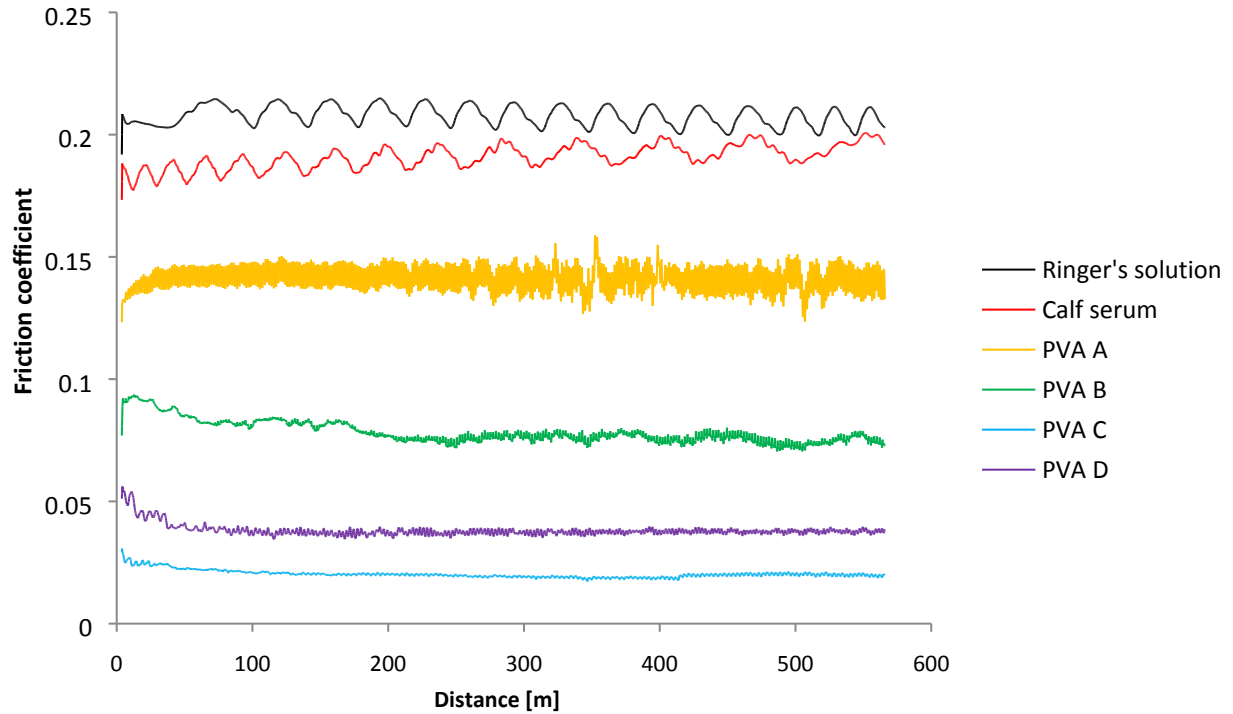
Figure 4.7: UHMWPE against PEEK friction coefficient experiment using different lubricants.

UHMWPE against Cobalt alloy showed the lowest friction coefficient for all the combinations, as shown in Figure 4.8. The highest friction coefficient for UHMWPE against Cobalt was 0.1 on average for Ringer's solution. The mean friction coefficient for calf serum was 0.08 which was lower than Ringer's solution for the same combination. The friction coefficient was 0.076 on average for PVA A and it has a close average value to calf serum for this combination. The mean friction coefficient was 0.05 when PVA B was used with this combination. The lowest friction coefficient for the same sliding distance was 0.009 on average for PVA C. The mean friction coefficient increased for PVA D to 0.06.
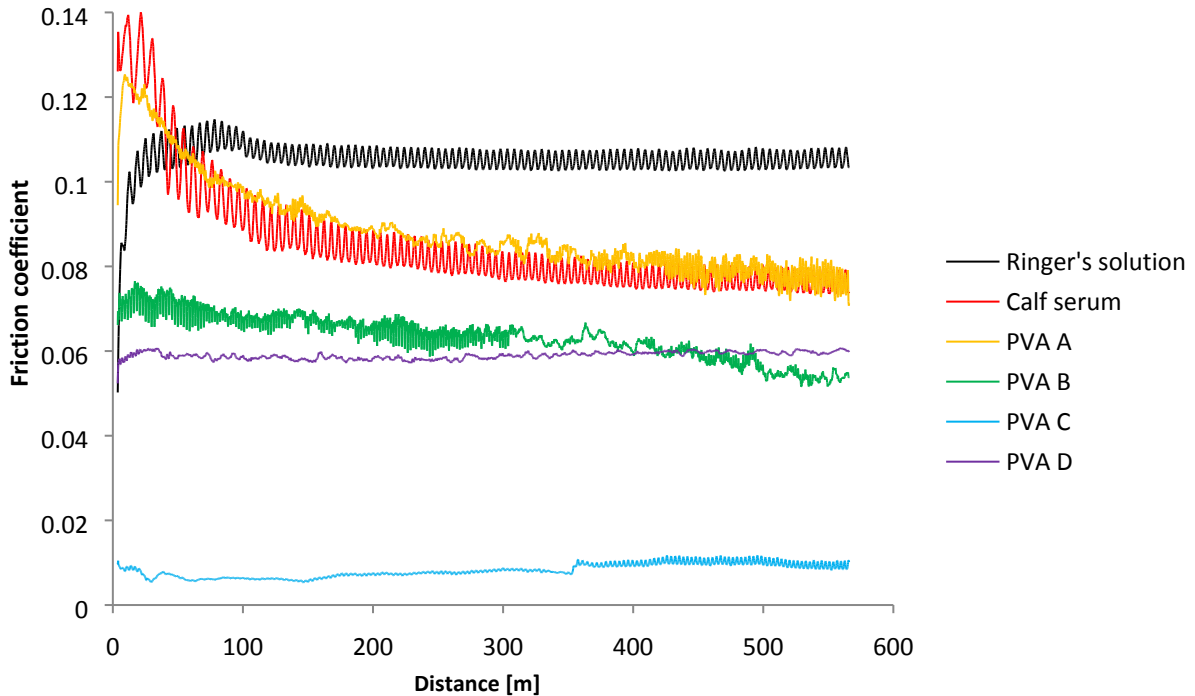
Figure 4.8: UHMWPE against Cobalt alloy friction coefficient experiment using different

lubricants.

Figure 4.9 shows the summary of the average steady state friction coefficients for the different

bearing material combinations with different lubricants. For all material combinations the

highest friction coefficient was found using Ringer's solution as the lubricant (range from 0.1 to

0.34). The friction coefficient was less when bovine calf serum was used. The friction coefficient

results for the PVA showed the same trend for all materials combinations with a decreasing

friction as the PVA percentage was increased between PVA A and PVA C. With PVA D the

friction was then found to increase. The lowest friction coefficient for all materials combinations

was for PVA C. The lowest friction coefficient (0.009) was for the UHMWPE against CoCr with

PVA C as the lubricant.
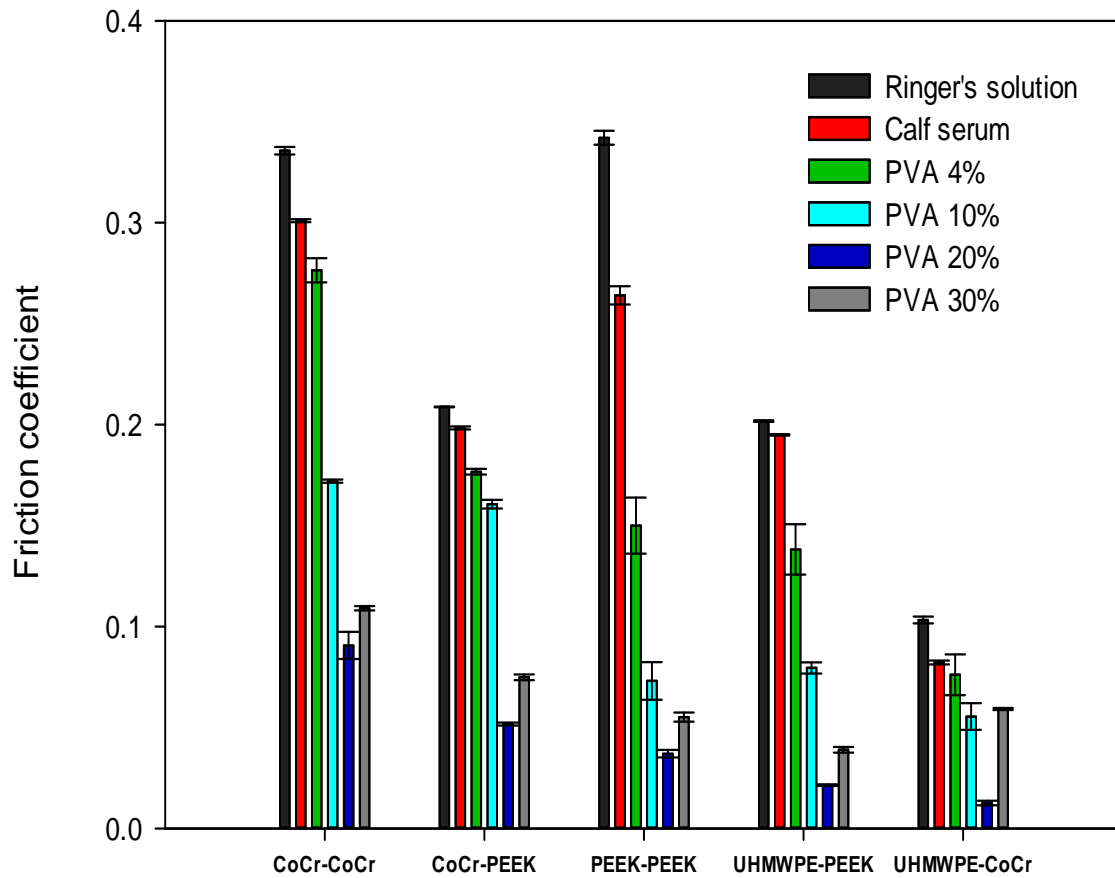
Figure 4.9: Friction coefficient for all material combinations with the different lubricants. Error

bars represent standard error.

4.5 Discussion

The aim of this chapter was to investigate the friction coefficient for different biomaterials for

disc replacement implants using biocompatible lubricants. These experiments were undertaken to

help determine suitable biomaterials and lubricants that could be used in an encapsulated disc replacement implant.

All the lubricants have shown shear thinning with the increase of the shear rate as shown in Figure 4.3. PVA A, Ringer's solution and calf serum had similar viscosities as mentioned earlier for the tested parameters. However, there was a slight increase in the viscosity of Ringer's solution, calf serum and PVA A at high shear rates, and this phenomenon has been observed by others (Yao *et al.*, 2003). The increase of the PVA concentration led to an obvious increase in viscosity as shown in Figure 4.3.

Tribologically, the Ringer's solution and bovine calf serum gave the highest friction coefficient for all combinations. The diluted serum had lower friction compared to the Ringers solution and this may have been caused by the development of a protein layer. This layer, adsorbed on to the frictional surfaces, would have improved boundary lubrication conditions by providing a phase between the surface and lubricant, leading to reduced friction. This is a phenomenon that has been observed by Scholes and Unsworth (2006). However, Brockett *et al.* (2007) found that a protein concentration in the calf serum increased the friction factor from nearly 0.05 for water as a lubricant to nearly 0.07 for 100% concentration of calf serum for CoCr against UHMWPE.

The PVA concentrations used in these experiments produced lubricants that induced lower frictional results even though viscosity of the PVA A was similar to the bovine calf serum. The results were smoother, reducing fluctuations which were the result of poor lubrication conditions, as shown in Figures 4.4 - 4.8, for example. By increasing the concentration of PVA, the viscosity increased. When the viscosity of the fluid increased, the friction coefficient decreased to a certain

value and then increased as shown in Figure 4.9. The incremental increase in the viscosity led to a thicker lubrication film which in turn would increase the squeeze time (i.e. the time required to reduce the film thickness to minimum) between the film and the two bearing surfaces (Roberts, 1982; Roberts *et al.*, 1982). For all material combinations the lowest friction coefficient was obtained using PVA C where the lubricant was viscous enough to support the bearing loads and separate the surfaces to reduce the friction coefficient to the lowest value. In addition, the steady-state friction coefficient was smoother when PVA C was used for all material combinations.

The viscosity of PVA D increased the friction coefficient instead of decreasing it, as shown in Figure 4.9. The reason for this increment was due to an increase in frictional forces caused by high viscosity shear; in addition, the fluid flow may be restricted, performing somewhat like a foam (Hamrock *et al.*, 2004; Thong *et al.*, 2014).

This study has found that the polymer lubricants were more effective than Ringer's solution and calf serum in reducing the friction coefficient. This is supported by Wathier *et al.* (2013) where they found that the polymer lubricants helped in reducing the friction coefficient more than synovial fluid and saline solution with common biomaterials.

Metal sliding against metal showed in general the highest friction coefficients and this can be seen clearly in the CoCr/CoCr results for most lubricants in Figure 4.4. The sliding of CoCr/PEEK shows a lower friction coefficient than the metal against metal. When UHMWPE was used with PEEK and CoCr, it showed lower friction again. The lowest friction was for UHMWPE against CoCr.

Figure 4.9 shows that all the friction coefficient for PVA C fall within the range of 0.009 to 0.09, which according to Bhushan (2013) falls within the mixed lubrication regime. PVA C and PVA D for UHMWPE against CoCr are shown in Figure 4.10. By using UHMWPE/ CoCr with PVA C as a lubricant the friction coefficient was 0.009 which is close to the hydrodynamic lubrication conditions. The CoCr/CoCr falls within the boundary lubrication regime as shown in Figure 4.9. Gispert *et al.* (2006) found in their study that the friction coefficient of UHMWPE/CoCr lubricated using Hanks' balanced salt solution, 0.39 MPa contact stress, 46 mm/s sliding velocity and surface roughness of (2.1, 0.3) μm was 0.085. The results from this study are in agreement with those of Gispert *et al.* (2006).
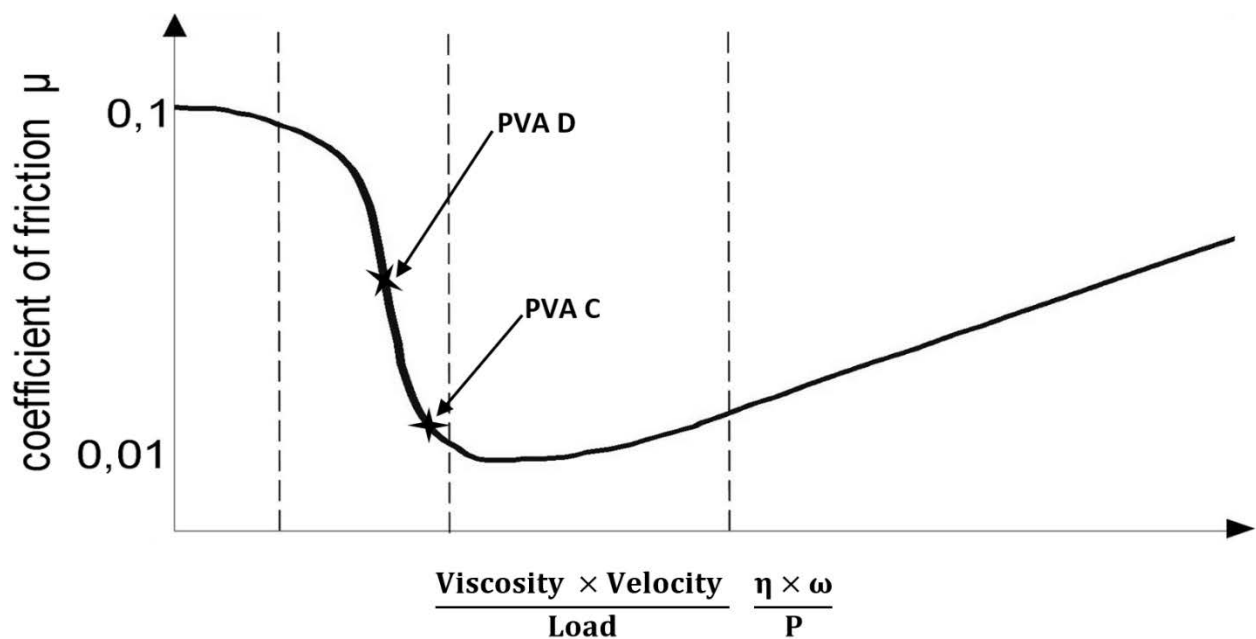
Figure 4.10: Hypothesised PVA D and PVA C points on the Stribeck curve for UHMWPE pin against CoCr disc.

4.6   Conclusion

The chapter aimed to screen and compare the different lubricants with different common articulating materials that might be used in an encapsulated artificial disc. A comparison has been made between the bio-lubricant polyvinyl alcohol (PVA) with varying concentrations, and other commonly used lubricants in-vitro tribological tests against common implant biomaterials, for potential use in encapsulated implants. Experiments measured viscosity and the frictional behaviour of the test fluids with a range of bearing material combinations. The conclusions from this chapter are:

- The PVA lubricant lowered the friction coefficient for CoCr/CoCr, CoCr/PEEK, PEEK/PEEK, UHMWPE/PEEK and UHMWPE/CoCr in comparison with Ringer's solution and bovine calf serum.

- Increasing the concentration of PVA gave a higher viscosity, which in most cases led to a lower friction coefficient. However, this effect was superseded by shear losses when the viscosity exceeded 2.08 Pa.s, as was observed for the PVA D (30 g per 100 mL of distilled water).

- PVA C (20 g per 100 mL of distilled water) with 1.650 ± 0.01 Pa.s viscosity showed the lowest friction coefficient for all combinations compared with other lubricants.

- UHMWPE/CoCr was the optimum material combination with the lowest friction coefficient for all lubricants.

- In light of these findings, PVA C with an UHMWPE/CoCr material combination will be used in the later chapters for the development of an encapsulated joint replacement implant.

5 Crack nucleation and growth in medical-grade silicone and polyurethane ether elastomers

5.1 Overview

This chapter presents the fatigue life of the most commonly used biomedical elastomers and the effect of ageing and sterilization on them. In the second section of the chapter, there is an introduction to the different elastomeric materials that have been used in biomedical implants; their biocompatibility and fatigue life are detailed in section 5.2. After this in section 5.3 there is a description of the materials and methods. In section 5.4, the results are presented. The results are then discussed and compared with the literature in section 5.5. The last section concludes the chapter. The work and the results of this chapter have been published in Alnaimat *et al.* (2017)

5.2 Introduction

A polymeric sheath has been suggested for artificial joints to encapsulate the ball and socket articulation surfaces to prevent the migration of wear particles to tissues, thus preventing an inflammatory response (Yao and Skorecki, 1985; Zhang *et al.*, 2009). Such a capsule should be biocompatible, flexible to allow the required motion of the artificial disc and should withstand millions of loading cycles without failure, as described in chapter 3. When the artificial disc is encapsulated, a formulated lubricant can be held inside the capsule helping to reduce both friction and wear. Chapter 4 tested a variety of formulated synthetic bio-lubricants as potential lubricants for an encapsulated artificial disc. For the encapsulating sheath, elastomers are ideal with the ability to withstand large strains without fracture. Su *et al.* (2006) used finite element analysis to investigate the effect of the capsule using silicone of thicknesses 0.5, 1, 1.5 and 2 mm. They found that stresses throughout the cross sectional area of the capsule decreased with thickness, with the 2 mm thick material showing the lowest stresses. Polyurethane and silicone elastomers have been shown to have improved biocompatible properties over other materials when they are implanted for long periods of time in the human body (Pinchuk, 1994). Silicone elastomers have been used and tested widely in finger joints, breast implants, electrodes and catheters (Bondurant *et al.*, 2000; Curtis and Colas, 2013; Naples *et al.*, 1988; Swanson, 1969). Polyurethane can be used in similar applications, but offer improved mechanical properties such as higher tensile strength, tear and abrasion resistance over silicone elastomers (Chauvel-Lebret *et al.*, 2001; Wasikiewicz *et al.*, 2013).

Boretos and Pierce (1968) investigated the use of the polyurethane ether in a heart-assist pump and compared it with silicone. They found that the polyurethane performed better in flexural

endurance, wear resistance and blood biocompatibility than silicone. Polyurethane has found further use in tri-leaflet heart valves (Butterfield *et al.*, 2001; Mackay *et al.*, 1996). In addition, it has also been used in the Bryan artificial disc as an outer flexible sheath (Kurtz, 2006; U.S. Food and Drug Administration, 2009) . Fan *et al.* (2012) reported a case of polyurethane sheath failure of the Bryan disc where a 5 mm transverse crack appeared on the sheath which led to revision surgery.

When selecting an elastomer for use as a sheath, long-term durability is a critical issue as a result of the strains that will be applied throughout the life of the joint. Fatigue performance, therefore, becomes a primary consideration for selecting an elastomer. A definition of fatigue life includes the propensity for crack nucleation (crack initiation), defined as the number of cycles required for a certain size crack to form in the specimen. There is also a second stage, after crack nucleation, as the crack grows (crack propagation) which is defined as the rate of propagation through the material with cyclic strain (Mars and Fatemi, 2002).

A requirement for *in-vivo* use would require the elastomer to be sterilized. Gamma radiation and electron beam are the most commonly used methods to sterilize medical devices (Lambert *et al.*, 2001). Gamma radiation produced from the cobalt isotope (60 Co) is ideal for medical products such as knee and hip replacements, syringes and bone implants. The most commonly used dose of this radiation to sterilize medical devices is 25 kGy (Benson, 2002). This radiation energy can degrade elastomeric materials and affect mechanical properties, reducing the tensile strength, moduli and fatigue life of the material (Gorna and Gogolewski, 2003; Mars and Fatemi, 2004).

After the implant is sterilized it will be implanted inside the human body and it should not face unacceptable changes in properties during the implantation period (Hukins *et al.*, 2008). To determine some of the likely changes in the materials, as a result of the ambient conditions within the body, a process of accelerated ageing can be used. This method is based on using elevated temperatures, for certain calculated time periods, to simulate the implantation time inside the human body (Lambert *et al.*, 2001). The fatigue and elastic properties of polymers in general are affected by ageing and are likely to lead to faster crack growth (Mars and Fatemi, 2004).

Chapter 3 described in detail the design requirements of the required sheath that will be used as an encapsulation sheath for the artificial disc from a design point of view. In addition, different conceptual designs relating to how the shape of the sheath and the way of attaching it to the artificial disc were also evaluated.

The aim of this chapter was to compare the fatigue life of biomedical silicone and polyurethane ether elastomers as a potential encapsulation sheath, including the effect of elastomer thickness, sterilization and accelerated ageing.

5.3 Materials and methods

5.3.1 Materials

Translucent silicone sheets 1.2 m wide x 1 m long with thicknesses of 1, 1.5 and 2 mm were bought from Silex Ltd (Bordon, UK). Yellow polyurethane ether sheets 0.5 m wide x 3 m long with thicknesses of 1.5 and 2 mm were bought from Bonaprene Products Ltd (Wrexham, UK). Rectangular specimens with 100 x 35 mm dimensions were cut using a ruler and scalpel (Swann-

Morton, Sheffield, UK) from all the different thicknesses of the silicone and polyurethane sheets. An initial crack of length 20 mm was cut into the rectangular specimens, as shown in Figure 5.1. The rectangular specimens were used in the crack growth experiments. Dumbbell specimens were cut from all sheets by using a hand-operated cutter with a dumbbell cutting die (Wallace Instruments, Kingston, UK), with the dimensions shown in Figure 5.2, and these were used in the crack nucleation experiments (ASTM D4482-11, 2011). Table 5.1 shows the mechanical properties of the silicone and polyurethane sheets.

Table 5.1: Mechanical properties as provided from the manufacturers of Silex silicone and Bonathane polyurethane elastomer sheets.

Mechanical properties	Silex silicone GP40	Bonathane ether polyurethane
Hardness (Shore A)	40	40
Tensile strength (MPa)	7	10.7
Elongation at break %	450	800
Tear strength (kN /m)	10.2	19.3
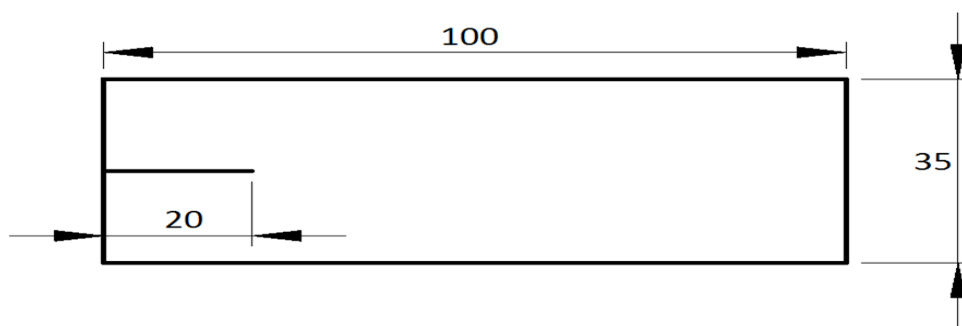
Figure 5.1: Rectangular specimen used for the crack growth experiments. All dimensions are in mm.
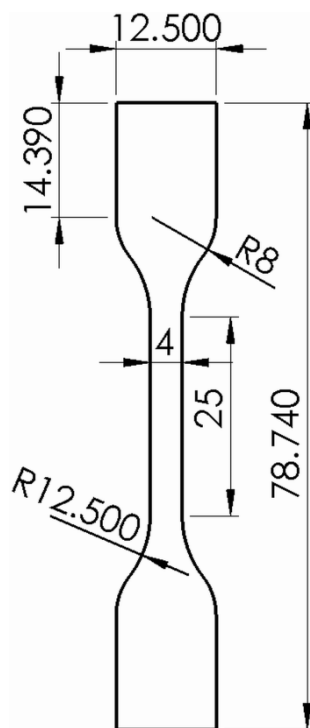
Figure 5.2: Dumbbell specimen used for the crack nucleation experiments. Dimensions satisfy the ASTM D4482-11 standard (ASTM D4482-11, 2011).

5.3.2 Methods

5.3.2.1 Specimen groups

The dumbbell and rectangular specimens were separated into four groups. The first group was the control group where specimens were not subjected to either sterilisation or ageing. The second group was the aged group (A group) in which accelerated ageing was applied to the specimens. The third group was the sterilized group (S group) where the specimens were sterilised by gamma radiation. The last group was the sterilized/aged group (S+A group) where specimens were both sterilised and aged, as described in Tables 5.2 and 5.3. Test sheets and test specimens were stored before testing in a dark place at a standard laboratory temperature and they were stored in different bags to prevent any contact with other materials, and hence prevent cross contamination that may affect the fatigue life, as described in the BS ISO 6943:2011 standard (BS ISO 6943, 2011).

5.3.2.2 Ageing of the elastomers

For ageing the specimens of silicone and polyurethane they were placed in polypropylene sample jars and immersed in saline solution (9.5 g/L of sodium chloride in deionized water). The jars were then placed in a Carbolite laboratory oven (Carbolite, Hope Valley, UK) for 149 days at a temperature of 50 °C; this temperature equated to an ageing time, t_a, of 1 year according to the following equation (Lambert *et al.*, 2001):

$$t_a = \frac{t_e}{2^{(T_e - T_\gamma)/10}}$$

where t_e is the real time equivalent (365 days), T_e is the elevated temperature (50°C) and T_γ is the reference temperature which was body temperature (37°C).

5.3.2.3 Sterilization of elastomers

Twelve samples from each material, six dumbbells and six rectangular specimens, were sterilized using gamma radiation produced from the cobalt isotope (60 Co). The sterilization have been done in a vacuum chamber to avoid oxidative embrittlement from gamma sterilizing in air. The radiation dose of the gamma was 25 kGy performed by Synergy Health Sterilisation UK Ltd (Swindon, UK).

5.3.2.4 Bose ElectroForce 3300 testing machine

The Bose ElectroForce 3300 testing machine (Bose Corporation, ElectroForce Systems Group, MN, USA) was used in the crack initiation and growth tests, as shown in Figure 5.3. The upper grip was attached to a single actuator which gave an axial tension or compression while the other grip was attached to the bottom plate which is a stationary plate. A 3000 N load cell (Bose 1010CCH-1K-B) was attached to the bottom plate and is calibrated by the manufacture every twelve months. The upper plate is manually moved up or down to adjust the displacement between the upper grip and lower grip. In addition, the upper grip can be controlled by the device software to move ± 12 mm in the axial direction. The device is connected to a desktop computer and controlled by WinTest® 4.1 software (Bose Corporation, ElectroForce Systems Group, MN, USA).

Figure 5.3: Bose ElectroForce 3300 testing machine.

5.3.2.5 Crack nucleation

Crack nucleation experiments were performed using the Bose ElectroForce 3300 testing machine (Bose Corporation, Minnesota, USA) shown above. The data were obtained using Wintest software (Bose Corporation, Minnesota, USA). The experiments were performed according to the standards ASTM D4482-11 and BS ISO 6943:2011 (ASTM D4482-11, 2011; BS ISO 6943, 2011). The dumbbell specimens were attached to the Bose machine using two grips. The testing

involved applying a sinusoidally varying displacement at 10 Hz. The testing was performed at room temperature. The applied strain was 50% which is more than the expected strain resulting from the different motions of the artificial disc, measured from the length between the two grips, at 17 mm. The testing continued until complete failure of the sample occurred or until five million cycles had been completed, which is the equivalent to five years implanted inside the human body. The crack nucleation testing was undertaken for the control group and the sterilized/aged group (which represented the worst case). The detailed test conditions are described in Table 5.2.

Table 5.2: Crack nucleation testing conditions (S+A: Sterilized/Aged group).

Group	Materials	Thickness mm	Samples (n) from each material	Ageing	Sterilization
Control group	Silicone	1, 1.5, 2	1	No	No
	polyurethane	1.5, 2	1	No	No
S+A group	Silicone	1, 1.5, 2	1	yes	Yes
	polyurethane	1.5, 2	1	yes	Yes

5.3.2.6 Crack growth

The crack growth tests were completed in accordance with ASTM E647 – 15 (ASTM E647-15, 2011). Single edge crack tension growth experiments were undertaken at room temperature using the same Bose testing machine detailed above. A sinusoidally varying tensile strain was applied

in displacement control. The cyclic strain was cycled from 0% to 30% (in accordance with strain that the designed artificial disc was expected to be exposed to) from the distance of the sample between the two grips, which again was 17 mm. A 70% cyclic strain was used with the aged and sterilized/aged polyurethane samples because there was not any crack growth at 30% strain due to changes in the hardness of the material from the ageing process. All crack growth tests were undertaken at 2 Hz. Slippage was monitored by force measurement, and none was observed during the experiments. A starting crack of 20 mm length was produced in each sample. The test was stopped periodically to take crack growth readings; crack length was measured three times using digital callipers (Fisher Scientific, Leicestershire, UK). The mean and standard error (as described in section 5.3.2.9) was calculated for the number of samples used from each material. Testing was stopped when the crack had grown by 70 mm from the initial 20 mm length and before the failure of the samples. Linear interpolation was used for the data points before and after 70 mm to calculate the number of cycles required to reach the 70 mm crack. The detailed test conditions are described in Table 5.3 and Figure 5.4.

Table 5.3: Crack growth testing conditions (S+A: Sterilized/aged group, A: Aged group, S: Sterilized group). Number of independent observations (n) used for calculating standard error.

Group	Materials	Thickness mm	Samples (n) from each material	Ageing	Sterilization
Control group	Silicone	1, 1.5, 2	3,2,3	No	No
	polyurethane	1.5, 2	3,3	No	No
A group	Silicone	1, 1.5, 2	2,2,3	Yes	No
	polyurethane	1.5, 2	1,1	Yes	No
S group	Silicone	1, 1.5, 2	2,2,1	No	Yes
	polyurethane	1.5, 2	2,2	No	Yes
S+A group	Silicone	1, 1.5, 2	2,2,2	yes	Yes
	polyurethane	1.5, 2	1,1	yes	Yes

```
                          ┌─────────────────────┐
                          │ Encapsulation sheath│
                          └─────────────────────┘
```

Silicone			Polyurethane	
Thickness 1 mm	Thickness 1.5 mm	Thickness 2 mm	Thickness 1.5 mm	Thickness 2 mm
No. of Samples (n):	No. of Samples (n):	No. of Samples (n):	No. of Samples (n):	No. of Samples (n):
Control: 3	Control: 2	Control: 3	Control: 3	Control: 3
A: 2	A: 2	A: 3	A: 1	A: 1
S: 2	S: 2	S: 1	S: 2	S: 2
S+A: 2	S+A: 2	S+A: 2	S+A: 1	S+A: 1
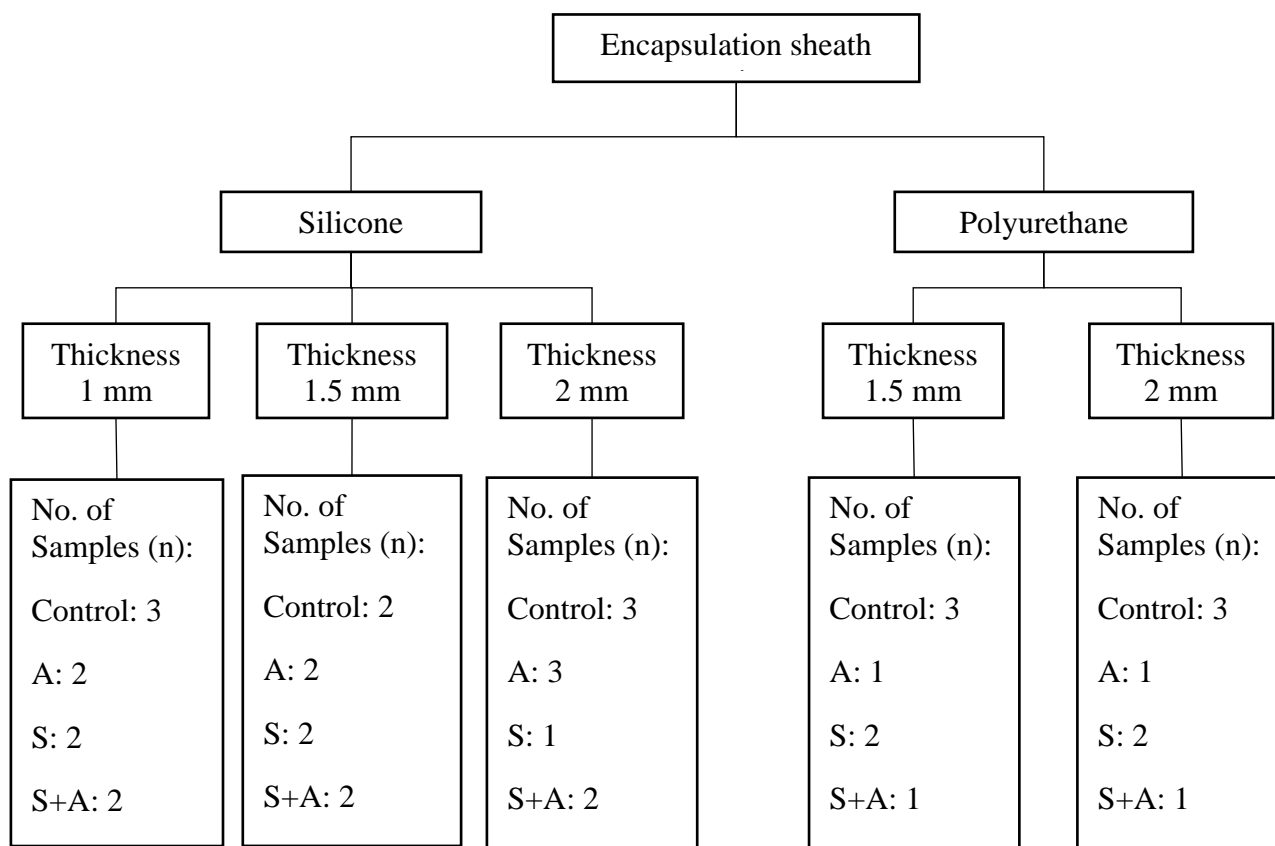
Figure 5.4: Number of samples (n) used for crack growth testing (S+A: Sterilized/aged group, A: Aged group, S: Sterilized group).

5.3.2.7 Surface imaging and roughness

Samples were scanned using an Alicona G5 InfiniteFocus (Alicona, Raaba, Austria) using 10× magnification. Three samples of each material from each group were scanned nine times and the mean surface roughness and standard error was calculated (Standard error is described in section 5.3.2.9). The undamaged outer surface was scanned to view the degradation that was potentially

caused by sterilization, ageing and sterilization/ageing and to compare them with the control group (without ageing or sterilization).

5.3.2.8 Hardness testing

Shore A hardness was measured for all the 2 mm thick samples according to the standards ASTM D2240-15 and BS ISO 7619-1:2010 (ASTM D2240-15, 2015; BS ISO 7619-1, 2010) using a shore A durometer (HUATEC Group Corporation, Beijing, China). The Durometer was held for 20 seconds until the reading was stable (giving a fixed reading). Three samples from each group were measured 9 times and the mean was calculated for the readings.

5.3.2.9 Standard error

Standard error of the mean is the measure of the accuracy with which a sample represents a population. It is the standard deviation divided by the square root of the number of observations in that sample (Logan, 2011).

$$Standard\ error = \frac{\sigma}{\sqrt{n}} \hspace{4cm} [1]$$

Where σ is the standard deviation and n is the sample size.

5.4 Results

5.4.1 Crack nucleation results

No silicone or polyurethane dumbbell specimens failed from the control group after five million cycles during the cyclic fatigue tests with 50% strain. In addition, no dumbbell specimens failed from the sterilized/aged group in the crack nucleation test after five million cycles.

5.4.2 Crack growth results

Crack growth was affected by the thickness of the sheath for all the materials, as shown in Figures 5.5 and 5.6. The rate of crack growth reduced with increasing thickness of the samples. Polyurethane ether samples showed a better resistance to crack growth than the silicone elastomer, as shown in Figures 5.5 and 5.7. The 2 mm thickness polyurethane from the control group reached 70 mm (without the initial crack) after approximately 421k cycles of the crack growth test, while the 2 mm thickness silicone from the control group reached 70 mm after 221k cycles.

Crack growth for the polyurethane samples for the thicknesses of 1.5 and 2 mm followed the same trend. The aged samples had the slowest crack growth rate between all the groups followed by the sterilized/aged samples. The aged and sterilized/aged group polyurethane samples were affected by the grips attachment area. Crack growth was not affected but there was evidence of deformation of the polyurethane, at the site of the grips and sample in the aged and sterilized/aged group. The control group had a higher crack growth rate than the sterilized/aged

group and the sterilized group had the highest crack growth rate compared to the other groups, as shown in Figures 5.5 and 5.6.
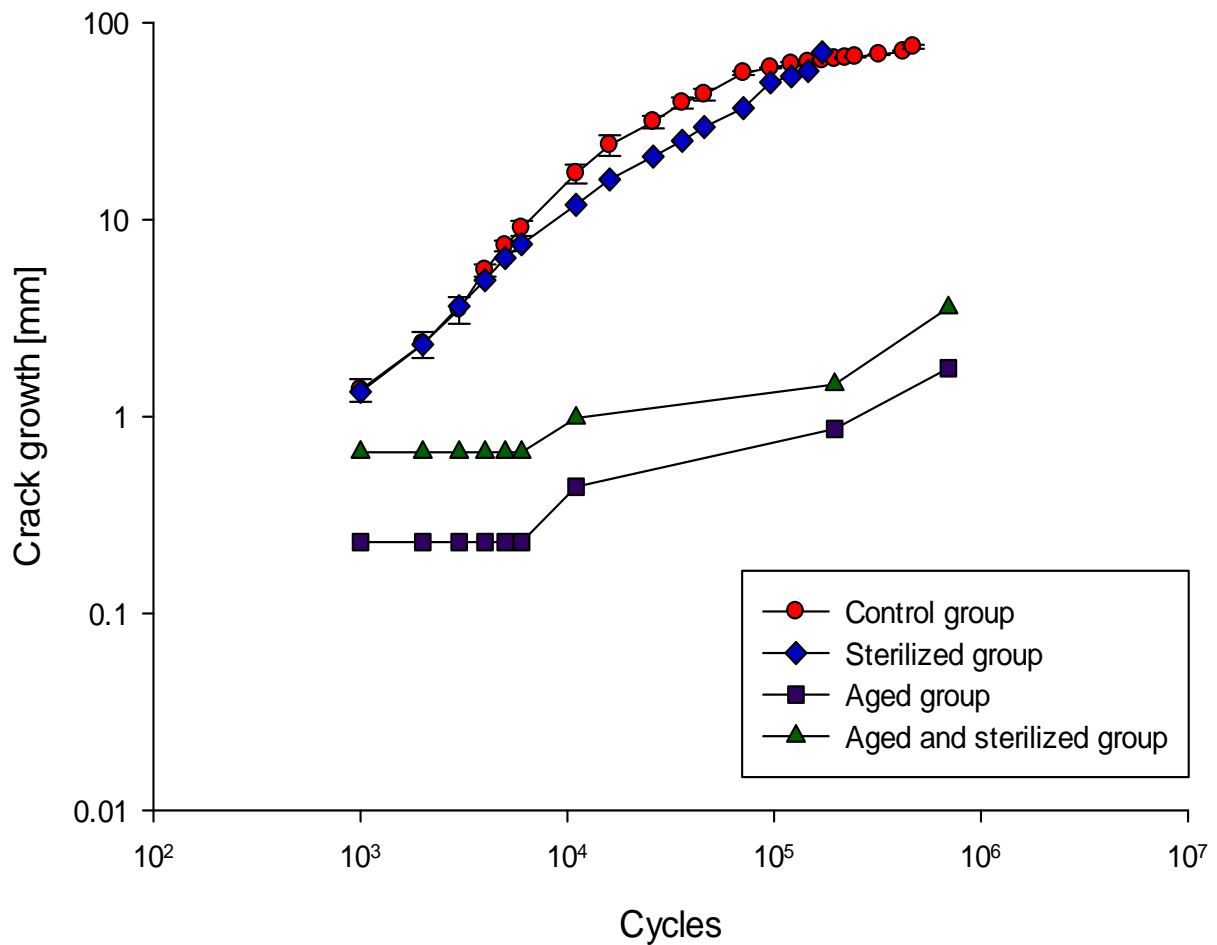
Figure 5.5: Crack growth for the 2 mm polyurethane ether samples; x and y-axis are on a logarithmic scale base 10. Error bars represent standard error. No error bars for n < 3.
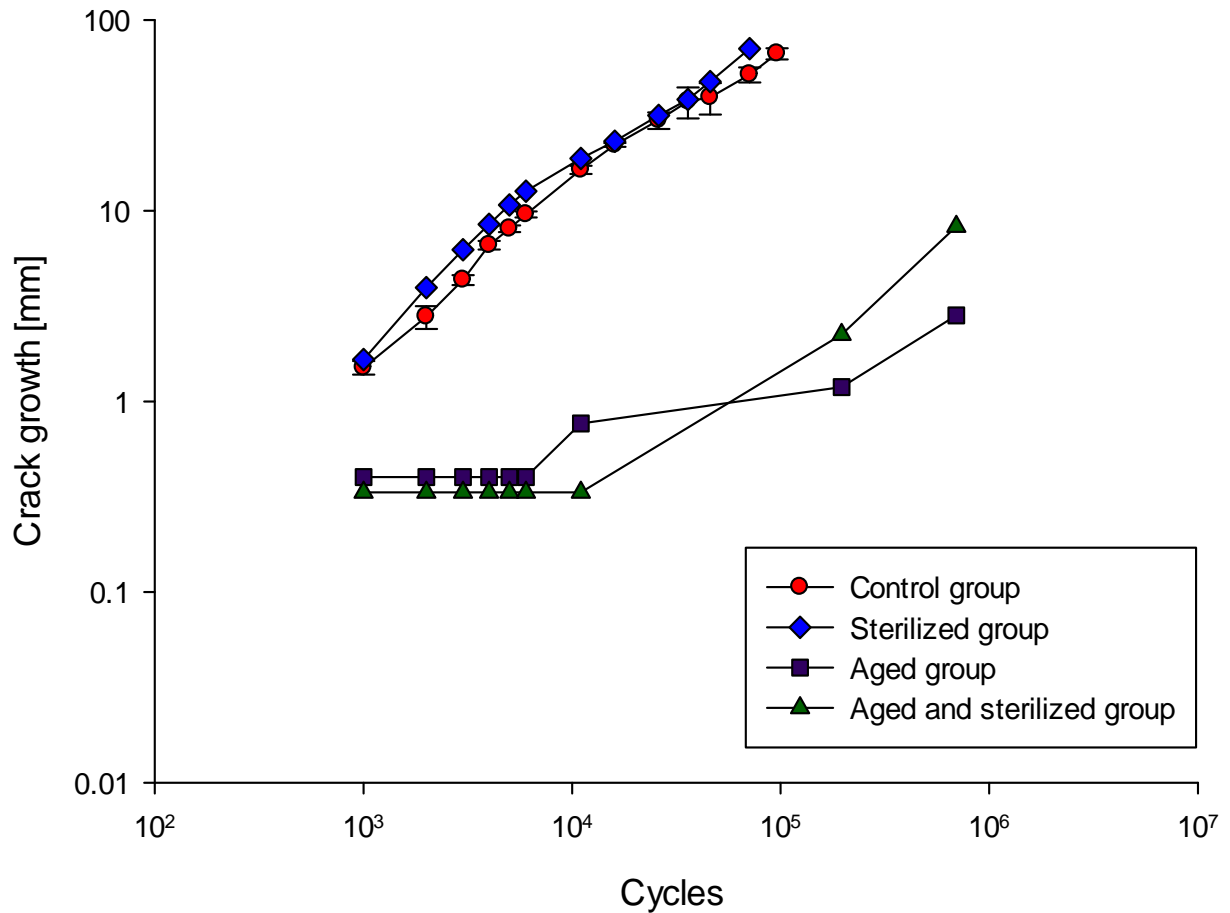
Figure 5.6: Crack growth for the 1.5 mm polyurethane ether samples; x and y-axis is on a logarithmic scale base 10. Error bars represent standard error. No error bars for n < 3.

The silicone samples with the different thicknesses had the same crack growth trends. The control group for all the silicone samples had the slowest crack growth rate of all the groups followed by

the sterilized group. Then there was the aged samples followed by the sterilized/aged group, with the fastest rate of crack growth rate between all the groups, as shown in Figures 5.7, 5.8 and 5.9.
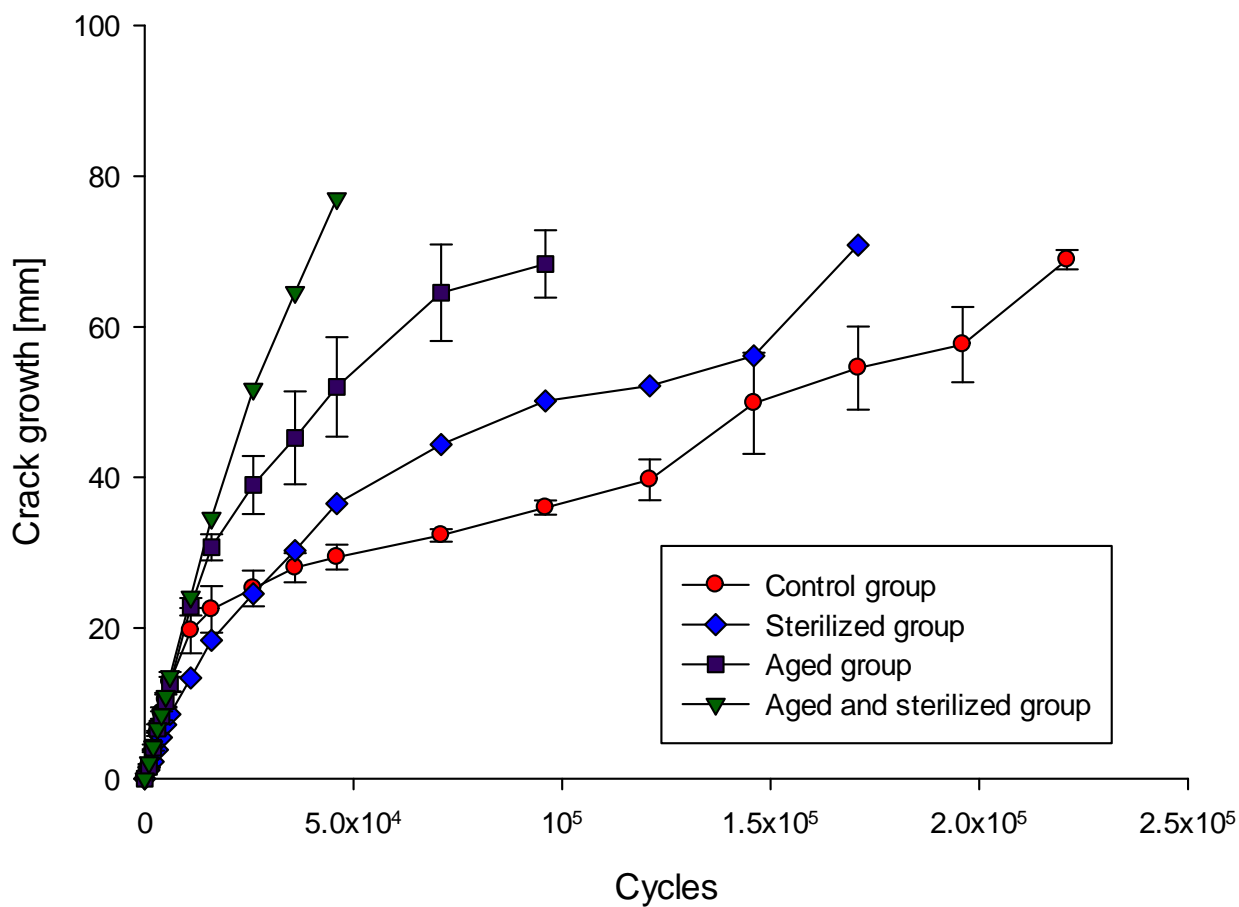
Figure 5.7: Crack growth for the 2 mm silicone samples. Error bars represent standard error. No error bars for $n < 3$.
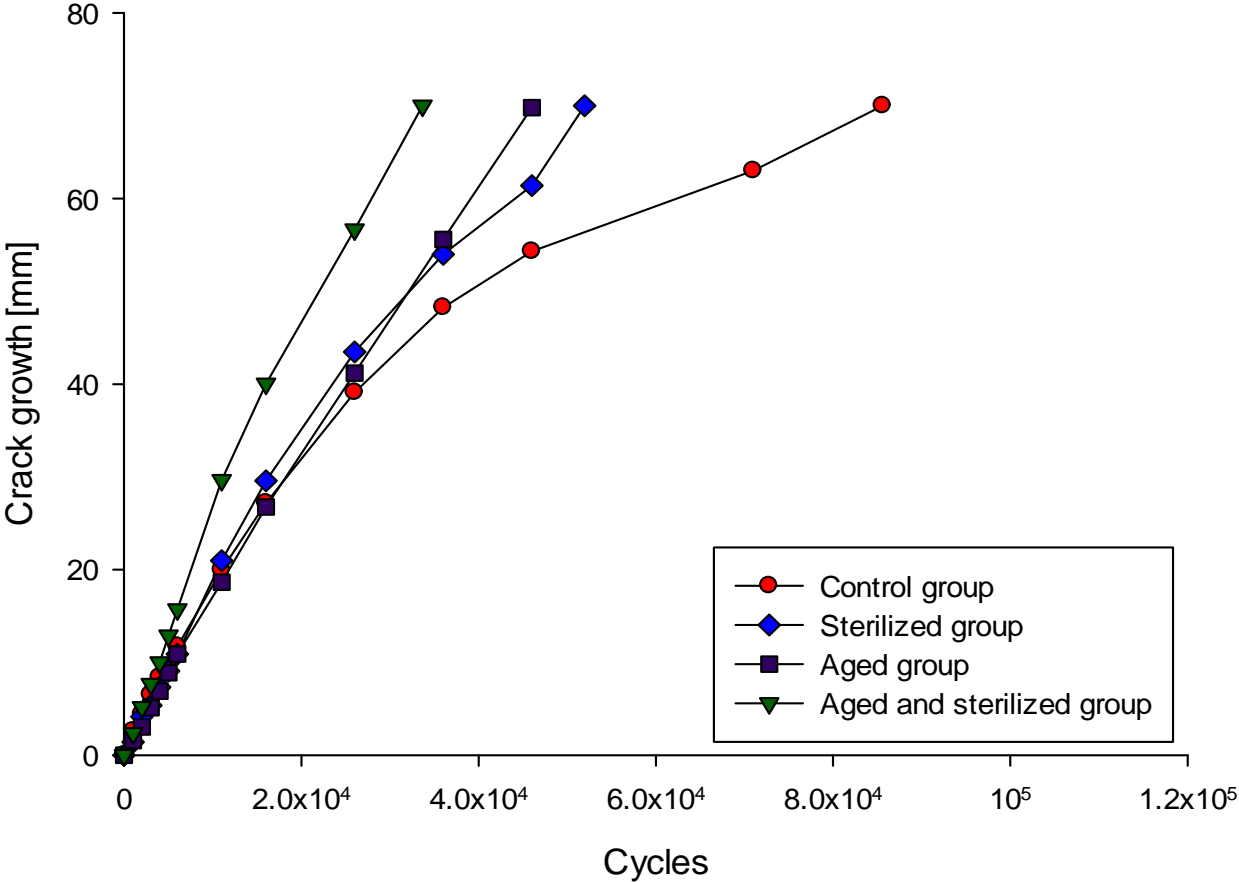
Figure 5.8: Crack growth for the 1.5 mm silicone samples. Error bars represent standard error. No error bars for n < 3.
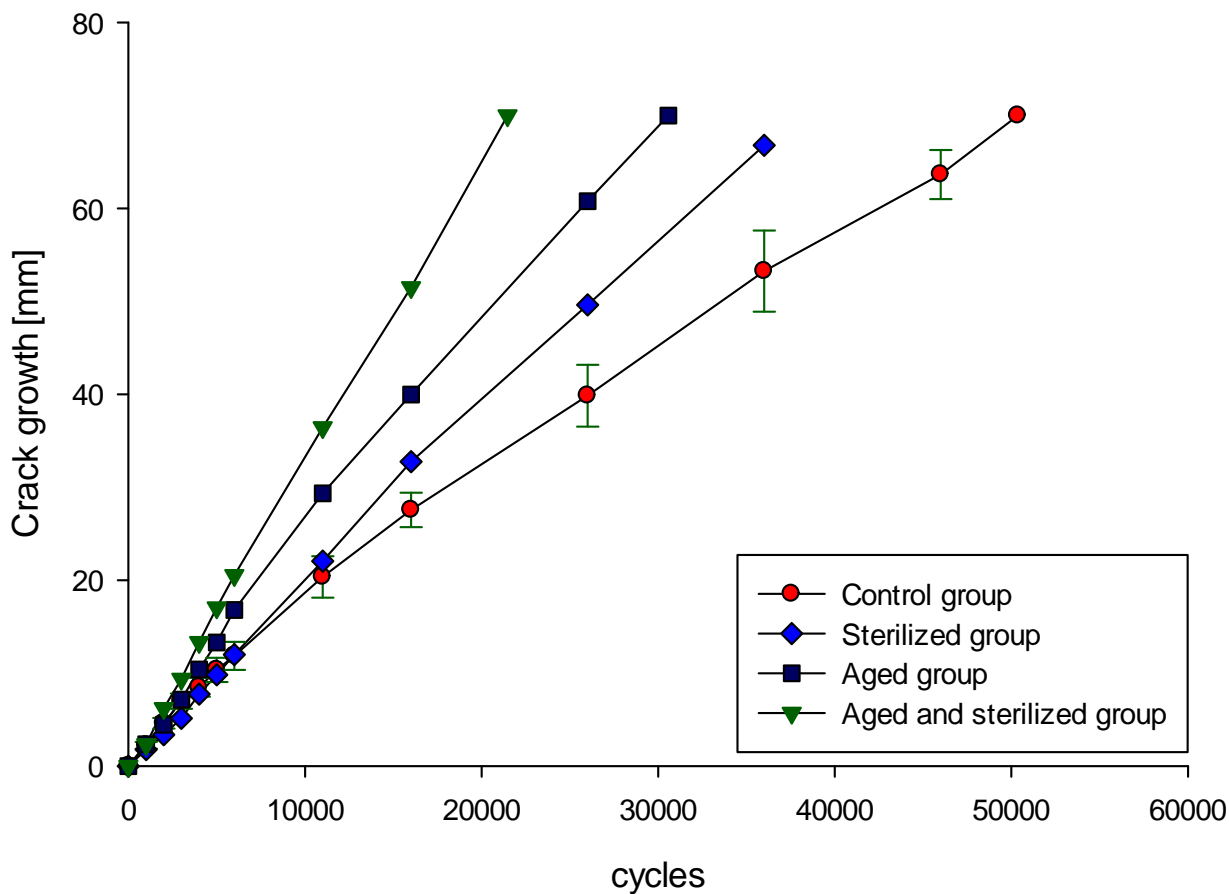
Figure 5.9: Crack growth for the 1 mm silicone samples. Error bars represent standard error. No error bars for n < 3.

5.4.3 Surface imaging and roughness results

Figure 5.10 shows the surfaces of the elastomers from the different groups. Figure 5.10 a is the polyurethane control group. There was no effect on the surface as a result of sterilizing the polyurethane, as shown in Figure 5.10 b. However, the ageing process caused surface degradation

and swelling of the surface, as shown in Figures 5.10 c and 5.10 d. There was no noticeable effect

on the surfaces of the different groups of silicone, as shown in Figures 5.10 e-h.
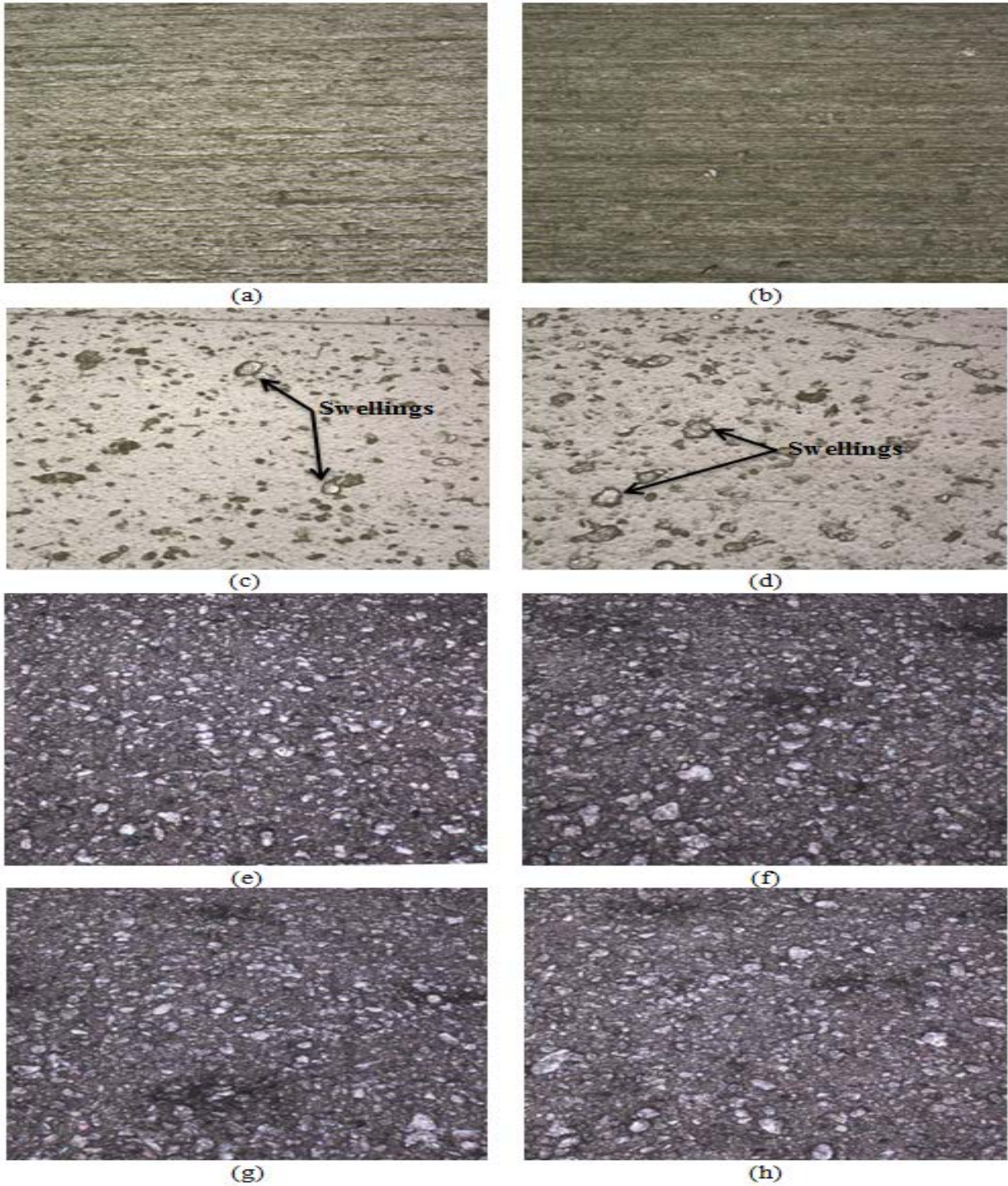
Figure 5.10: surface imaging by Alicona G5 InfiniteFocus for: a) Control polyurethane group. b) Sterilized polyurethane group. c) Aged polyurethane group. d) Sterilized/aged polyurethane group. e) Control silicone group. f) Sterilized silicone group. g) Aged silicone group. h) Sterilized/aged silicone group.

Figure 5.11 shows a polyurethane surface with topography plotted, from the red line, below. The peaks represent swellings, and their heights are given on the chart. The peak values of the swellings reached 8 μm from the nominal surface.
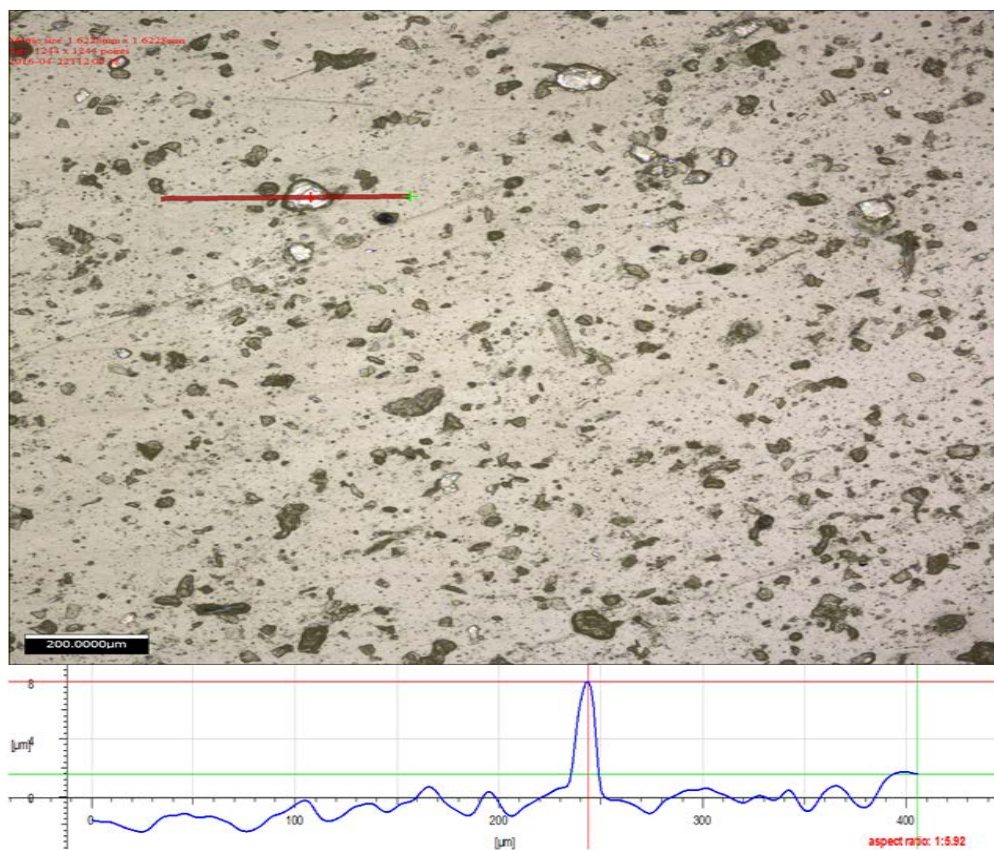
Figure 5.11: surface imaging by Alicona G5 InfiniteFocus for an aged polyurethane sample. The line chart represents the topography of the surface across the red line on the upper part of the Figure.

Table 5.4 lists the surface roughness measured from the tested samples. The mean values of Ra for aged and sterilized/aged polyurethane was lower than the sterilized and control group of the polyurethane. Also, the mean values of Ra for sterilized/aged silicone was lower than the control, sterilized and aged silicone samples.

Table 5.4: The mean surface roughness and standard error for the test specimens. There were no differences between the surface roughnesses; however, the mean values of R_a for aged and sterilized/aged polyurethane were lower than the sterilized and control group.

Group	R_a mean [μm]	Standard error [μm]
Control polyurethane	0.82	0.04
Sterilized polyurethane	0.89	0.1
Aged polyurethane	0.61	0.03
Sterilized/aged polyurethane	0.64	0.03
Control silicone	0.85	0.09
Sterilized silicone	0.79	0.1
Aged silicone	0.89	0.05
Sterilized/aged silicone	0.68	0.09

5.4.4 Hardness results

The hardness of the polyurethane was lower after the ageing process from 40 to 10 shore A; however, sterilization did not affect the hardness properties of the polyurethane samples. For the silicone samples, all combinations of sterilisation and ageing increased the hardness to 50, from the control level of 45 shore A. The results are listed in Table 5.5.

Table 5.5: The mean Shore A hardness for the test specimens.

Group	Mean shore A
Control polyurethane	40
Sterilized polyurethane	41
Aged polyurethane	10
Sterilized/aged polyurethane	10
Control Silicone	45
Sterilized Silicone	50
Aged Silicone	50
Sterilized/aged Silicone	50

5.5 Discussion

All of the dumbbell samples from the control group exceed 5 million cycles using 50% strain in the crack nucleation tests, as did all the dumbbell specimens from the sterilized/aged group. There was no noticeable complete failure in the samples from the crack nucleation tests for all the groups tested.

Polyurethane ether showed a greater crack growth resistance than the silicone elastomer with the same hardness for all the groups. There were also noticeable effects from the elastomer thickness on the crack growth rate, being higher for the thinner elastomers. The same effect of sample

thickness was described previously (Legorju-jago and Bathias, 2002; Mazich *et al.*, 1989) in which the crack growth rate was higher for thinner samples.

For the crack growth tests, the control group for the silicone groups produced the lowest rate of crack growth compared to the sterilised, aged and sterilised/aged groups. The sterilized samples had a lower crack growth life than the control group due to the effects of gamma irradiation on the materials. Hutchinson *et al.* (1997) observed the same negative effect of the gamma sterilization on polyurethane and silicone elastomers. In their experiments, there was a noticeable negative effect from gamma radiation on both materials and the polyurethane had slower crack growth rate more than the silicone elastomer. Gamma radiation has also been shown to increase crack growth rate for other polymers such as UHMWPE as reported previously (Baker *et al.*, 2000; Cole *et al.*, 2002). This reduction in the fatigue life of the UHMWPE is caused by the degrading of the mechanical and structural integrity of the UHMWPE (Baker *et al.*, 2000; Pruitt, 2003). This might be the same case for the silicone and the polyurethane elastomers.

Accelerated ageing had a different effect on both materials. For the silicone samples, ageing reduced fatigue life by increasing the rate of crack growth, compared to the control and sterilized samples. These results are similar to the effects described by Leslie *et al.* (2008) in which accelerated ageing reduced the mechanical properties of medical silicone elastomers Med82-5010-80 and C6-180. The rate of crack growth in the aged polyurethane ether samples was much slower when compared with the control group. The reduction of the crack growth rate in these samples was due to the reduction in strength and hardness due to the plasticization by water, as shown in Table 5.5. Davies and Evrard (2007) presented similar results in which they described a reduction in hardness and strength as a result of water driven plasticization. In this process the

water molecules with the help of temperature can destroy the links between the polymer chains as described by Boubakri *et al.* (2009).

The application of sterilization and ageing has a different effect on both of the tested materials. For the silicone samples, the sterilization and ageing had the largest effect on the increase of speed of crack growth rate between all the groups. The sterilized/aged polyurethane ether samples showed a lower crack growth rate when it is compared with silicone from the same group due to the plasticization by water which occurred due to the ageing process. However, they showed a faster crack growth rate than the aged polyurethane ether samples. The sterilized/aged samples had the fastest crack growth rate, as a result of gamma sterilization radiation and ageing effects on the silicone samples. The aged samples of the silicone were slightly improved but worse of all was the sterilised/aged silicone samples.

The polyurethane samples showed different results in which the aged samples had the lowest crack growth rate. The sterilized/aged polyurethane samples showed a slight increase in the crack growth rate. The reduction of the crack growth rate in these samples was due to the drop of the strength, due again to the plasticization by water. Water plasticization of the polyurethane was due to the water absorption during the accelerated ageing process as described previously (Apicella *et al.*, 1983). There was a noticeable effect on the surface of the aged and sterilized/aged polyurethane groups with swellings on the surfaces of both groups; the peak height of the swelling reached 8 µm in some areas, as shown in Figure 5.11. These swellings might be caused by the penetration of water molecules into the material structure. This phenomena was noticed by Boubakri *et al.* (2009) in which the same swellings appeared after accelerated ageing and immersion of the polyurethane material in distilled water.

The sterilization and accelerated ageing had no measurable effect on the surface roughness of the silicone samples. For the polyurethane, the aged and sterilized/aged samples showed a reduction in mean roughness, a likely result of water plasticization, as shown in Figures 5.10 c and 5.10 d.

The hardness for the polyurethane was the same for the control and sterilized group, but this reduced as a result of ageing, as mentioned earlier in Table 5.5. The reduction in hardness will also have been a product of water plasticization in the polyurethane samples due to the ageing process. Davies and Evrard (2007) noted a similar drop after ageing polyurethane in seawater for 1 month. The hardness of the silicone samples was increased to similar levels by both sterilization and ageing, this is again a phenomenon similar to that described by Dootz *et al.* (1994) in which the hardness increased from 30.4 to 34.6 shore A after the accelerated ageing for 900 hours at 110 °F (43.3 °C), with the distilled water spraying technique was used.

5.6 Conclusions

The following conclusions can be drawn from this chapter:

- For the crack nucleation tests no samples, of each thickness, from the control or the sterilized/aged group failed after the 5 million cycles.

- The rate of crack growth was slowest with the polyurethane ether elastomer. For example, the control group in the 2 mm polyurethane ether samples took 421k cycles to reach 70 mm crack length, whereas silicone elastomer from the same group and thickness took 221k cycles to reach the same crack length. The same trend was shown for all other groups.

- Crack growth life was dependant on the sample thickness in which the thicker elastomers took longer to crack.

- Accelerated ageing reduced the hardness of the polyurethane ether elastomer, created swellings on the surface of the material as a result of water plasticization and decreased the crack growth rate. For the silicone elastomer, there was no change in the surface of the elastomer but the hardness and the crack growth rate were increased.

- Gamma sterilization did not affect the hardness of the polyurethane ether elastomer; however, crack growth rate of the material was increased. The same sterilization process increased the hardness of the silicone elastomer and increased the crack growth rate.

Based on the results of this chapter the polyurethane ether elastomer exhibited superior performance over the silicone with a 2 mm thickness for use as a sheath for the development of an encapsulated artificial disc technology. The next chapter will be about the development and evaluation of the encapsulated artificial disc configurations.

6 Development and evaluation of the encapsulated artificial disc design

6.1 Overview

This chapter presents the preparation and evaluation of the encapsulated artificial disc design. Section 6.2 introduces the materials that have been chosen from the previous chapters (4 and 5) to be used in the encapsulated artificial disc. In section 6.3 the methods used to manufacture, assemble and evaluate the different encapsulation procedures are described. Section 6.4 includes the results of the different tests that were undertaken. Section 6.5 contains the discussion of these results in the context of the literature. Finally the conclusions of the chapter and recommendations, based on the results and discussion are given in section 6.6.

6.2 Introduction

The process of evaluating the encapsulated ball and socket artificial disc in this chapter came after choosing and manufacturing the design that satisfied the product design specifications from chapter 3. The choice of the articulation materials and lubricant was determined in chapter 4 where the coefficient of friction was evaluated for different bearing combinations. The outcome of chapter 4 was UHMWPE against CoCr for the articulation materials with the use of PVA C (20 g per 100 mL of distilled water). In chapter 5, different elastomeric materials were tested to choose the material that will be used for the outer sheath which will hold the lubricant during the articulation between the UHMWPE and CoCr. Polyurethane ether elastomer with a hardness of 40 shore A was suggested as an encapsulation sheath. In this chapter, the preparation of the manufactured encapsulated ball and socket artificial disc is presented in detail. This includes the evaluation of the assembly and in particular the attachment methods between the sheath and the ball and socket components, with various methods of connection tested and discussed throughout the chapter. However, this will not be the only evaluation for the encapsulated artificial disc as in chapter 7 there will be an evaluation of the tribology of the whole encapsulated artificial disc with and without encapsulation. The aim of this chapter is to evaluate and test a number of different attachment methods of the encapsulated ball and socket artificial disc.

6.3 Materials and methodology

6.3.1 Ball and socket manufacture

The socket was designed using SolidWorks (Dassault Systèmes SolidWorks Corp., Massachusetts, USA), as described in chapter 3, section 3.5. The UHMWPE socket was produced from a 250 mm length and 70 mm diameter natural white colour rod bought from PAR-group (Manchester, UK). Ten sockets were machined from the rod with an external diameter of 56 mm diameter and 10.015 mm radius, as shown in Figure 6.1. The machining of the socket samples was undertaken in the workshop of the School of Physics and Astronomy, University of Birmingham (Birmingham, UK) and predominantly manufactured using a Haas ST-25Y CNC lathe (Haas Automation, Inc., California, USA). The M1 hole was drilled in the socket without applying the thread by using a 0.75 mm drill bit on the same machine tool centre. The ball with 10 mm radius was designed and manufactured previously by Moghadas (2012), as described in chapter 3 section 3.5.

Figure 6.1: CoCr ball and UHMWPE socket.

6.3.2 Disc fixtures

The encapsulated ball and socket artificial disc were fitted to the spine simulator using the lower and upper plates, as shown in Figure 6.2. The plates were designed and manufactured by Moghadas (2012) in order to have the centre of rotation located from the top of the upper plate by 42.5 mm, as shown in Figure 6.2. The reason for this is that the centre of the ball has to match when it was fitted in the spine simulator to give the centre of rotation. By matching the centre of rotation of the machine and the centre of rotation of the artificial disc would prevent undesirable bending moments during the resistive torque and wear testing.
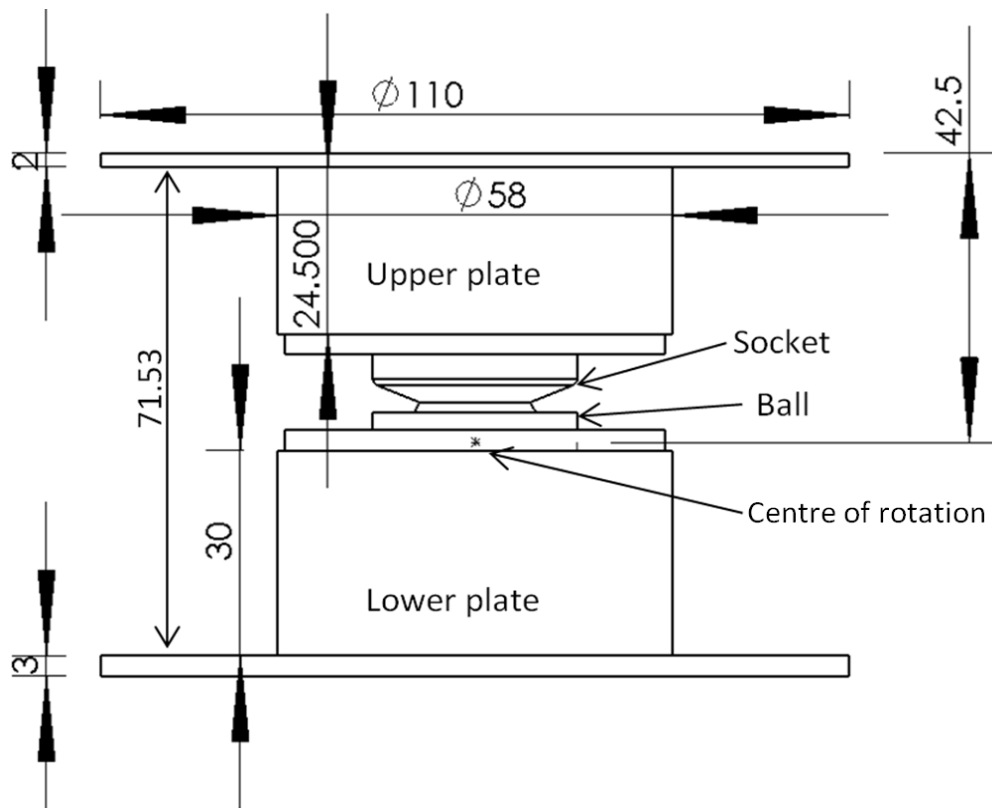
Figure 6.2: Artificial disc upper and lower plates fixation and centre of rotation point. All dimensions in mm.

6.3.3 General preparation of the samples for the measuring of weight, surface roughness and for preassembly

The general preparation and cleaning of the encapsulated artificial discs was achieved through different steps to prepare them for testing. The procedure for cleaning the samples was adopted from BS ISO 14242-2 (BS ISO 14242-2, 2016) and the Standard Operating Protocol for Spine Wear Simulator Studies (SOP01.6) which has been developed by the Institute of Medical and Biological Engineering, University of Leeds. The cleaning steps from 1 to 10 were used for all the configurations before every assembly. These steps are listed below:

1. The attachment surfaces between the capsule sheath and the artificial disc were roughened for the ball and socket specimens with sandpaper 120 grit sizes (KLINGSPOR Abrasives, Inc, North Carolina, USA) to increase the attachment strength of the adhesive, as shown in Figure 6.1.

2. All the specimens were washed with non-oily household detergent to remove the dirt and grease.

3. The ball and socket specimens were cleaned with alcohol (methanol) solution (70% with water (Sigma-Aldrich, St. Louis, MO, USA) prior to testing.

4. The ball specimens were soaked in Virkon disinfectant solution (10 mg of powder (Antec International, Sudbury, UK) with 1 L of water) to remove any bacterial contamination from 2 to 24 hours, the UHMWPE sockets were soaked for less than 20 minutes.

5. All specimens (balls, sockets and sheaths) were washed once with tap water and twice with distilled water and then left on low lint clean-room wipes (Cleanroom shop, Cumbria, UK) in open air to dry completely.

6. The ball and socket samples then were soaked in propan-2-ol (Scientific Laboratory Supplies, East Yorkshire, UK) in a beaker and were then ultrasonically cleaned using an ultrasonic cleaner (Scientific Laboratory Supplies, East Yorkshire, UK).

7. To remove all grease and dirt, all the ball and socket samples were finally washed with acetone (Sigma-Aldrich, MO, USA).

8. At the end of cleaning stage all the samples were dried and wiped with low lint cleaning wipes and left in a plastic box for 48 hours to ensure complete drying of the samples.

9. After 48 hours all the samples were weighed using an Ohaus GA200D balance with ± 0.2 mg precision (Ohaus Scales and Balances, Norfolk, UK) using the gravimetric measurement procedure as described in BS ISO 18192-1:2011 (BS ISO 18192-1, 2011).

10. All the samples were cleaned with an air duster to remove any dust particles on the surfaces and the surface roughness for each sample was measured three times using the procedure described in section 4.3.1.

6.3.4 Encapsulation configurations

6.3.4.1 Assembly configuration 1

A cast polyurethane ether sheath with a 30 mm inner diameter, 34 mm outer diameter and 13 mm length, with a 40 shore A hardness, was bought from the AAA-ACME Rubber Co. (Arizona, USA), as shown in Figure 6.3. The drawing of the polyurethane ether sheath is shown in Appendix A. The polyurethane ether sheath was selected based on the findings of chapter 5.

Figure 6.3: Polyurethane ether sheath used in the first assembly.

The first suggested method for attachment was developed using TRIZ, as detailed in chapter 3, and it involved using an adhesive to attach the artificial disc to the encapsulation sheath. The first adhesive selected was MED-1511 silicone adhesive (Polymer Systems Technology Ltd, Buckinghamshire, UK), as it was suitable for long term implantation in the human body as described in the datasheet of the adhesive. After the 10 steps of the general method of preparation of the ball and socket samples (section 6.3.3), there were several other specific steps for assembly of the ball and socket with the polyurethane ether sheath with MED-1511 silicone adhesive. The method of assembly of the first assembly configuration is described below:

1. A layer of MED-160 primer was applied using foam wipes on the PU sheath and a layer of MED-163 primer was applied using foam wipes on the UHMWPE attachment surfaces for the sheath and the socket. This was suggested by Nusil Technology (Nusil Technology, Buckinghamshire, UK) to enhance the bonding between the adhesive and the polymer.

2. The sheath and socket were left to dry after applying the primers for 24 hours.

3. A layer of the MED-1511 silicone adhesive was spread on the socket. The sheath was placed on the socket by applying a force on the top of the sheath to ensure a full attachment.

4. The attached socket and sheath were left for 24 hours for complete curing of the adhesive.

5. A layer of the MED-1511 silicone adhesive was then spread on the attachment surface of the ball and then the sheath was attached to the ball by applying a pressure on the top of the sheath to ensure full attachment.

6. The attached socket-sheath-ball were left for 24 hours to allow complete curing of the adhesive.

7. The PVA C lubricant was mixed with a red food colouring agent (Sainsbury's Supermarkets Ltd., London, UK) to help in determine any leakage during the test.

8. The PVA C lubricant (2 mL) was placed inside the encapsulated artificial disc with a syringe and needle through the 0.75 mm hole in the socket.

9. The ball and socket with the sheath were compressed using an F-clamp to give the curvature shape of the sheath and to remove air bubbles by compressing the lubricant, as shown in Figure 6.4.

10. M1 X 6 mm countersunk self-tapping bolt was inserted to seal and secure the lubricant.
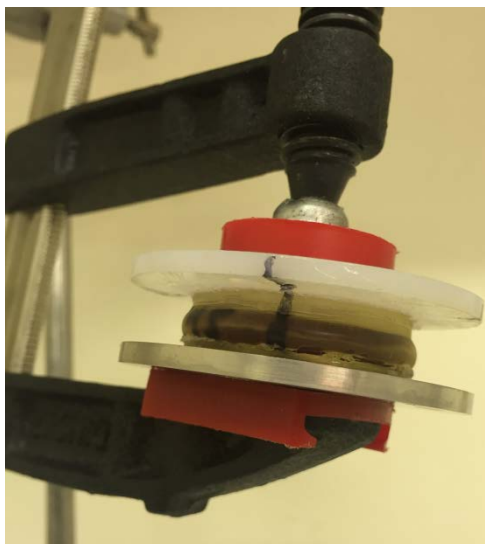
Figure 6.4: Compressed ball and socket artificial disc with polyurethane sheath using an F-clamp.

6.3.4.2 Assembly configuration 2

The second assembly configuration was to use different adhesives with a stronger bond with the UHMWPE. Super glue all plastics (Henkel Ltd, Hertfordshire, UK) was used as an alternative adhesive to bond the PU sheath with the ball and socket (S2-B2), as shown in Figure 6.5. This super glue was formulated for hard bonding plastics such as UHMWPE. This super glue package contained an activator and the super glue itself. The general cleaning of the ball and socket samples was applied before the assembly using this adhesive. The activator was used before the adhesive to stimulate the UHMWPE and PU surface and was placed on the attachment surfaces, increasing their bonding energy and to strengthen the joint. The adhesive was then placed on the attachment surfaces of the ball and socket, as described in the first configuration from step 3 to step 10, except super glue all plastics was used instead of using MED – 1511.

Figure 6.5: Ball and socket artificial disc with polyurethane sheath and Super glue all plastics.

6.3.4.3   Assembly configuration 3

Latex rubber was also used in the assembly configuration 3 as an alternative to assess the effect of the encapsulation sheath on testing. A latex balloon with wall thickness of 0.45 mm and outer diameter of 25 mm and 65 mm length was cut from the straight part (the neck of a balloon) and was taken and attached to the ball and socket artificial disc (S5-B4 and S6-B5) using MED – 1511, as shown in Figure 6.6. The general cleaning method was the same as in section 6.3.3. The assembly method was undertaken using the steps below:

1. A layer of MED – 1511 adhesive was spread on the attachment areas of the socket and then the socket was inserted inside the latex rubber from one side.

2. The attached sockets with the latex rubber left to dry for 24 hours.

3. A layer of MED – 1511 adhesive was spread on the attachment regions of the ball and then the ball was inserted inside the latex rubber.

4. Then the entire assembly configuration was left to dry for 24 hours.

5. After that, the steps from 8-10 from assembly configuration 1 was applied on this assembly configuration.

Figure 6.6: Latex rubber balloon attached to the ball and socket artificial disc using MED – 1511.

6.3.4.4   Assembly configuration 4

Butyl rubber (Halfords Group plc, Worcestershire, UK) with 0.9 mm thickness, 28 mm outer diameter and 65 mm length was used as a sheath to encapsulate the artificial disc (S1-B1), where S1 is socket 1 and B1 is ball 1, bonded using the super glue all plastics, as shown in Figure 6.7. The general cleaning method, as described in section 6.3.3, was applied to the ball and socket samples before the assembly. The assembly procedure was the same with the assembly configuration 3, but with changing the adhesive to super glue all plastics and changing the sheath to butyl rubber.

Figure 6.7: Butyl rubber attached to the ball and socket artificial disc using Super glue all plastics.

6.4 Mechanical testing

6.4.1 Wear testing

Wear tests were performed for the encapsulated artificial discs according to the standards BS ISO 18192-1:2011 (BS ISO 18192-1, 2011) standard and SOP01.6 using the Bose spine simulator SDWS-1 (Bose Corporation, Minnesota, USA). The sinusoidal motions used for the wear tests were +6º for the flexion motion, extension motion with -3º, lateral bending motion from -2º to +2º and axial rotation from -2º to +2º applied continuously with 1 Hz frequency. A sinusoidally varying load from 600 to 2000 N was applied at a frequency of 2 Hz, as shown in Figure 6.8. The lubricant PVA C (20 g per 100 mL of distilled water) was used inside the encapsulated artificial disc between the ball and socket joint. A saline fluid surrounded the encapsulated artificial discs during the tests and the temperature was maintained at 37º in the fluid bath. The wear tests were

run for two millions cycles under the different described motions and loads for three encapsulated artificial discs. The wear of artificial discs have previously been shown to reach a steady state value after the two millions cycles (Grupp *et al.*, 2009). The masses of the UHMWPE sockets were weighted using an Ohaus GA200D balance with $\pm$ 0.2 mg precision (Ohaus Scales and Balances, Norfolk, UK). Each specimen was weighted nine times and the mean mass was calculated for each specimen.
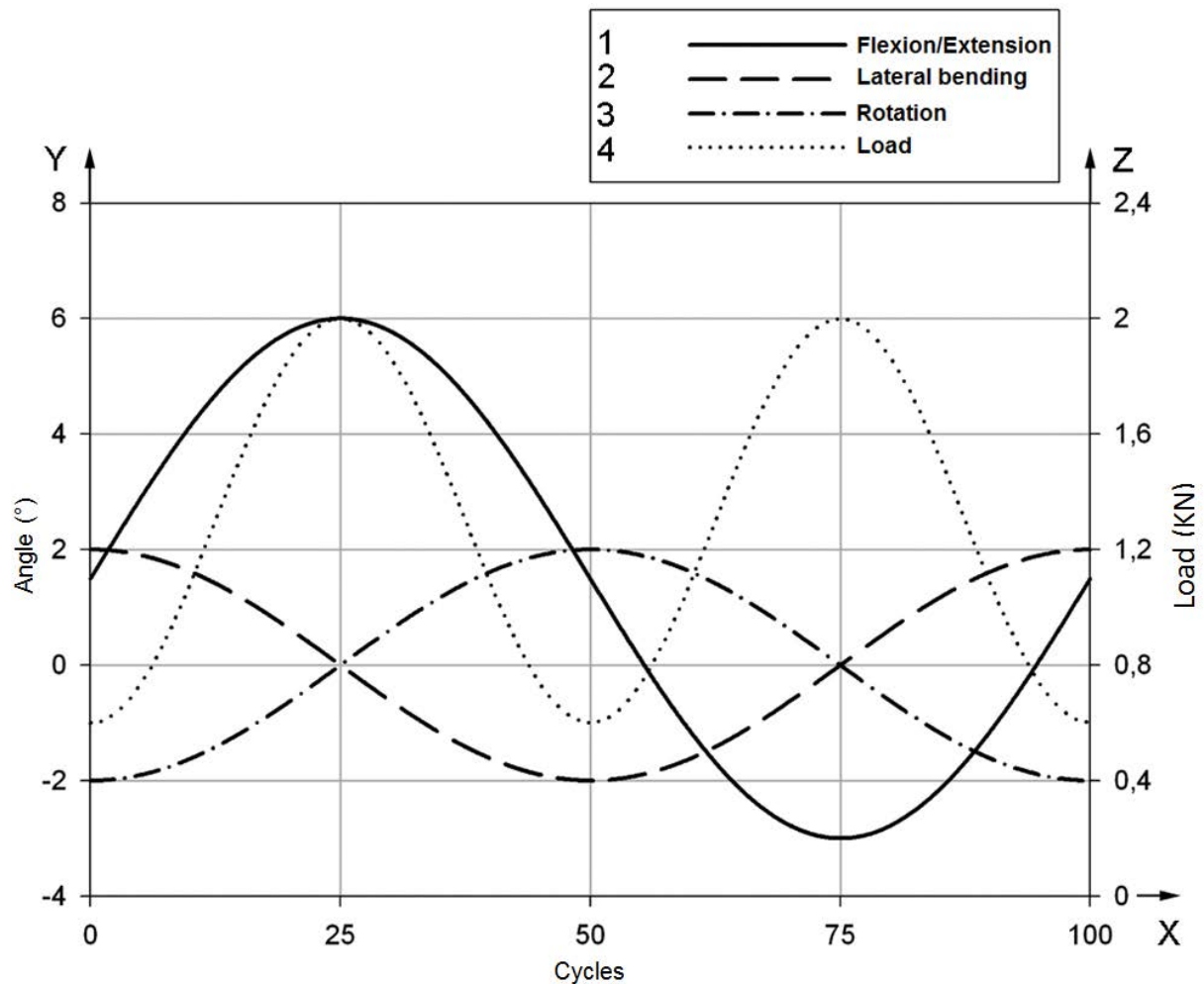
Figure 6.8: The different motions and load used in the wear testing (BS ISO 18192-1, 2011). The x-axis was magnified on the scale of 100:1.

6.4.2 Bose spine simulator

The Bose spine simulator SDWS-1 Simulator (Bose Corporation, ElectroForce Systems Group, MN, USA) is a device for testing artificial discs which will allow the different spine motions to be applied on the artificial disc. These devices are controlled using Bose's WinTest® 4.1

software (Bose Corporation, ElectroForce Systems Group, MN, USA). The simulators are capable of applying a 3000 N axial load with ± 15° flexion/extension, ± 12° lateral bend, ± 9° axial rotation with four degrees of freedom (DOF). Each of the spine simulators has a load cell attached to the bottom plate, as shown in Figures 6.9 and 6.10. Two of the spine simulators are used for the wear tests because the load cell (uni-axial Bose 1010CCH-1K-B) does not give frictional torque measurements. However, the third spine simulator can provide frictional torque measurements with a precision of 0.01 N.m as it incorporates a Bose multi-axial load cell (AMTI MC3-6-1000). All the load cells are calibrated every twelve months by the manufacturer. A Perspex chamber (water bath) can be fitted to the lower plate and the fluid contained within can be heated through the lower plate. The water bath was used to insert the artificial disc to the bottom plate and the temperature was transferred from the bottom plate. The heat was controlled by the heating controller and was connected with the computer to be controlled by the software. A thermocouple probe was attached to the chamber to give continuous temperature readings. Split clamps were used to attach the top and bottom plates to the spine simulator. The artificial disc was attached to the bottom and top plates using screws. The bottom plate moves vertically (Y axis) ± 12 mm and can move ± 5 mm in the horizontal directions (X axis), as shown in Figure 6.10. However, the top plate cannot move vertically or horizontally. The clearance between the upper and lower plate is 100 mm at the zero position, which is controlled by the software.
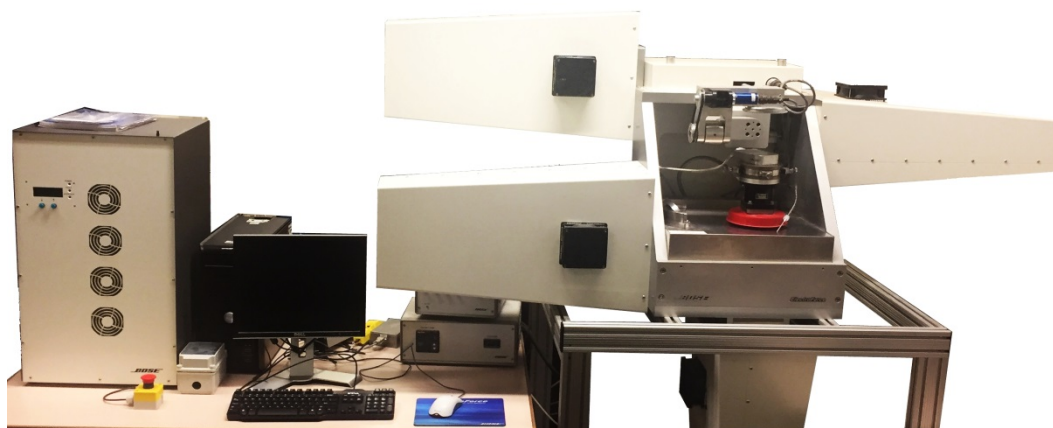
Figure 6.9: Bose spine simulator SDWS-1 Simulator, with multi-axial AMTI MC3-6-1000 load.
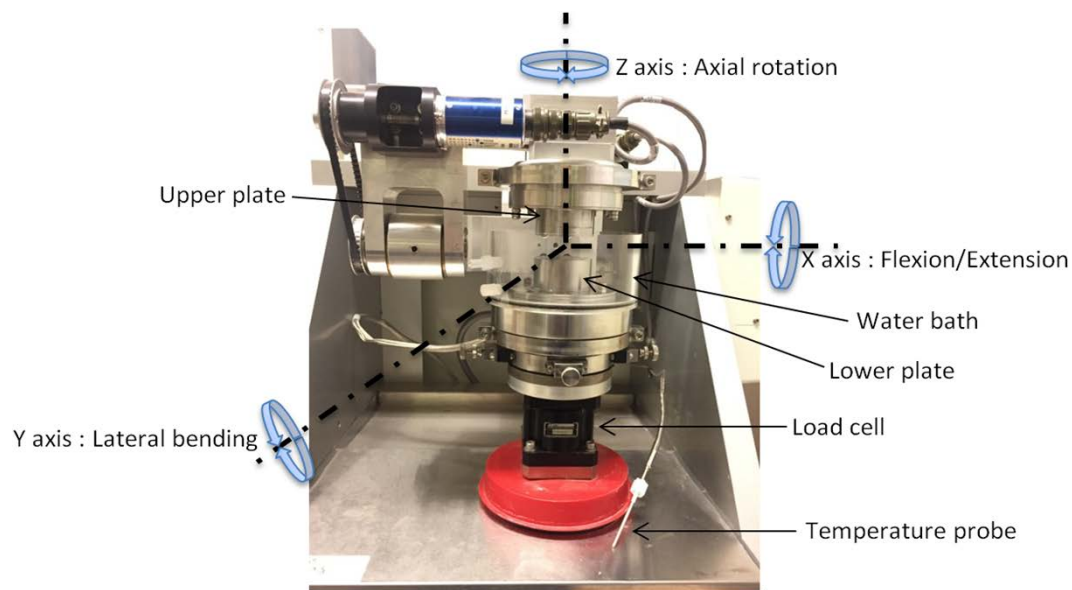
Figure 6.10: Features of the testing chamber of the Bose spine simulator SDWS-1 Simulator.

6.4.3 Assembly configuration tests

S1-B1 and S2-B2 in configuration 1 encapsulated artificial discs were wear tested, as described in section 6.4.1) using the Bose spine simulator SDWS-1. Both the configurations showed lubricant leakage before reaching 10000 cycles, as shown in Table 6.1. The lubricant leakage was from the attachment between the UHMWPE and the PU sheath. Configuration 2, with the use of the S2-B2 disc and PU sheath with super glue all plastics, started to leak lubricant before 7500 cycles which led to stopping the test. The latex sheath was peeling from configuration 3 or detaching from the adhesive before testing, due to the weak bonding between the latex and the MED – 1511 adhesive. The butyl rubber with the super glue in configuration 4 formed a very strong bond with the artificial disc. It was noticed that it was difficult to remove the sheath using acetone without damaging the UHMWPE socket or leaving some pieces of butyl rubber attached to the socket that means that after the wear tests there will be a few pieces of butyl rubber after cleaning the samples (using acetone), affecting the mass measurements.

Table 6.1: The different assembly configurations with the wear testing results. S refers to the socket and B refers to the ball.

Assembly configuration	Socket	Ball	Sheath	Method of attachment	Wear Cycles achieved before failure wear testing
Assembly configuration1	S1	B1	PU	MED - 1511	Less than 10000
Assembly configuration1	S2	B2	PU	MED - 1511	Less than 10000
Assembly configuration2	S2	B2	PU	Super glue all plastics	Less than 7500 cycles
Assembly configuration3	S5	B4	Latex balloon 0.45 mm thickness	MED – 1511	Latex was peeling off easily from adhesive before wear testing
Assembly configuration3	S6	B5	Latex balloon 0.45 mm thickness	MED – 1511	Latex was peeling off easily from adhesive before wear testing
Assembly configuration4	S1	B1	Butyl inner tube	Super glue all plastics	Causing damage to sample after removal before wear testing

6.5   Discussion

The main performance indicator in the evaluation of the encapsulated artificial disc was to keep the lubricant inside the capsule by preventing any leakage to the surroundings. In the case of leakage this will be a sign of failure because wear particles will start to reach the surrounding tissue and the main problem of osteolysis caused by wear debris, as mentioned in chapter 2, of the ball and socket artificial disc will remain.

Configuration 1 failed before reaching 10000 cycles as mentioned in the results. This was due to the low surface energy of the UHMWPE which does not allow the adhesive to have a strong bond with the PU sheath. The most important factor for the successful adhesive bonding is the spreading of the adhesive on the surfaces that need to be bonded and the wettability of the adhesive on the bonded surfaces. In order to achieve a strong adhesive bonding the bonded surfaces must have a high surface energy to overcome the surface tension forces resulting from the adhesive and leading to a strong bond (Ebnesajjad and Ebnesajjad, 2006). Some plastics, such as polyethylene and fluoroplastics, have a low surface energy (Dunn, 2003). Therefore, a special treatment (such as plasma treatment) is needed for these plastics to increase their low surface energy and thus increase their ability to bond (Noeske *et al.*, 2004). Plasma treatment is the procedure of exposing the target area of the polymer to a gas such as oxygen that is activated by radiofrequency energy. It will remove the weak boundary layers on the bonding surface and will oxidise the surface which will lead to increase the adhesive bonding strength on that surface (Dunn, 2004). Unfortunately, this treatment could not be applied on the sockets in this chapter due to the lack of equipment needed for this process.

The encapsulated artificial disc, using super glue all plastics with the polyurethane sheath, in configuration 2 lasted for less than 7500 cycles. The reason behind this was again the low surface energy of the UHMWPE. It was concluded that the UHMWPE has to be treated by plasma to give the required adhesion which might last for longer wear testing. In addition, the thickness of the polyurethane sheath, which is 2 mm, might lead to greater stiffness during the angular motions (flexion, extension and lateral bending) which will produce a higher peeling force and thus will reduce the life time of the adhesive bond. The peeling force is a force applied on a flexible sheath bonded by an adhesive with a rigid body by applying a constant force with a peeling angle between 20 to 170 degrees, as shown in Figure 6.11 (Williams and Kauzlarich, 2004). Latex rubber with 0.45 mm thickness was used to replace the polyurethane sheath with the use of the MED-1511 adhesive, as described in configuration 3. However, the smooth surface of the latex meant that the MED-1511 adhesive was ineffective in bonding and started to detach during the assembly and before starting the wear test. The latex sheath was replaced with butyl inner tube and this time super glue all plastics was used instead of the MED-1511 due to the weak bond that was noticed with the previous sheaths, as described in configuration 4. The butyl inner tube formed a strong bond with the socket and ball parts, but it might lose the bond with the long wear testing (two million cycles at least). However, it was not tested on the wear test because it was very difficult to remove it from the socket part after the wear test. The removal of the adhesives is usually undertaken using acetone. However, the butyl inner tube formed a barrier between the acetone and the adhesive which made the sheath difficult to remove without using a scalpel. Removing the sheath this way could damage the UHMWPE.
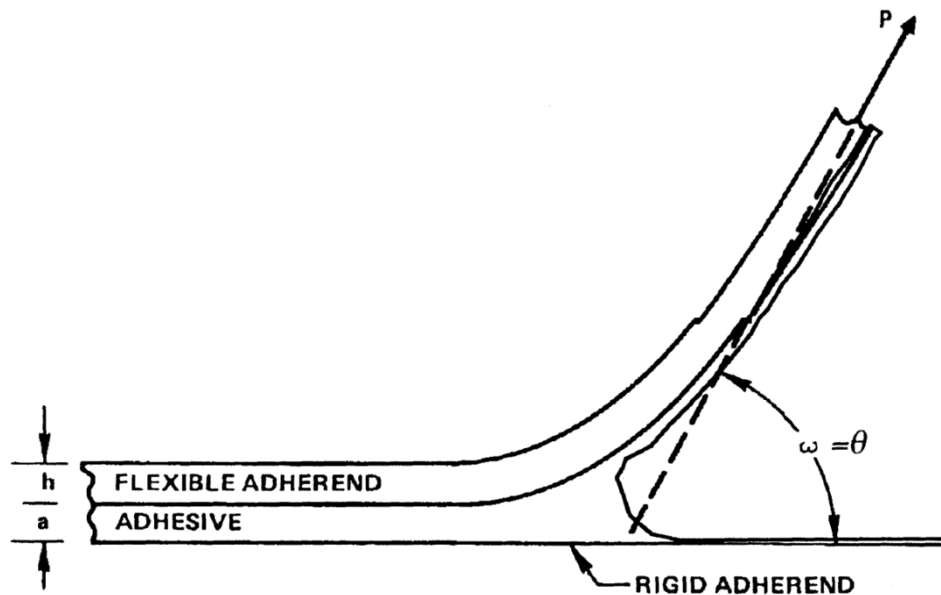
Figure 6.11: Simplified view of peeling force affecting the adhesive bond with the sheath (Williams and Kauzlarich, 2004). Reprinted with permission from Taylor & Francis.

6.6   Conclusion

This chapter evaluated the attachment methods of the encapsulated artificial discs. The conclusions from this chapter are:

- Assembly configuration 1 with MED – 1511 and polyurethane sheath started leaking before reaching 10000 cycles of wear testing.

- Super glue all plastics lasted less than 7500 cycles during the wear test using the polyurethane sheath in assembly configuration 2.

- The UHMWPE surface should be treated to increase the surface energy and thus increase the bond strength with adhesives.

- Sheath thickness and hardness might lead to a stiffer sheath which will lead to weakening the adhesive bond by applying a higher peeling force.

Another configuration which solved most of the limitations discussed here will be presented in chapter 7. Further testing on the resistive torque and wear will be discussed in the coming chapter.

7 The effect of encapsulating the ball and socket artificial disc on the resistive torque and wear

7.1 Overview

This chapter presents the effect of encapsulating the ball and socket artificial disc on the resistive torque and the wear of the final design. In section 7.2 there will be an introduction to the resistive torque and wear of artificial discs. After that, in section 7.3, there is a description of the methods used to perform the different tests on the encapsulated artificial disc. In section 7.4, the results of the different tests that were undertaken are presented. After that the results are discussed and compared with previous literature in section 7.5. The last section is the conclusions of the chapter.

7.2   Introduction

Prior to any clinical trial there must be a series of comprehensive pre-clinical mechanical tests which will include tribological analysis measuring both resistive torque and wear. Resistive torque, for the purposes of this work is defined as the frictional torque from the rolling and sliding of the socket against the ball and the stiffness resulting from the resistance in the elastomer sheaths. In the previous chapter there was an evaluation of the method of attachment and the different sheaths that have been used for encapsulation. However, in this chapter there will be an understanding of wear produced during the articulation of the bearing surfaces within the artificial disc. In addition, testing the resistive torque and comparing it with other studies is a valuable factor that should be focused on, as a high resistive torque could lead to loosening of the artificial disc as has been described for hip implants (Brockett *et al.*, 2007; Simon *et al.*, 1975) which could have the same effect on the artificial discs.

The encapsulation with a lubricant inside was applied on the ball and socket artificial discs for the lumbar region in this study, as shown in Figure 7.1. The aim of this chapter was to compare the resistive torque of the artificial discs with and without encapsulation for the different motions (flexion, extension and lateral bending). A further aim was to generate Stribeck curves for the artificial discs without encapsulation at different frequencies for the different motions. In addition to this the gravimetric wear rate after encapsulating the artificial disc after two million cycles *in vitro* was also measured.
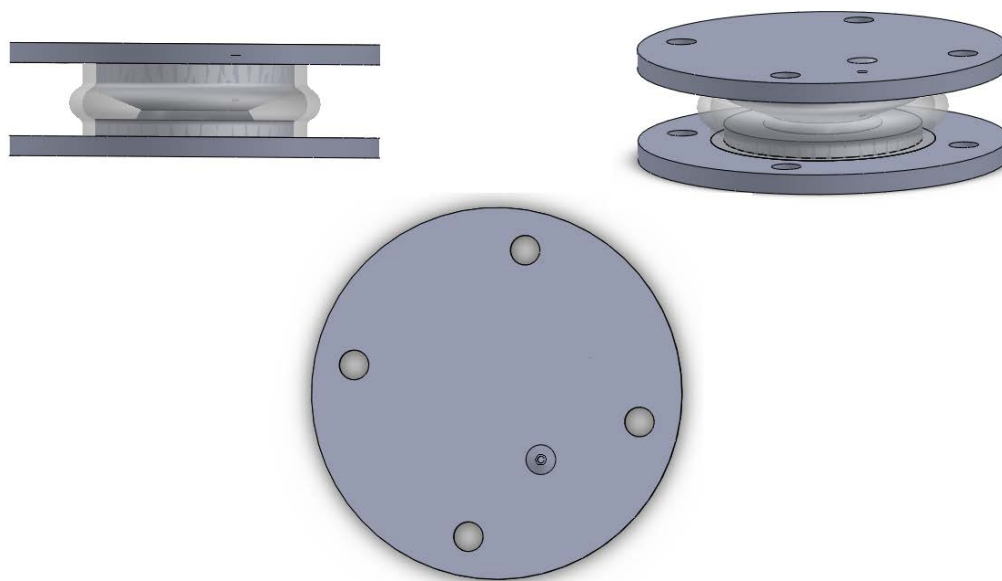
Figure 7.1: Encapsulated ball and socket artificial disc with the polyurethane sheath.

7.3   Materials and methods

7.3.1 Assembly configuration 1

Assembly configuration 1 was used in this chapter for both the resistive torque and wear testing. This assembly configuration was fully described in chapter 6 in section 6.3.4.1.

7.3.2 Assembly configuration 5

In configuration 5, a wire hose clamp was used as a sealing and attachment method instead of adhesive, as the adhesives required more surface treatment as discussed in section 6.5. A

polyolefin (polyethylene) heat shrink tube (Hilltop Products Ltd, Greater Manchester, UK) was used instead of polyurethane sheath as an encapsulation sheath from a 1 m length tube with a 0.8 mm wall thickness and a diameter of 60 mm diameter with 95 shore A hardness, bought from Hilltop Products Ltd (Greater Manchester, UK). The sheath was cut into different pieces with the same thickness and with 80 mm length, then was fitted using a heat gun (Bosch, Stuttgart, Germany) to the artificial disc with final dimensions of 58 mm diameter and 74 mm length, as shown in Figure 7.2. The wire hose clamp and the polyolefin (polyethylene) heat shrink were used after the failure of the adhesive and the polyurethane sheath in configuration 1 as described in details in section 6.4.3. The polyethylene heat shrink sheath was fitted to the lower and upper plates using a double wire hose clamp (WilTec Wildanger Technik GmbH, Eschweiler, Germany), as shown in Figure 7.3. The lubricant, PVA C, was selected based on the previous study reported in chapter 4. This configuration was used just to continue with the wear testing of the encapsulated artificial disc but it was not a final solution for the main encapsulated artificial disc design which is configuration 1.

Figure 7.2: The ball attached to the polyethylene heat shrink sheath and the lower plate using a double wire hose clamp before inserting the lubricant.

Figure 7.3: The assembly configuration 5, mounted on the Bose spinal simulator. The sheath is fixed using a double wire hose clamp, the PVA C lubricant contains a red dye and the whole device is surrounded by saline solution (9.5 g/L of sodium chloride in deionized water).

7.3.3 Resistive torque tests

The resistive torque tests were undertaken according to the standards BS ISO 18192-1:2011 and ASTM F2423-05 (ASTM F2423 - 05, 2005; BS ISO 18192-1, 2011) which describe wear testing procedures for artificial disc implants. The resistive torque represents the frictional torque produced from the ball and socket articulation and the stiffness resulting from the sheath. All the

resistive torque tests were performed using the Bose spine simulator SDWS-1 (Bose Corporation, Minnesota, USA), as described in section 6.4.2. All the tests were performed under a 1200 N constant axial compressive force. The flexion tests were from 0 to 6 °, the extension tests from 0 to 3° and lateral bending tests were performed from -2 to 2°. All tests were completed at frequencies from 0 to 2 Hz with 0.25 increments. Each resistive torque test was performed for 100 cycles and the mean for the last 10 peak values was taken as the resistive torque. The standard error (as described in section 5.3.2.9) was measured for the number of artificial discs that have been used for each lubricant. The resistive torques were measured for different sockets and balls with encapsulation and without (as a benchmark) three times for all the different motions, as described in Table 7.1 and Figure 7.4. A graph with the resistive torque against frequency was plotted for each movement using Microsoft Excel (Microsoft Office, Washington, USA).

Table 7.1: Resistive torque testing conditions for the artificial discs with and without encapsulation.

Socket (UHMWPE)	Ball (CoCr)	Sheath (PU)	Lubricant	Number of tests
S5	B4	None	PVA C: 20 g per 100 mL of distilled water	3
S6	B5	None	PVA C: 20 g per 100 mL of distilled water	3
S7	B3	None	PVA C: 20 g per 100 mL of distilled water	3
S1	B1	SH4 (PU)	PVA C: 20 g per 100 mL of distilled water	3
S2	B2	SH5 (PU)	PVA C: 20 g per 100 mL of distilled water	3
S4	B3	SH6 (PU)	PVA C: 20 g per 100 mL of distilled water	3
S3	B3	Heat shrink sheath	PVA C: 20 g per 100 mL of distilled water	3
S9	B1	Heat shrink sheath	PVA C: 20 g per 100 mL of distilled water	3
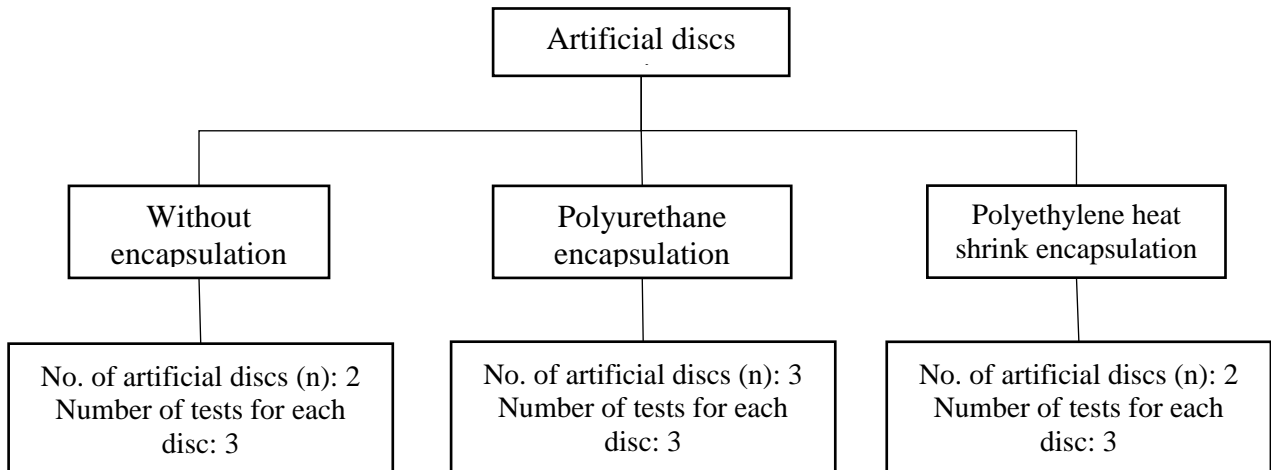
Figure 7.4: Number of samples (n) used for resistive torque testing conditions for the artificial discs with and without encapsulation.

7.3.4 Stribeck analysis

To analyse the lubrication regimes between the ball and socket artificial disc without encapsulation, Stribeck analysis was used (Jin *et al.*, 2006). The friction factor (*f*) was plotted against the Sommerfeld number (Z) to determine the lubrication regime as has been performed previously (Moghadas *et al.*, 2012a; Scholes and Unsworth, 2006). Resistive torque measurements were taken from the Bose spine simulator and the friction factor *f* was calculated from equation [1]:

$$f = \frac{T}{rL} \qquad\qquad [1]$$

where T is the resistive torque between the bearing surfaces, r is the radius of the ball and L is the applied load on the artificial disc. The Sommerfeld number (Z) was calculated from equation [2]:

$$Z = \frac{\eta u r}{L} \qquad [2]$$

where η is the viscosity of the lubricant and u is the entraining velocity between the two bearings surfaces which was calculated from equation [3]:

$$u = \frac{\omega r}{2} \qquad [3]$$

where ω is the angular velocity used during testing (Mattei *et al.*, 2011; Moghadas *et al.*, 2012a; Shaheen and Shepherd, 2007). The angular velocity was calculated from equation [4]:

$$\omega = \frac{2\theta f \pi}{180} \qquad [4]$$

where θ is the angular displacement and f is the motion frequency.

A constant friction factor with increasing Sommerfeld number would be indicative of a boundary lubrication regime, while a decreasing friction factor with increasing Sommerfeld number would be a sign of a mixed lubrication regime. An increasing friction factor with increasing Sommerfeld number is suggestive of a fluid film regime (Brockett and Fisher, 2013; Jones *et al.*, 2009). The lubricant used was PVA C 31,000-50,000 g/mol, 98-99% hydrolysis (20 g of PVA per 100 mL of distilled water) with 1.650 ± 0.01 Pa.s at 22 ºC viscosity, as described previously in chapter 4. At 37 ºC the viscosity of this lubricant dropped to 1.2 ± 0.4 Pa.s at 1000 s^{-1} shear rate; the full graph is shown in appendix B.

7.3.5 Wear testing

The wear test was described in chapter 6, section 6.4.1. The lubricant PVA C (20 g per 100 mL of distilled water) was used inside the encapsulated artificial disc between the ball and socket joint, as detailed in Table 7.2. The encapsulation sheath was the polyethylene heat shrink tube as described in section 7.3.1. A saline fluid surrounded the encapsulated artificial discs during the tests and the temperature was maintained at 37° C in the fluid bath. The wear tests were run for two millions cycles under the different described motions and loads for three encapsulated artificial discs. The sinusoidal motions used for the wear tests were $+6^o$ for the flexion motion, extension motion with -3°, lateral bending motion from -2° to $+2^o$ and axial rotation from -2° to $+2^o$ applied continuously with 1 Hz frequency. A sinusoidally varying load from 600 to 2000 N was applied at a frequency of 2 Hz. The wear tests were undertaken with four degrees of freedom. The wear of artificial discs have previously been shown to reach a steady state value after 2 million cycles (Grupp *et al.*, 2009). The masses of the UHMWPE sockets were weighted before and after testing and using an Ohaus GA200D balance with $\pm$ 0.2 mg precision (Ohaus Scales and Balances, Norfolk, UK). Each specimen was weighted nine times and the mean mass and standard error (as described in section 5.3.2.9) were calculated for each specimen.

There will be no soak control as the PVA lubricant will be inserted in the encapsulated artificial disc exactly before the implant. In addition, the PVA lubricant form a thin layer on the polymer (UHMWPE) which preventing the water from getting absorbed by the polymer (UHMWPE) that it is lubricating (Krantz *et al.*, 1986). Furthermore, Liao and Hanes (2006) have found that the soaking has no significance effect on the wear performance of the polyethylene.

Table 7.2: Wear testing conditions for the encapsulated artificial discs.

Socket (UHMWPE)	Ball (CoCr)	Sheath (PU)	Lubricant
S8	B4	polyethylene heat shrink tube	PVA C: 20 g per 100 mL of distilled water
S7	B5	polyethylene heat shrink tube	PVA C: 20 g per 100 mL of distilled water
S10	B2	polyethylene heat shrink tube	PVA C: 20 g per 100 mL of distilled water

7.3.6 Surface roughness

The surface roughness of the ball and socket was measured using an Alicona G5 InfiniteFocus (Alicona Imaging GmbH, Raaba, Austria) using 10× magnification before and after the resistive torque and wear tests. Each socket and ball was measured three times in different positions on the bearing surfaces to calculate the mean surface roughness and standard deviation.

7.4   Results

7.4.1 Resistive torque and Stribeck curve results

The mean resistive torque changed with frequency for the flexion motion of the artificial discs with and without encapsulation. The mean resistive torque was the lowest for the polyethylene heat shrink encapsulated artificial discs in flexion motion. The mean resistive torque increased in

the flexion motion for the polyurethane encapsulated artificial discs. The highest mean resistive torque was for the artificial discs without any encapsulation. The mean resistive torque decreased with frequency for all artificial discs with and without encapsulation for flexion motion, as shown in Figure 7.5. The highest mean resistive torque for the artificial disc without encapsulation was for the flexion motion which reached 4.7 N.m at 0.25 Hz frequency and the lowest point was at 2 Hz with 4.15 N.m. For the same motion the polyurethane encapsulated artificial disc had a highest mean resistive torque of 3.9 N.m at 0.25 Hz frequency and a lowest mean resistive torque of 2.9 N.m at 2 Hz frequency. For the same motion the polyethylene heat shrink encapsulated artificial disc had the highest mean resistive torque of 1.9 N.m at 0.25 Hz frequency and the lowest was 1.73 N.m at 2 Hz frequency.
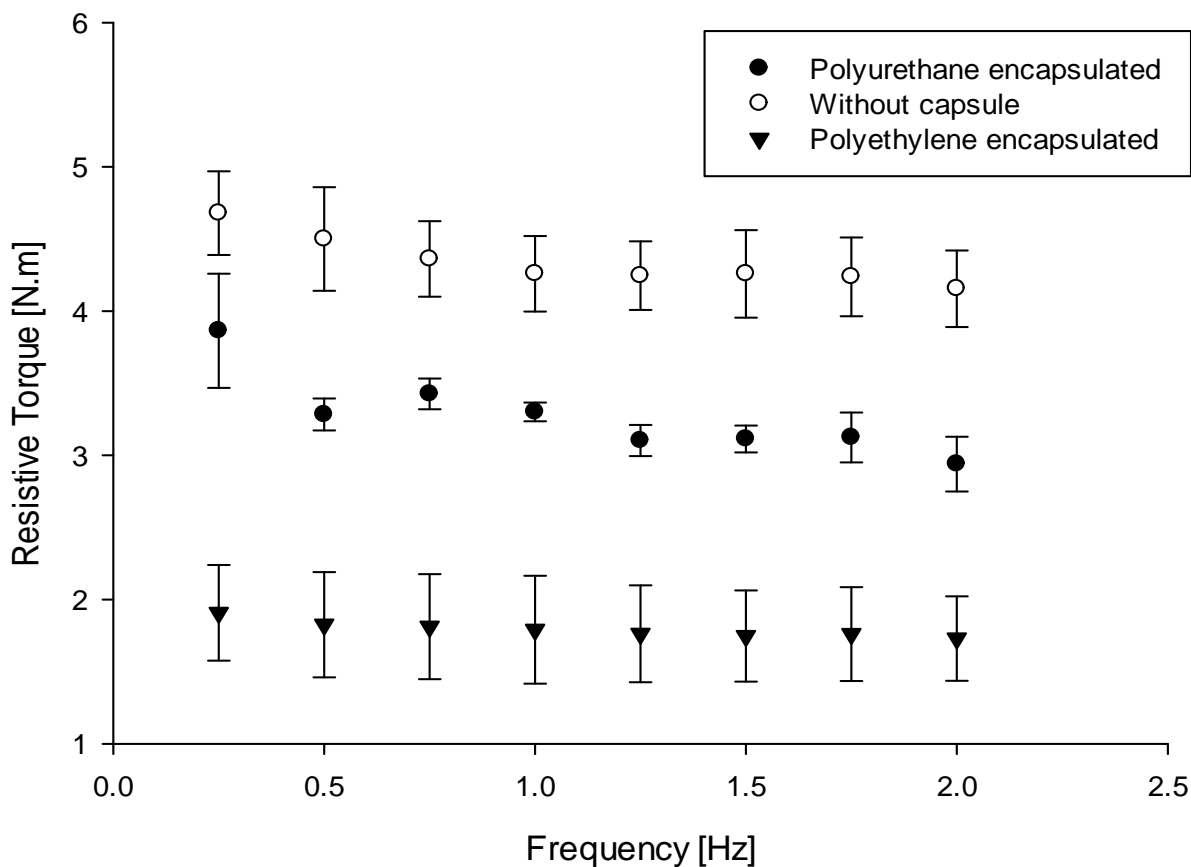
Figure 7.5: Mean resistive torque with frequency for the three artificial discs with and without encapsulation for flexion motion. Error bars represent standard error.

The mean resistive torques for the extension motion for the artificial discs with and without encapsulation, are shown in Figure 7.6. The mean resistive torque was lower for the polyurethane encapsulated artificial disc than the artificial discs without encapsulation at all the different frequencies for the extension motion. The lowest mean resistive torque was for the polyethylene

heat shrink encapsulated artificial disc. The mean resistive torque was nearly constant with frequency for the artificial disc without encapsulation for the extension motion. However, resistive torque did increase with frequency for the same motion for both the encapsulated artificial discs with polyurethane and polyethylene heat shrink encapsulations. The mean resistive torque for the extension motion for the artificial disc without encapsulation was about 2 N.m for all the frequencies. The mean resistive torque for the polyurethane encapsulated artificial disc was 0.96 at 0.25 Hz and 2 N.m at 2 Hz for the extension motion. The mean resistive torque for the polyethylene heat shrink encapsulated artificial discs was 0.94 N.m at 0.25 Hz and 1.3 N.m at 2 Hz for the same motion.
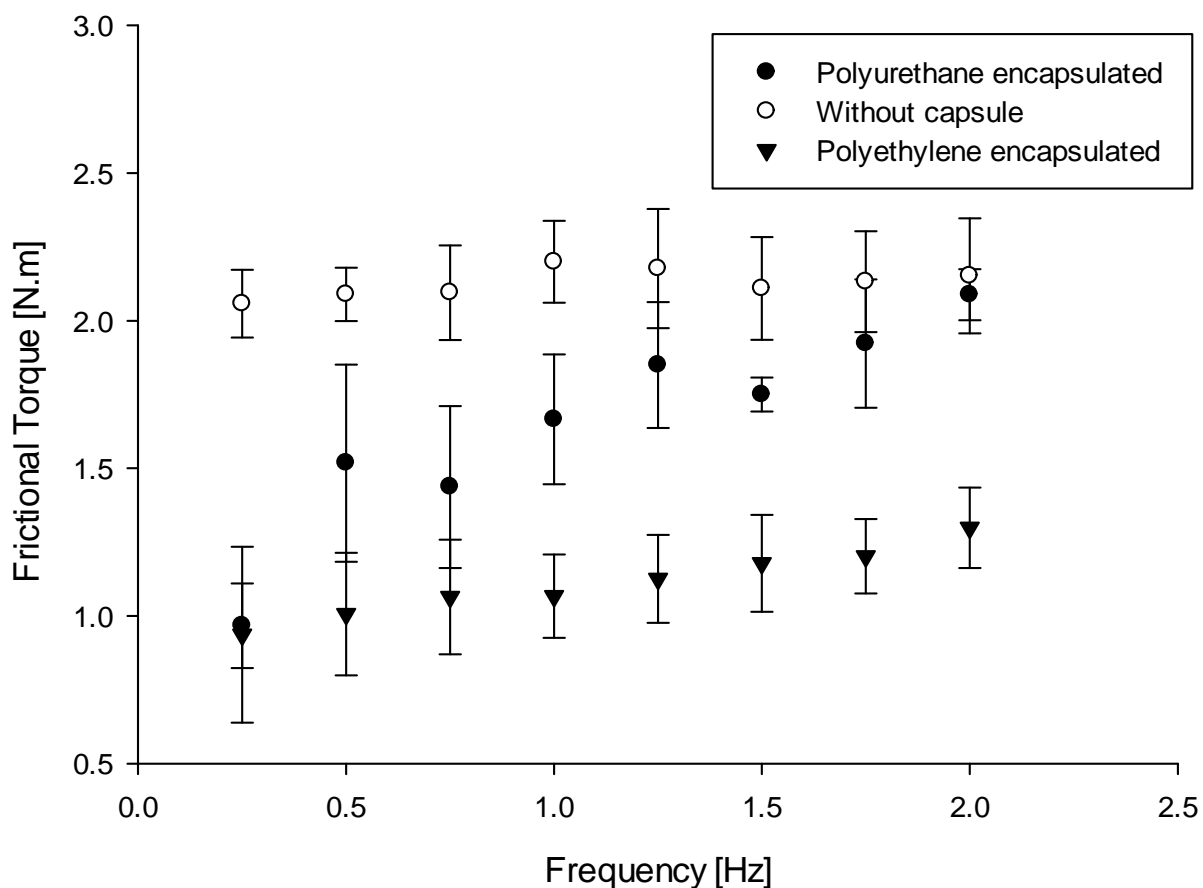
Figure 7.6: Mean resistive torque with frequency for the three artificial discs with and without encapsulation for extension motion. Error bars represent standard error, for clarity only positive error bars have been added.

The mean resistive torque for lateral bending decreased with frequency for the artificial discs without encapsulation. However, it increased with frequency for both encapsulated artificial discs for the same motion, as shown in Figure 7.7. The highest mean resistive torque for the artificial

discs without encapsulation was 1.03 N.m at 0.5 Hz and the lowest was 0.86 N.m at 2 Hz for lateral bending motion. The lowest mean resistive torque for the artificial discs with polyurethane encapsulation for lateral bending motion was 0.85 N.m at 0.25 Hz and the highest was 1.1 N.m at 2 Hz. The lowest mean resistive torque for the artificial discs with polyethylene heat shrink encapsulation for lateral bending motion was 0.64 N.m at 0.25 Hz and the highest was 0.96 N.m at 2 Hz, as shown in Figure 7.7.
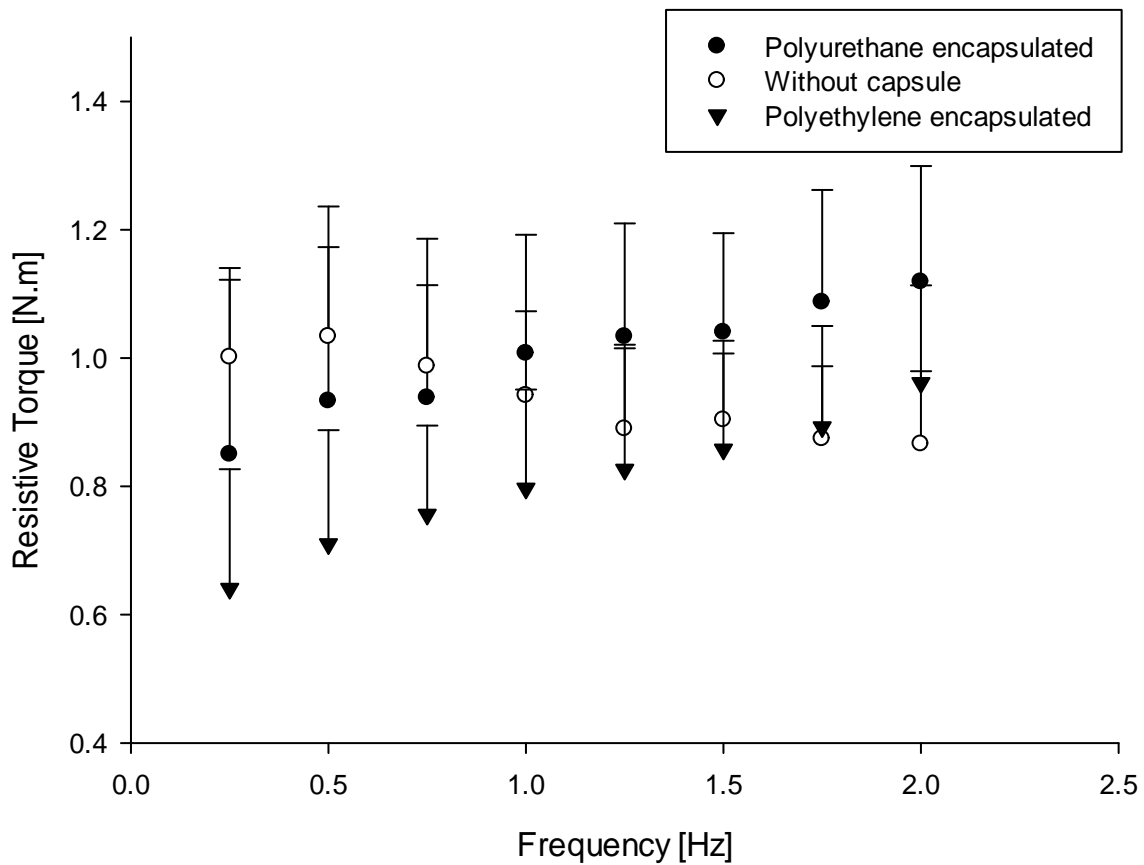
Figure 7.7: Mean resistive torque with frequency for the three artificial discs with and without encapsulation for lateral bending motion. Error bars represent standard error, for clarity only positive error bars have been added.

The mean resistive torque was the highest for the flexion motion in the artificial discs without encapsulation. The mean resistive torque was lower for the extension motion than the flexion motion in the artificial discs without encapsulation. The lowest mean resistive torque was for

lateral bending motions in the artificial discs without encapsulation, as shown in Figure 7.8. This trend was the same as well for all the encapsulated artificial discs.
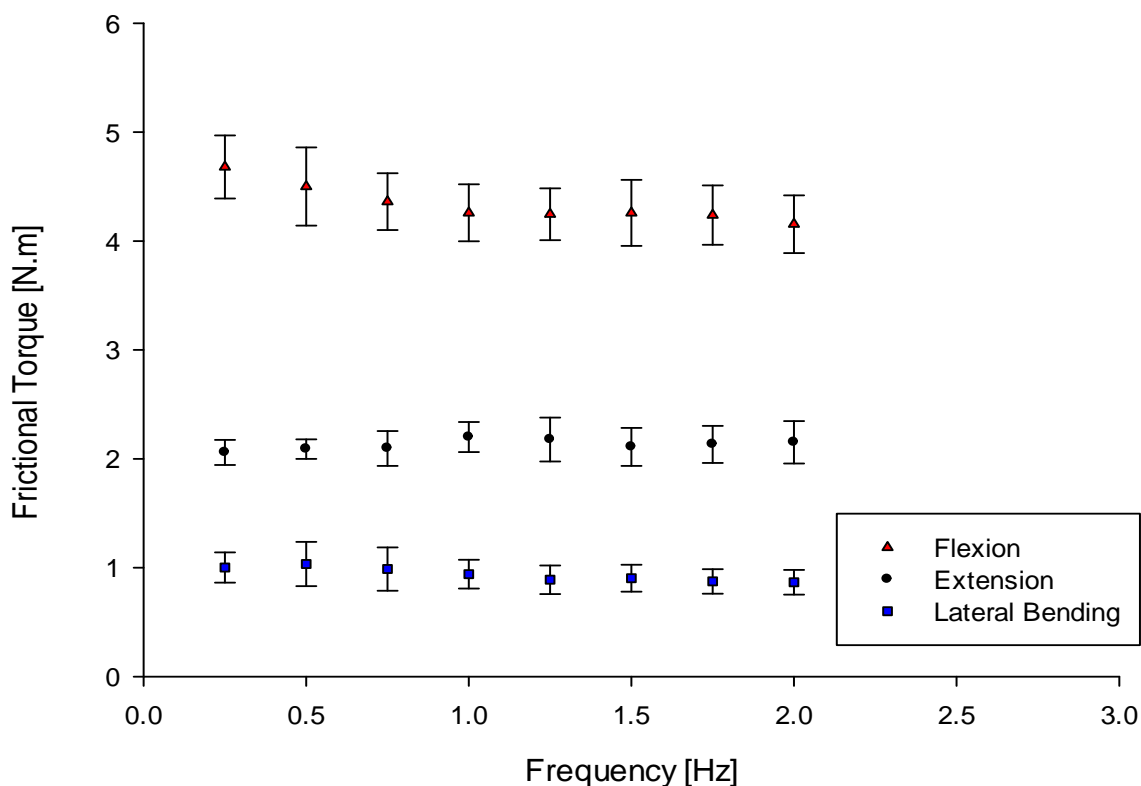
Figure 7.8: Mean resistive torque with frequency for the artificial discs without encapsulation for flexion, extension and lateral bending motion. Error bars represent standard error.

Stribeck curves were plotted to identify the lubrication regimes for the different motions for the three artificial discs without encapsulation. The flexion and lateral bending motion for the discs without encapsulation decreased with increasing Sommerfeld number, which indicated a mixed lubrication regime. However, the extension motion showed a constant friction factor with the

increment of the Sommerfeld number which indicated a boundary lubrication regime, as shown in Figure 7.9.
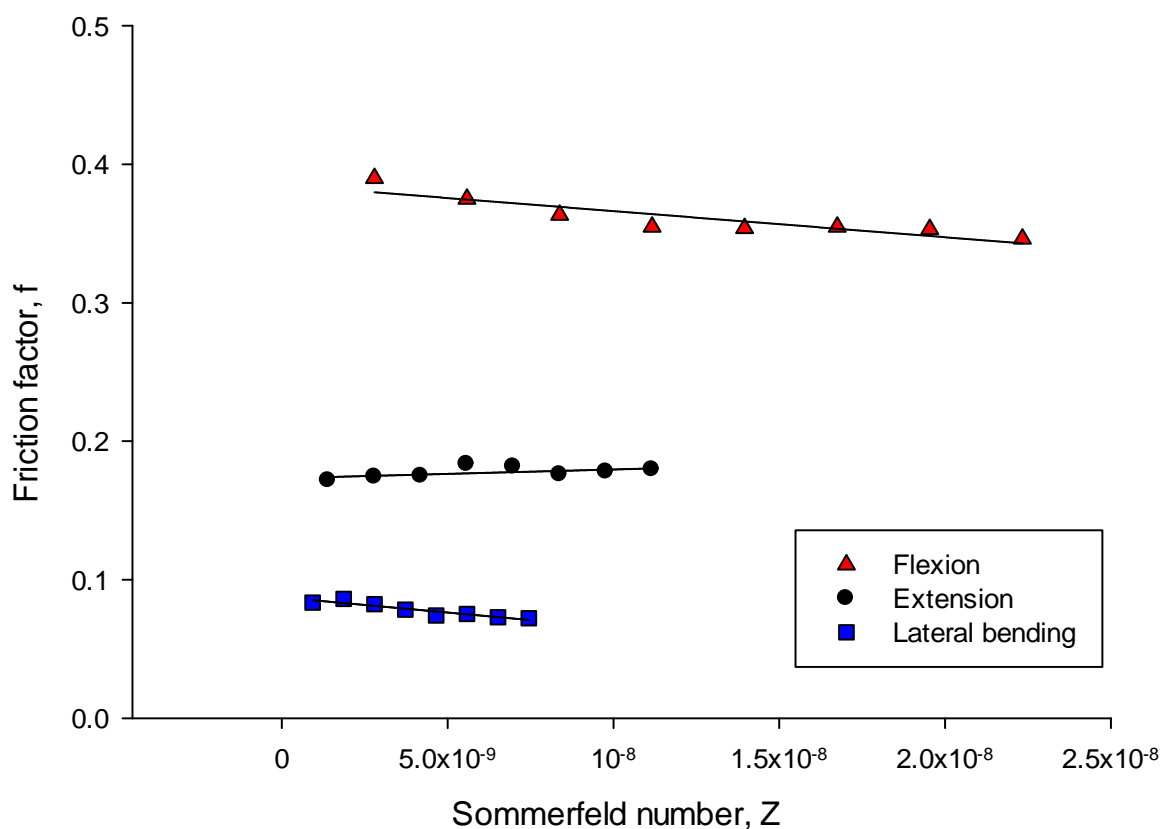
Figure 7.9: Stribeck cure for the three artificial discs for the three different motions without encapsulation.

7.4.2 Wear results

The wear tests lasted for two million cycles without any sign of encapsulation sheath failure or any signs of PVA C lubricant leakage into the surrounding saline solution as it maintained a clear

colour and there was no coloured dye visible from the disc lubricant. The wear tests for the S8-B4 encapsulated artificial disc showed the lowest wear between all the other encapsulated artificial discs. The mean wear mass for S8 was 20.3 ± 0.03 mg which is 10.15 ± 0.02 mg/million cycles and the mean wear volume for the S8 was 21.6 ± 0.03 mm^3. The S7-B5 encapsulated artificial disc showed similar wear results as the S8-B4 encapsulated artificial disc. However, the wear results were slightly higher for the S7-B5 encapsulated artificial disc. The mean wear mass for S7 was 22.6 ± 0.02 mg which is 11.3 ± 0.01 mg/million cycles and the mean wear volume for the same part was 24 ± 0.03 mm^3 after two million cycles. The S10-B2 encapsulated artificial disc had a different trend to the previous two artificial discs showing a high wear mass and volume. The mean wear mass for S10 was 134.1 ± 0.03 mg which is 67.05 ± 0.02 mg/million cycles and the mean wear volume for the same part was 142.7 ± 0.04 mm^3, as shown in Table 7.3.

Table 7.3: The mean mass and volume of the wear resulted from the wear testing and the standard error.

UHMWPE part name	Mean wear mass ± Standard error (mg)	Mean wear volume ± Standard error (mm³)	Mass loss (mg/ million cycles)	Volume loss (mm³/ million cycles)
S8	20.3 ± 0.03	21.6 ± 0.03	10.15 ± 0.02	10.8 ± 0.02
S7	22.6 ± 0.02	24 ± 0.03	11.3 ± 0.01	12 ± 0.02
S10	134.1 ± 0.03	142.7 ± 0.04	67.05 ± 0.02	71.35 ± 0.02

The wear rate for the S10-B2 artificial disc was higher than the other two encapsulated artificial discs. The socket surface showed a smooth surface around the bottom of the socket, as shown in Figure 7.10 denoted by the red colour. However, there was a peak shaped material cluster on the bottom of the socket, as shown in Figure 7.10 with the blue colour.

a   b
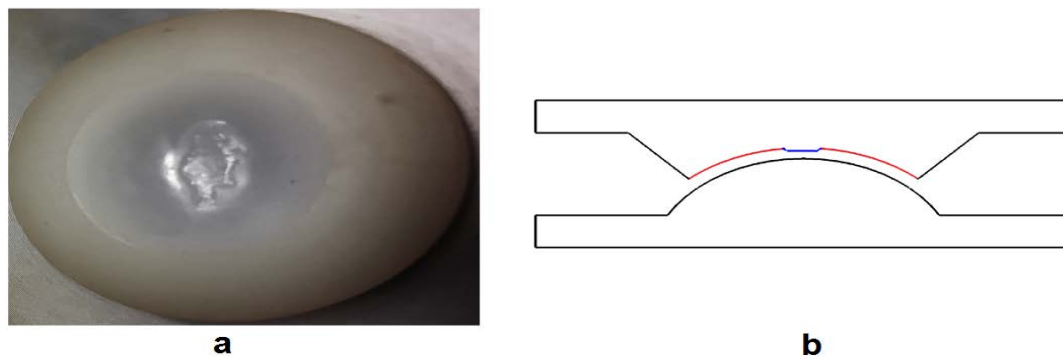
Figure 7.10: S10 socket: a) S10 socket after wear test. b) S10 illustration after 2 million cycles wear testing.

The profile of the edges of the blue peak area and the smooth red area were imaged by normal camera, as shown in Figure 7.11. The profile of the surface showed that the surface had changed to become a peak directly above the centre of rotation then decreased again. The black spots in the images were due to points that could not be picked up by the reflection of the light to the microscope, as this can happen with the scanning of the curved surfaces using the Alicona, as shown in Figure 7.11.
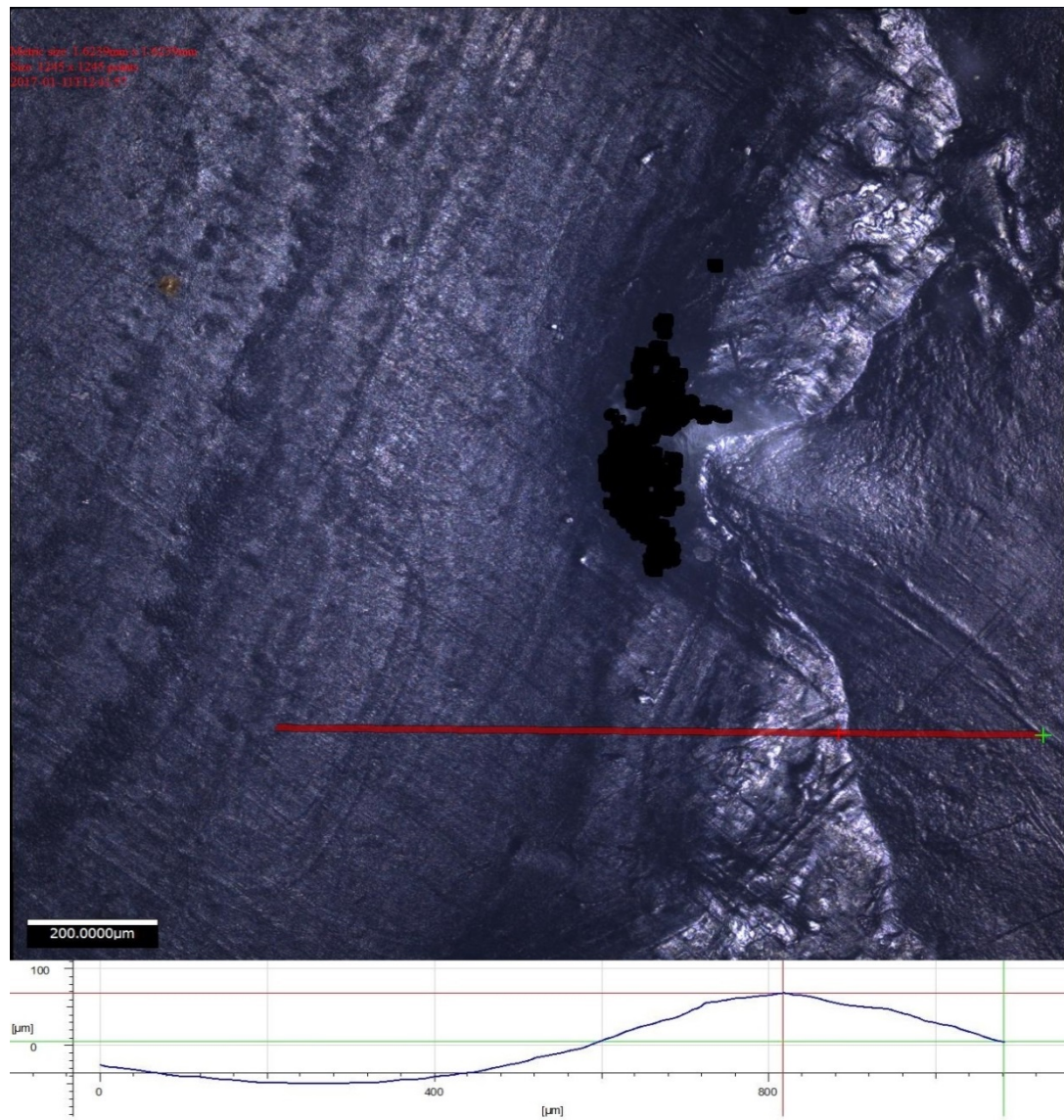
Figure 7.11: Surface imaging by Alicona G5 InfiniteFocus for the bottom of S10 socket. The line chart represents the topography of the surface across the red line on the upper part of the figure.

7.4.3 Surface roughness

The surface roughness was measured for all the samples before the resistive torque and wear testing. In addition to this, the surface roughness was measured for all the samples after wear testing. For the UHMWPE sockets the wear testing resulted in a smoothing of the surface after the testing. However, the effect of the wear testing on the CoCr balls after wear testing was the opposite in which they become more rough in the contacting area, as they were mirror polished before the wear testing, as shown in Table 7.4 and Table 7.5.

Table 7.4: Mean Surface roughness for the different specimens before resistive torque and wear testing.

Specimen number	Mean surface roughness (Ra) (µm)	Standard Deviation (µm)
S1	4.66	1.26
S2	5.34	0.65
S3	3.26	0.35
S4	5.14	1.25
S5	3.29	0.37
S6	3.20	0.46
S7	3.33	0.81
S8	3.88	0.30
S9	3.23	0.22
S10	3.56	0.08
B1	1.67	0.049
B2	1.68	0.119
B3	1.63	0.069
B4	1.75	0.04
B5	1.83	0.045

Table 7.5: Mean Surface roughness for the different specimens after resistive torque and wear testing.

Specimen number	Mean surface roughness (Ra) (µm)	Standard Deviation (µm)
S7	1.7	0.07
S8	1.85	0.01
S10	2.38	0.02
B2	1.7	0.02
B4	2.15	0.03
B5	1.86	0.02

7.5   Discussion

The mean resistive torque results varied for the different motions for the artificial discs with and without capsulation. The flexion motion had the highest resistive torque followed by the extension and the lowest resistive torque was for lateral bending motion. This might be due to the degree of motions for each of them in which the flexion motion within the socket would travel 6° forward and extension motion allowed the socket to travel 3° backward and lateral bending has $\pm2^o$ motion, which is lower than the previous two motion angles, as shown in Figure 7.8. This phenomena could be explained as the friction varies with the sliding distance for UHMWPE as it has been reported previously by McKellop *et al.* (1978). The maximum resistive torque for the polyurethane encapsulated artificial disc was 3.9 N.m for the flexion motion. The maximum mean resistive torque for the polyethylene encapsulated artificial disc was 1.9 N.m for the same motion. The maximum flexural moment for a sheep lumbar functional spinal unit was 7.5 N.m when articulating to 6° of flexion motion which was comparable in the same study with the

human lumbar (Wilke *et al.*, 1997). Thus, all the encapsulated artificial discs achieved lower resistive torque than the natural intervertebral discs under the same motion.

The resistive torque for the encapsulated artificial discs with the polyethylene sheath showed a lower resistive torque for all motions than the encapsulated artificial discs with polyurethane sheath. This can be explained by the polyethylene heat shrink sheath encapsulation being harder (and hence stiffer) than the PU sheath. There is a relationship between the hardness and Young's modulus; as the hardness increases the Young's modulus increases, as shown in Figure 7.12. Young's modulus has a direct relationship with the stiffness as described in this function $k=EA/L$, in which K is stiffness, E is Young's modulus, A is cross sectional area and L is the sheath length (Leckie and Bello, 2009). Using a Young's modulus from Figure 7.12 and calculating the cross sectional area for both sheaths can be used to calculate the stiffness for both of them. The stiffness was 53.1 kN/m for polyurethane sheath and 668.5 kN/m for the polyethylene heat shrink sheath. Therefore, the harder the sheath is the higher the Young's modulus and it would be stiffer taking into consideration the cross sectional area and the sheath length for both materials. The stiffness will result in reducing the total resistive torque by allowing the lubricant to pressurise.

In addition, the method of assembly for both encapsulated artificial discs is different. The encapsulated artificial disc with PU sheath was compressed with an F-clamp as mentioned in step 9 in section 6.3.4.1. However, the assembly method for the polyethylene heat shrink encapsulation was different as described in section 7.3.1. The encapsulation method for the polyethylene heat shrink encapsulation as described in section 7.3.1 in which the socket and upper plate were inserted over the lubricant which was inserted over the ball and the lower plate. This might lead to lubricant separation between the socket and the ball because PVA C is a

viscous lubricant. When the 1200 N load was applied by the spine simulator the volume inside the sheath decreases, increasing the pressure by moving the lubricant from under the contact zone and increasing the pressure within the encapsulation. The polyethylene heat shrink encapsulation is harder than the PU sheath, as described previously. Thus, the harder sheath would have a higher Young's modulus and will retain a higher pressure and the sheath will not expand easily. This will lead to partial separation of the ball and socket during the articulation and will lead to a lower mean resistive torque.
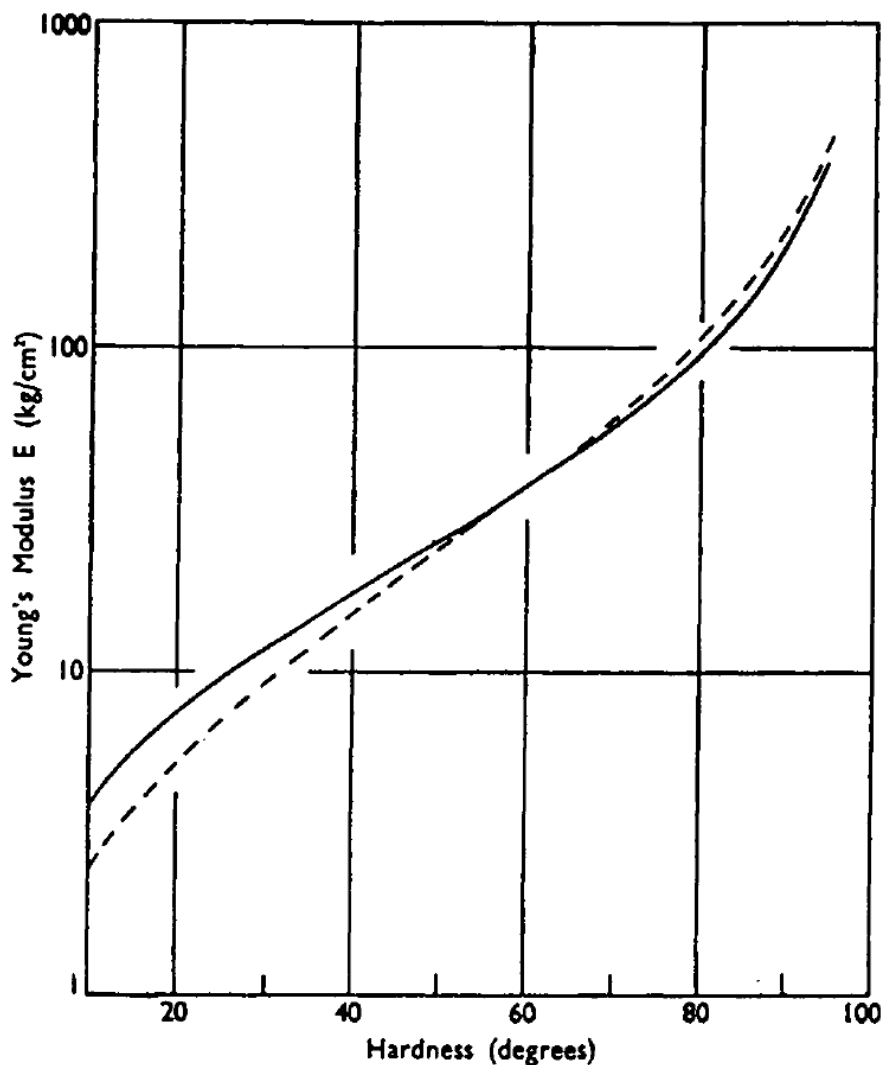
Figure 7.12: relationship between Young's modulus and hardness. The full line is the theoretical measurements and the broken line is the experimental results of different rubbers from BS903 and international rubber hardness (Gent, 1958).

The mean resistive torque for the flexion motion slightly reduced with increasing frequency for the artificial discs, with and without encapsulation, as shown in Figure 7.5. For the extension

motion, the mean resistive torque increased with increasing frequency for the artificial discs with and without encapsulation. Except for the artificial discs without encapsulation which were constant with frequency, as shown in Figure 7.6. For lateral bending, the mean resistive torques for the encapsulated discs increased with frequency, and the opposite was observed when the encapsulation was removed, as shown in Figure 7.7.

The Stribeck curves were plotted for the three artificial discs without encapsulation to identify the lubrication regimes. In flexion motion, the resistive torque decreased with increasing Sommerfeld number which indicates a mixed lubrication regime during the flexion motion. The Stribeck curves for the extension motion showed a boundary lubrication regime. Lateral bending motion indicated a mixed lubrication regime for the artificial discs without encapsulation. The mixed and boundary lubrication regime were shown previously for an UHMWPE socket against CoCr ball without encapsulation, using diluted calf serum (30 ± 2 g/L) as the lubricant (Moghadas, 2012).

Configuration 5 which has the wire hose clamp and the polyolefin (polyethylene) heat shrink sheath were used instead of the main design configuration which is configuration 1 after the failure of the adhesive to continue with the wear testing. This was happened due to the failure of the attachment between the adhesive and the polyurethane surface due to the low surface energy as described in section 6.5. Also, the polyolefin (polyethylene) heat shrink sheath was used instead of the polyurethane sheath to just continue with the wear testing.

The surface roughness of the CoCr samples were high due the previous testing of the ball samples by Moghadas (2012). However, the surface roughness R_a of the metallic components such as the ball should not exceed 0.5 μm (BS EN ISO 21534, 2009).

For the S8 polymer socket the mean mass loss was 10.15 ± 0.02 mg/million cycles and the mass loss for the S7 socket was 11.3 ± 0.01 mg/million cycles. This is a comparable with the previous work on the Charité artificial disc that was wear tested using calf serum lubricant and under similar testing conditions by Moghadas (2012) where the mean mass loss was 12.03 ± 1.4 mg/ million cycles. Also, the mean wear mass for the ProDisc-L was found to be 12.7 ± 2.1 mg/million cycles when previously tested using calf serum lubricant and under similar testing conditions (Vicars *et al.*, 2010). In addition, The mean wear volume for the ProDisc-L with ISO 18192-1 was found to be 17.2 mm^3/ million cycles (Hyde *et al.*, 2015) and 14.4 ± 2.1 mm^3/ million cycles for Charité artificial disc with the same standard (Hyde, 2012; Hyde *et al.*, 2017). There was no evidence of the sheath leaking, hence wear debris was all contained within the device and it was prevented from migrating away from the device. It is difficult to make a direct comparison between the results presented above with those presented in the literature, as very few tests have been conducted for encapsulated devices and none in the lumbar region. The overwhelming majority of *in-vivo* testing of artificial discs are conducted with simulated lubricants, unsheathed and in most cases, the lubricant is changed periodically after thousands of cycles. The result of this is to remove debris from the test and to refresh the lubricant. In the encapsulated tests the lubricant will have been the same throughout the full duration of the tests. Hence this is perhaps a more realistic approximation of *in-vivo* conditions.

The S10-B2 encapsulated artificial disc showed much higher wear results than the other two encapsulated artificial discs (S8-B4 and S7-B5). This is may be due to an air bubble or air pocket formed above the head of the B2 ball head, as shown in Figure 7.13. This air bubble may have prevented the ball and socket from contacting in this region and subsequently distributed further

stresses to the surrounding regions, as shown in Figure 7.13. Increasing the stress on the surrounding regions would increase the friction and thus increase the wear rate. However, an air pocket or bubble might not be the reason behind the high wear rate because this air bubble could circulate outside the ball and socket articulation region during the movement or sliding of the socket against the ball.
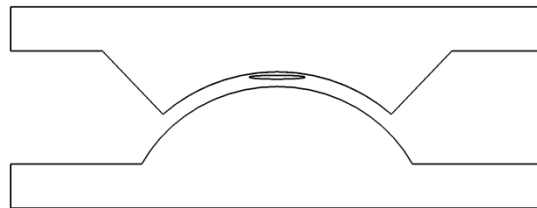
Figure 7.13: Air bubble formed between the ball and socket of the artificial disc.

Another explanation for the higher wear rate in the S10 socket could be as a result of compacted debris that gathered during the wear test near from the top area of the ball and stayed above the original shape of the socket. However, this would not cause the large reduction in the mass of the socket. The wear particles removed from certain parts of the socket and compacted on the bottom of the socket formed peaks of wear debris. This phenomenon did not occur in the other two encapsulated artificial discs. There have been reports of compacted wear debris phenomenon with for example, a steel ball sliding against a polymethyl methacrylate disc. The wear debris compaction formed a peak shape on the polymethyl methacrylate disc (Chateauminois and Briscoe, 2003).

The third explanation for this high wear rate is due to a manufacturing defect in the socket. A nipple shape was formed by a manufacturer defect at the bottom of the socket, as shown in Figure 7.14. This manufacturing defect led to cause small scratches at this area and increase the wear rate to the surrounding regions of the bottom area of the socket.
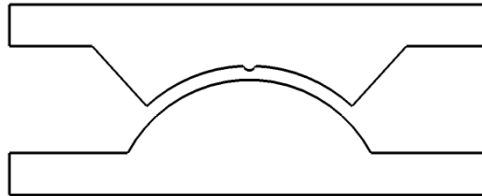
Figure 7.14: A nipple shape caused by a manufacturing defect during the manufacturing process.

The final explanation is similar to the third one in which a manufacturing defect led to cause a flattened surface at the bottom of the socket, as shown in Figure 7.15. The shallow depth of the socket or the flattened shape increased the stress on the sides of the socket during the wear test and led to increase the friction and thus increase the wear rate in that region.
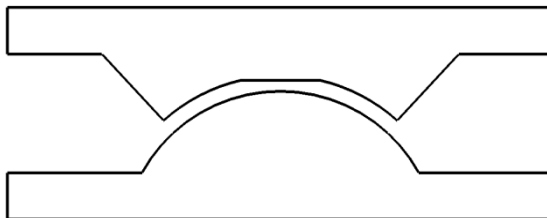
Figure 7.15: A flattened shape caused by a manufacturing defect during the manufacturing process.

7.6   Conclusion

The tribological performance of the encapsulated ball and socket artificial discs were evaluated and compared against artificial discs without encapsulation. The following conclusions can be drawn from this chapter:

- In all tests the mean resistive torque in flexion was the highest followed by extension, with the lowest torque recorded in lateral bending.

- Encapsulating the ball and socket artificial disc reduced the mean resistive torque for all motions.

- polyethylene heat shrink encapsulation produced the lowest resistive torque followed by PU and finally the highest resistive torque was recorded for the un-encapsulated device for all motions.

- The mean resistive torque changed with frequency for the different motions. In some motions the mean resistive torque increased and decreased for other motions with the increment of frequency.

- The highest mean resistive torque was 4.7 N.m at 0.25 Hz frequency for the artificial discs without encapsulation. The lowest mean resistive torque was 1.73 N.m at 2 Hz for the polyethylene heat shrink encapsulated artificial disc for flexion motion.

- At 1 Hz the mean resistive torque was 2.2 N.m which was the highest for the artificial discs without encapsulation. The lowest mean resistive torque was 0.94 N.m at 0.25 Hz for the polyethylene heat shrink encapsulated artificial disc for extension motion.

- The mean resistive torque was 1.1 N.m at 2 Hz frequency and was the highest for the artificial discs with polyurethane encapsulation. The lowest mean resistive torque was 0.64 N.m at 0.25 Hz for the polyethylene heat shrink encapsulated artificial disc for lateral bending motion.

- Un-encapsulated the discs operated under the boundary and mixed lubrication regimes according to the generated Stribeck curves.

- For the S8 polymer socket the mean mass loss was 10.15 ± 0.04 mg/million cycles and the mass loss for the S7 socket was 11.3 ± 0.03 mg/million cycles.

Encapsulating the artificial disc could help in preventing the wear particles from reaching the surrounding tissues; in addition, it would help in reducing the resistive torque and wear by using lubricant inside it.

8 General discussion and conclusions

8.1 General discussion

This work and thesis aimed to design and test a new encapsulated ball and socket artificial disc. The aim was achieved by understanding the challenges that face the current ball and socket artificial disc. Then applying a design process that carefully studied the needs to improve the current ball and socket artificial discs. The design process included different stages; the first stage was to determine a product design specification related specifically to the artificial discs to gain a better understand of the new and old performance requirements in the artificial discs in general. The second step was to produce different conceptual designs using the TRIZ methodology to meet the product design specification. An evaluation matrix was created to evaluate the different conceptual designs to help choose the most successful design to proceed with to the next stage of development which is the detailed design stage. In the detailed design stage a detailed design for the ball and socket were modelled using SolidWorks.

Different bio-lubricants and different biomaterials were tested using a pin-on-disc tribometer to investigate the tribology for the different combinations. All the lubricants (Ringer's solution, bovine calf serum and PVA with all concentrations) showed a shear thinning effect with increasing shear rate for the viscosity values. The diluted bovine calf serum showed slightly higher viscosity results than the Ringer's solution and had a lower coefficient of friction with all materials combinations than Ringer's solution. This is due to the protein absorption on the surfaces of the materials during the frictional tests (Scholes and Unsworth, 2006). The PVA

lubricants with all concentrations showed a lower coefficient of friction than Ringer's solution and bovine calf serum. With increasing the concentration of the PVA diluted in distilled water it was found that the viscosity increased and the coefficient of friction reduced for all the material combinations. This could be explained by the increment of the viscosity leading to a thicker film which helped to increase the squeeze time between the film and the two bearing surfaces and increased the chance of separating the two surfaces of the bearings (Roberts, 1982; Roberts *et al.*, 1982). The lowest coefficient of friction for all the material combinations was for PVA C (20 g per 100 mL of distilled water). However, increasing the concentration of the lubricant more than that led to an increase in the coefficient of friction as noticed with PVA D (30 g per 100 mL of distilled water). The increment of the coefficient of friction for this lubricant was due to the high viscosity shear and fluid flow was maybe restricted because this lubricant performed like a foam (thick lubricant) which is circulating slowly between the articulating materials (Hamrock *et al.*, 2004; Thong *et al.*, 2014). Between all the materials that were tested using the pin on disc tribometer, the UHMWPE against CoCr gave the lowest coefficient of friction, as discussed in chapter 4.

Polyurethane and silicone were suggested to be used as the encapsulation materials as they are known to be used for long implantation periods in the human body (Pinchuk, 1994). The fatigue life of these materials, which is represented by the crack nucleation and growth was tested and discussed in chapter 5. For the crack nucleation with using a 50% strain none of the dumbbell samples completely failed during the test after 5 million cycles. For the crack growth, the polyurethane ether elastomer showed a greater resistance for the crack growth more than the silicone elastomers. In addition, the thickness of the elastomer had an impact on the crack growth

life of the different elastomers. The thicker elastomer showed a higher resistance to crack growth and had a higher crack growth rate. This phenomena was described previously (Legorju-jago and Bathias, 2002; Mazich *et al.*, 1989) in which the crack growth rate was higher for thinner samples. The crack growth was affected by sterilization using gamma radiation produced from a cobalt isotope (60 Co). The gamma sterilization caused an increase in the crack growth rate for all the samples of polyurethane and silicone. Therefore, the crack growth of the sterilized samples showed a higher crack growth rate than the control samples which have not been sterilized. Hutchinson *et al.* (1997) noted the same negative effect of the gamma sterilization on silicone and polyurethane elastomers. Accelerated ageing was applied to one of the groups of the polyurethane and silicone samples as described in chapter 5. The ageing was undertaken using a Carbolite laboratory oven where the samples were soaked in saline solution at a temperature of 50 °C for 149 days which is the equivalent to 1 year implantation in the human body. The accelerated ageing affected the crack growth of silicone and polyurethane differently. The ageing increased the crack growth rate of the silicone samples and they had a higher crack growth rate than the sterilized and control samples. However, it reduced the strength and hardness of the polyurethane samples which led to a reduction in the crack growth rate. The aged samples of polyurethane had a lower crack growth rate than the sterilized and control samples. This was caused by the plasticization of water resulting in the reduction of strength and hardness of the polyurethane which was noticed previously by Davies and Evrard (2007). The sterilized/aged group of silicone samples had the highest crack growth rate between the samples. This was due to the sterilization and aged effect on the samples. The sterilized/aged group of polyurethane ether samples had a lower crack growth rate than the control and sterilized groups, but higher than the

aged polyurethane samples. There were noticeable swellings on the surface of the aged and sterilized/aged polyurethane samples where the peak height of the swelling reached 8 µm in some areas. These swellings were likely due to the penetration of water molecules into the material structure and this phenomena was previously observed by Boubakri *et al.* (2009). The hardness of the polyurethane samples was the same for the control and sterilized groups; however, it reduced for the aged and sterilized/aged groups. The reduction of the hardness was as a result of water plasticization caused by long accelerated ageing applied on the samples using saline solution. This phenomena was described previously where the hardness dropped after accelerated ageing of the polyurethane samples for one month (Davies and Evrard, 2007). The hardness of the silicone samples was increased for aged and sterilized groups and this was described previously by Dootz *et al.* (1994).

In chapter 6 the different configuration assemblies were wear tested in accordance with the standard BS ISO 18192-1:2011 (BS ISO 18192-1, 2011), as described in chapter 6 section 6.4.1. Configuration 1 (polyurethane sheath attached with ball and socket using MED – 1511 adhesive) failed before reaching 10000 cycles. This was due to the low surface energy of the UHMWPE which does not allow the adhesive (MED – 1511) to have a strong bond between the PU sheath and the ball and socket. The low surface energy which was described in chapter 6 could be solved by applying special treatments on the surface such as plasma treatments (Noeske *et al.*, 2004). Plasma treatment is done exposing the polymer to a gas such as oxygen that is activated by radiofrequency energy which will remove the weak boundary layers on the bonding surface and will oxidise the surface, as described in section 6.5 (Dunn, 2004). Configuration 2 which was a polyurethane sheath bonded with the ball and socket artificial disc; super glue all plastics was

used as the adhesive, but it lasted for less than 7500 cycles for the same reason which led to the failure of Configuration 1. For both configuration 1 and 2 the polyurethane sheath with 2 mm thickness was used and this may have led to a greater stiffness during the angular motions (flexion, extension and lateral bending) which led to a high peeling force applied on the adhesive from the sheath itself during the motions as described in chapter 6. Other configurations were tested using adhesive and different sheaths as described in chapter 6. It was concluded from the different assembly configurations that UHMWPE needed special treatment to increase the bond strength between the sheath and the UHMWPE. In addition, when using the adhesive as way of bonding the sheath with the artificial disc the sheath should be thin and flexible to not cause a peeling force and weaken the adhesive bond by this force. Therefore, a mechanical attachment was used in chapter 7 to replace the adhesive in configuration 5 in which a wire hose clamp was used as an attachment method and polyethylene heat shrink as an encapsulation sheath. The configuration 5 with the mechanical attachment passed 2 million cycles without any leakage of the lubricant or any type of failure of the sheath or attachment. Both configuration 1 and configuration 5 where tested using a resistive torque test before wear testing and compared with artificial discs without encapsulation. The mean resistive torque was different for each motion for artificial discs with and without encapsulation. The highest resistive torque was for the flexion motion and then the extension motion; the lowest resistive torque was for the lateral bending motion. This was explained by the angle of motion in which the flexion had the largest angular motion as was noticed previously (Moghadas, 2012). The resistive torque in general was higher for all the motions for the artificial discs without encapsulation. For the encapsulated artificial discs with polyethylene heat shrink sheath, they showed a lower resistive torque for all motions

compared with the polyurethane encapsulated artificial discs, as explained in detail in chapter 7. The Stribeck curves for the artificial discs without encapsulation showed a boundary or mixed lubrication regime as was described previously with the use of diluted calf serum (30 ± 2 g/L) as the lubricant (Moghadas, 2012).

The wear testing showed comparable results to artificial discs that have been used commercially such as the Charité and ProDisc-L devices. The mean mass loss was 10.15 ± 0.02 mg per million cycles for the S8 polymer socket and the mass loss for the S7 polymer socket was 11.3 ± 0.01 mg/MC. These results are comparable to the previous literature where a calf serum lubricant was used and the tests were performed under similar conditions; the mean mass loss was 12.03 ± 1.4 mg/10^6 cycles by Moghadas (2012) for the Charité artificial disc. Also the mean wear mass for ProDisc-L was found to be 12.7 ± 2.1 mg/MC when previously tested (Vicars *et al.*, 2010). The results are difficult to compare with the literature because all the wear studies in the literature are related to artificial discs where the lubricant was changed after thousands of cycles (500000 cycles) or every one million cycles. This will affect the wear rate because a fresh lubricant will be inserted which is not the same case as *in vivo*.

The key limitations of this study can be concluded below:

- The polyethylene attachment surface with the polyurethane sheath was not treated with plasma treatment to increase the adhesion strength of the adhesive in the encapsulated artificial disc and this led to failure of the bond between the artificial disc and the sheath.

- The surface roughness of the CoCr samples were high due to the previous usage of the CoCr balls during a previous tests. The focus of this work was on testing the effect of the

PVA C lubricant on the encapsulated artificial disc without taking in consideration the surface roughness. This could be improved by re-polishing the samples again and using them in the near future with the same lubricant to see the effect of the surface roughness on the resistive torque and wear testing.

8.2 Future Work

Encapsulation of an artificial disc was studied here as a concept to open a wide knowledge that could be used in the near future to help improve artificial discs to survive for longer and thus help patients to have a better life. The future work that can be undertaken on the artificial discs are listed below:

- More biomedical lubricants could be developed to be used as a lubricant inside the artificial discs to help in improving the lubrication regimes inside them.

- Encapsulation sheaths could be used with flexible core artificial discs which are mimicking the intervertebral disc such as the Acroflex artificial disc to prevent the damaged particles of the flexible core from migrating to the surrounding tissues and cause chronic inflammations, osteolysis, subsidence of the implant and then revision surgery.

- Using adhesive to bond the artificial discs with the encapsulation sheath could be applied by treating the surfaces of the UHMWPE and all the other plastics and elastomers to become more suitable for bonding using adhesives instead of using mechanical attachment methods.

- A deep study of the wear particles resulted from encapsulating the artificial disc and compare them with particles produced from un-encapsulated artificial discs.

8.3 Conclusions

The major findings from this entire project are listed below:

- UHMWPE/CoCr was the optimum material combination with the lowest friction coefficient for all lubricants. PVA C (20 g per 100 mL of distilled water) with 1.650 ± 0.01 Pa.s viscosity gave the lowest friction coefficient for all combinations compared with other lubricants tested using pin-on-disc tribometer.

- None of the dumbbell samples of polyurethane ether or silicone elastomer (control or the sterilized/aged) from the crack nucleation tests failed after the 5 million cycles.

- The polyurethane ether elastomer had a slower crack growth rate than the silicone elastomer. For example, the control group in the 2 mm polyurethane ether samples reached 70 mm crack length after 421k cycles whereas silicone elastomer from the same group and thickness took 221k cycles to reach the same crack length.

- Accelerated ageing affected the polyurethane samples by reducing the hardness and reduced the crack growth rate for them. However, it increased the hardness and the crack growth rate for the silicone elastomer samples.

- Gamma sterilization increased the crack growth rate of the polyurethane samples and did not affect the hardness of the same material. However, it increased the hardness of the silicone samples and increased the crack growth rate of the same material.

- The polyurethane ether with 2 mm thickness was suggested to be used as an encapsulation sheath in the artificial disc.

- Encapsulating the ball and socket artificial disc decreased the mean resistive torque for all motions.

- The mean resistive torque varied with frequency for the different motions for artificial discs with and without encapsulation. In some motions, the resistive torque increased and in other motions the resistive torque decreased with frequency.

- The flexion motion, had the highest mean resistive torque which was 4.7 N.m at 0.25 Hz frequency for the artificial discs without encapsulation. For the same motion the lowest mean resistive torque was 1.73 N.m at 2 Hz for the polyethylene heat shrink encapsulated artificial disc for flexion motion.

- The extension motion at 1 Hz gave mean resistive torque of 2.2 N.m which was the highest for the artificial discs without encapsulation and the lowest was 0.94 N.m at 0.25 Hz for the polyethylene heat shrink encapsulated artificial disc.

- The mean resistive torque for the lateral bending motion was 1.1 N.m at 2 Hz frequency and was the highest for the artificial discs with polyurethane encapsulation. The lowest mean resistive torque for the same motion was 0.64 N.m at 0.25 Hz for the polyethylene heat shrink encapsulated artificial disc for the lateral bending motion.

- Un-encapsulated discs operated under the boundary and mixed lubrication regimes according to the generated Stribeck curves.

- The mean mass loss during wear testing applied on encapsulated artificial disc was 10.15 ± 0.04 mg/MC for the S8 polymer socket and the mass loss for the S7 socket was 11.3 ± 0.03 mg/MC.

- Encapsulation of the ball and socket artificial discs could help in preventing the wear particles from migrating to the surrounding tissues and cause chronic inflammations, osteolysis, subsidence of the implant and then revision surgery. In addition, it could help in reducing friction and wear by using lubricant to lubricate the articulating ball and socket artificial disc.

Appendix A

Engineering drawings

The engineering drawings of the pin and disc used in section 4.3.1.

Ø8

15

If in doubt ask

		UNLESS OTHERWISE SPECIFIED:		NAME	DATE			
		DIMENSIONS ARE IN mm ANGULAR: ±0.5° Whole numbers ± 0.25 TWO PLACE DECIMAL ±0.1 THREE PLACE DECIMAL ±0.05	DRAWN	F. Alnaimat	02/04/14		TITLE:	
			CHECKED					
			ENG APPR.				Pin	
			MFG APPR.					
		INTERPRET GEOMETRIC TOLERANCING PER:	Q.A.					
PROPRIETARY AND CONFIDENTIAL			COMMENTS:					
THE INFORMATION CONTAINED IN THIS DRAWING IS THE SOLE PROPERTY OF UNIVERSITY OF BIRMINGHAM. ANY		MATERIAL PEEK, UHMWPE, CoCr				SIZE	DWG. NO.	REV
REPRODUCTION IN PART OR AS A WHOLE WITHOUT THE WRITTEN PERMISSION OF		FINISH				**A**	Pin	
UNIVERSITY OF BIRMINGHAM IS PROHIBITED.	NEXT ASSY	USED ON						
		APPLICATION	DO NOT SCALE DRAWING			SCALE: 1:1	WEIGHT:	SHEET 1 OF 1

SECTION A-A

90°

10

ϕ8

ϕ8 $\overline{\downarrow}$ 10
ϕ 18 X 90°

ϕ78

A   A

If in doubt ask

		UNLESS OTHERWISE SPECIFIED:		NAME	DATE				
		DIMENSIONS ARE IN mm	DRAWN	F. Alnaimat	18/03/14				
		ANGULAR: ±0.5° Whole numbers ± 0.25 TWO PLACE DECIMAL ±0.1 THREE PLACE DECIMAL ±0.05	CHECKED			TITLE:			
			ENG APPR.				Disc		
			MFG APPR.						
PROPRIETARY AND CONFIDENTIAL		INTERPRET GEOMETRIC TOLERANCING PER:	Q.A.						
THE INFORMATION CONTAINED IN THIS DRAWING IS THE SOLE PROPERTY OF UNIVERSITY OF BIRMINGHAM. ANY REPRODUCTION IN PART OR AS A WHOLE WITHOUT THE WRITTEN PERMISSION OF UNIVERSITY OF BIRMINGHAM IS PROHIBITED.		COMMENTS:							
		MATERIAL PEEK, CoCr				SIZE **A**	DWG. NO. Disc		REV
NEXT ASSY	USED ON	FINISH							
	APPLICATION	DO NOT SCALE DRAWING				SCALE: 1:1	WEIGHT:		SHEET 1 OF 1

5   4   3   2   1

Appendix B

The graph of the different lubricants viscosities at 37 ºC.
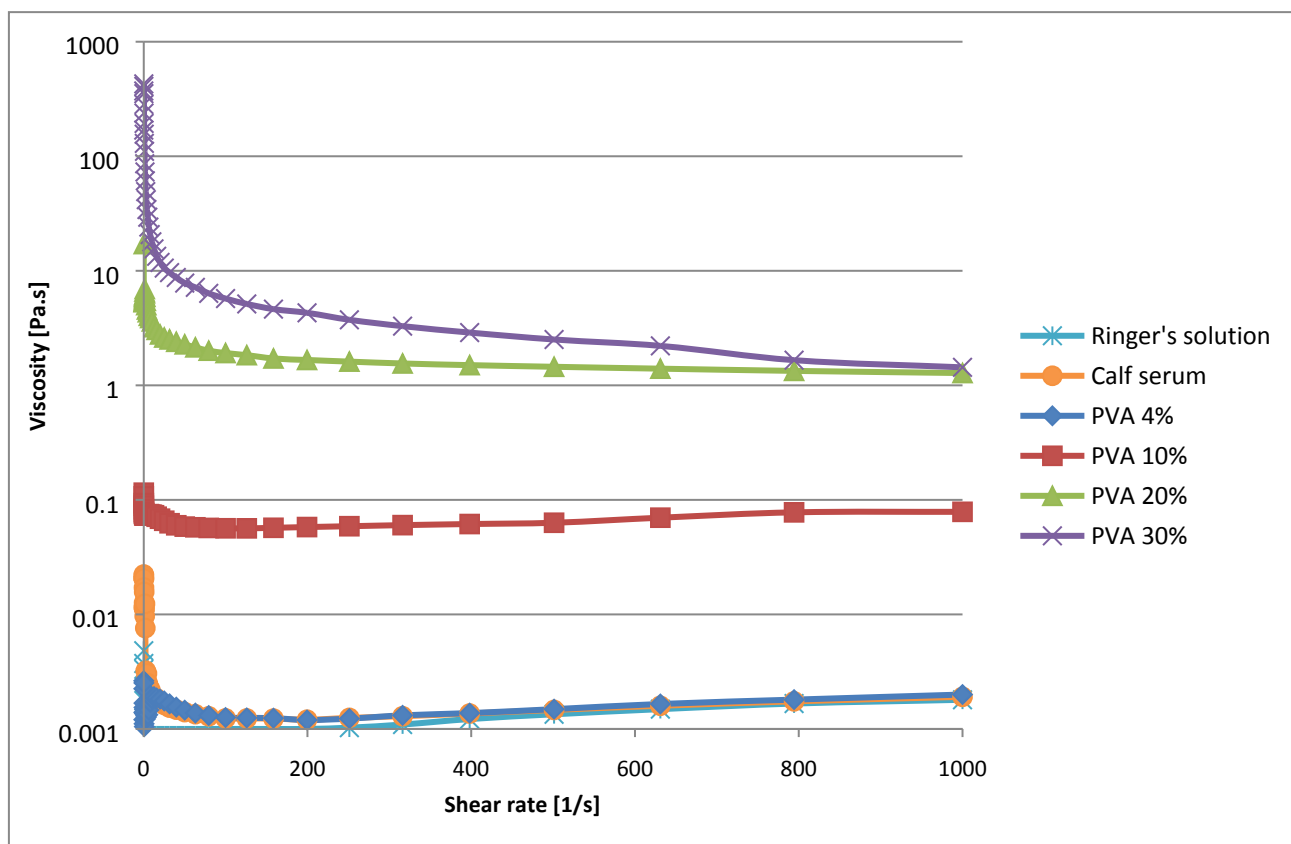
References

Acton, Q. A. (2013) *Lower Back Pain: New Insights for the Healthcare Professional: 2013 Edition: ScholarlyBrief*. Georgia, USA: ScholarlyEditions.

Adams, M. A., Burton, K. and Bogduk, N. (2006) *The Biomechanics of Back Pain*. Pennsylvania, USA: Churchill Livingstone Elsevier.

Adams, M. A. and Roughley, P. J. (2006) 'What is intervertebral disc degeneration, and what causes it?', *Spine,* 31(18), pp. 2151-2161.

Alnaimat, F. A., Shepherd, D. E. T. and Dearn, K. D. (2016) 'The effect of synthetic polymer lubricants on the friction between common arthroplasty bearing biomaterials for encapsulated spinal implants', *Tribology International,* 98, pp. 20-25.

Alnaimat, F. A., Shepherd, D. E. T. and Dearn, K. D. (2017) 'Crack growth in medical-grade silicone and polyurethane ether elastomers', *Polymer Testing,* 62, pp. 225-234.

Anderson, P. A., Sasso, R. C., Rouleau, J. P., Carlson, C. S. and Goffin, J. (2004) 'The Bryan Cervical Disc: wear properties and early clinical results', *The Spine Journal,* 4(6), pp. S303-S309.

Apicella, A., Migliaresi, C., Nicolais, L., Iaccarino, L. and Roccotelli, S. (1983) 'The water ageing of unsaturated polyester-based composites: influence of resin chemical structure', *Composites,* 14(4), pp. 387-392.

Arida, D., Kabra, A., Lowe, C., Szafranski, A. M. and Milestone, D. (2006) *The Charité: Lesson in the Launch of a New Medical Device.* [online].

http://www.kellogg.northwestern.edu/biotech/faculty/articles/charite_device.pdf Northwestern University Kellogg (Accessed 17 Sept 2015).

ASTM D2240-15 (2015) *Standard Test Method for Rubber Property-Durometer Hardness.* PA, USA: ASTM International.

ASTM D4482-11 (2011) *Standard Test Method for Rubber Property—Extension Cycling Fatigue.* Pennsylvania, United States: ASTM International.

ASTM E647-15 (2011) *Standard Test Method for Measurement of Fatigue Crack Growth Rates.* PA, United States: ASTM International.

ASTM F75-98 (2001) *Standard Specification for Cobalt-28 Chromium-6 Molybdenum Alloy Castings and Casting Alloy for Surgical Implants (UNS R30075).* Pennsylvania, United States: ASTM International.

ASTM F90-09 (2009) *ASTM Standard F90-09: Standard Specification for Wrought Cobalt-20Chromium-15Tungsten-10Nickel Alloy for Surgical Implant Applications (UNS R30605).* Pennsylvania, United States: ASTM International.

ASTM F2423 - 05 (2005) *Standard Guide for Functional, Kinematic, and Wear Assessment of Total Disc Prostheses.* West Conshohocken, PA, United States: ASTM International.

ASTM G99-05 (2010) *ASTM Standard G99-05: Standard Test Method for Wear Testing with a Pin-on-Disk Apparatus.* Pennsylvania, United States: ASTM International.

Baker, D., Hastings, R. and Pruitt, L. (2000) 'Compression and tension fatigue resistance of medical grade ultra high molecular weight polyethylene: the effect of morphology, sterilization, aging and temperature', *Polymer,* 41(2), pp. 795-808.

Baker, M. I., Walsh, S. P., Schwartz, Z. and Boyan, B. D. (2012) 'A review of polyvinyl alcohol and its uses in cartilage and orthopedic applications', *Journal of Biomedical Materials Research Part B: Applied Biomaterials,* 100B(5), pp. 1451-1457.

Bao, Q.-B. and Yuan, H. A. (2000) 'Artificial disc technology', *Neurosurgical Focus,* 9(4), pp. 1-7.

Barberá-Tomás, D. (2015) 'Uncertainty in the Hybridization of New Medical Devices: The Artificial Disc Case', in Consoli, D.;Mina, A.;Nelson, R.R. & Ramlogan, R. (Eds.) *Medical Innovation: Science, Technology and Practice.* London, UK, Taylor & Francis, pp. 69-87.

Benson, R. S. (2002) 'Use of radiation in biomaterials science', *Nuclear Instruments and Methods in Physics Research Section B: Beam Interactions with Materials and Atoms,* 191(1–4), pp. 752-757.

Berry, J. L., Moran, J. M., Berg, W. S. and Steffee, A. D. (1987) 'A morphometric study of human lumbar and selected thoracic vertebrae', *Spine,* 12(4), pp. 362-367.

Bhushan, B. (2013) *Principles and Applications of Tribology*. Ohio, Usa: Wiley.

Blumenthal, S., McAfee, P. C., Guyer, R. D., Hochschuler, S. H., Geisler, F. H., Holt, R. T., Garcia Jr, R., Regan, J. J. and Ohnmeiss, D. D. (2005) 'A prospective, randomized, multicenter food and drug administration investigational device exemptions study of lumbar total disc replacement with the CHARITE™ artificial disc versus lumbar fusion: part i: evaluation of clinical outcomes', *Spine,* 30(14), pp. 1565-1575.

Bogduk, N. (2012) *Clinical and Radiological Anatomy of the Lumbar Spine*. Edinburgh, UK: Elsevier Health Sciences UK.

Bondurant, S., Ernster, V., Herdman, R., Implants, C. S. S. B. and Medicine, I. (2000) *Safety of Silicone Breast Implants*. Washington, USA: National Academies Press.

Boretos, J. W. and Pierce, W. S. (1968) 'Segmented polyurethane: A polyether polymer. An initial evalution for biomedical applications', *Journal of biomedical materials research,* 2(1), pp. 121-130.

Boubakri, A., Elleuch, K., Guermazi, N. and Ayedi, H. (2009) 'Investigations on hygrothermal aging of thermoplastic polyurethane material', *Materials & design,* 30(10), pp. 3958-3965.

Brockett, C. and Fisher, J. (2013) 'Chapter 2. Experimental Wear Studies of Total Joint Replacements', in Davim, J.P. (Ed.) *Biotribology.* London, UK, Wiley, pp. 51-86.

Brockett, C., Williams, S., Jin, Z., Isaac, G. and Fisher, J. (2007) 'Friction of total hip replacements with different bearings and loading conditions', *Journal of Biomedical Materials Research Part B: Applied Biomaterials,* 81(2), pp. 508-515.

BS EN ISO 13485 (2003) *Medical devices. Quality management systems. Requirements for regulatory purposes.* London, UK: British Standard Institution.

BS EN ISO 14971 (2012) *Medical devices. Application of risk management to medical devices.* Geneva, Switzerland: British Standard Institution.

BS EN ISO 21534 (2009) *Non-active surgical implants Joint replacement implants -Particular requirements.* London, UK: British Standard Institution.

BS EN ISO 21535 (2009) *Non-active surgical implants. Joint replacement implants. Specific requirements for hip-joint replacement implants.* London, UK: British Standard Institution.

BS EN ISO 21536 (2007) *Non-active surgical implants. Joint replacement implants. Specific requirements for knee-joint replacement implants.* London, UK: British Standard Institution.

BS ISO 6943 (2011) *Rubber, vulcanized. Determination of tension fatigue.* Geneva, Switzerland: British Standard Institution.

BS ISO 7619-1 (2010) *Rubber, vulcanized or thermoplastic - Determination of indentation hardness - Part 1: Durometer method (Shore hardness).* Geneva, Switzerland: British Standard Institution.

BS ISO 14242-2 (2016) *Implants for surgery. Wear of total hip-joint prostheses. Methods of measurement.* London, UK: British Standard Institution.

BS ISO 18192-1 (2011) *Implants for surgery - Wear of total intervertebral spinal disc prostheses - Part 1: Loading and displacement parameters for wear testing and corresponding environmental conditions for test.* London, UK: British Standard Institution.

Buckwalter, J. A. (1995) 'Aging and degeneration of the human intervertebral disc', *Spine,* 20(11), pp. 1307-1314.

Burczak, K., Gamian, E. and Kochman, A. (1996) 'Long-term in vivo performance and biocompatibility of poly(vinyl alcohol) hydrogel macrocapsules for hybrid-type artificial pancreas', *Biomaterials,* 17(24), pp. 2351-2356.

Burke, D. W., O'Connor, D. O., Zalenski, E. B., Jasty, M. and Harris, W. H. (1991) 'Micromotion of cemented and uncemented femoral components', *Journal of Bone and Joint Surgery, British Volume,* 73(1), pp. 33-37.

Butterfield, M., Wheatley, D. J., Williams, D. F. and Fisher, J. (2001) 'A new design for polyurethane heart valves', *The Journal of heart valve disease,* 10(1), pp. 105-110.

Campbell, P., Doorn, P., Dorey, F. and Amstutz, H. C. (1996) 'Wear and morphology of ultra-high molecular weight polyethylene wear particles from total hip replacements', *Proceedings of the Institution of Mechanical Engineers. Part H, Journal of engineering in medicine,* 210(3), pp. 167-174.

Chan, D., Song, Y., Sham, P. and Cheung, K. M. C. (2006) 'Genetics of disc degeneration', *European Spine Journal,* 15(3), pp. 317-325.

Chand, N., Dwivedi, U. and Sharma, M. (2007) 'Development and tribological behaviour of UHMWPE filled epoxy gradient composites', *Wear,* 262(1), pp. 184-190.

Chateauminois, A. and Briscoe, B. (2003) 'Nano-rheological properties of polymeric third bodies generated within fretting contacts', *Surface and Coatings Technology,* 163, pp. 435-443.

Chauvel-Lebret, D. J., Auroy, P. and Bonnaure-Mallet, M. (2001) 'Biocompatibility of Elastomers', in Dumitriu, S. (Ed.) *Polymeric Biomaterials, Revised and Expanded.* Second ed. New York, USA, Taylor & Francis, pp. 311-360.

Cobb, W. S., Burns, J. M., Kercher, K. W., Matthews, B. D., James Norton, H. and Todd Heniford, B. (2005) 'Normal Intraabdominal Pressure in Healthy Adults', *Journal of Surgical Research,* 129(2), pp. 231-235.

Cole, J. C., Lemons, J. E. and Eberhardt, A. W. (2002) 'Gamma irradiation alters fatigue-crack behavior and fracture toughness in 1900H and GUR 1050 UHMWPE', *Journal of Biomedical Materials Research Part A,* 63(5), pp. 559-566.

Cooke, A., Dowson, D. and Wright, V. (1978) 'The rheology of synovial fluid and some potential synthetic lubricants for degenerate synovial joints', *Engineering in Medicine,* 7(2), pp. 66-72.

Cortes, D. H. and Elliott, D. M. (2014) 'The Intervertebral Disc: Overview of Disc Mechanics ', in Shapiro, I.M. & Risbud, M.V. (Eds.) *The Intervertebral Disc: Molecular and Structural Studies of the Disc in Health and Disease.* New York, USA, Springer Vienna, pp. 17-32.

Cramer, G. D. (2014) 'Chapter 2 - General Characteristics of the Spine', in Cramer, G.D. & Darby, S.A. (Eds.) *Clinical Anatomy of the Spine, Spinal Cord, and Ans.* Third ed. Saint Louis, Mosby 15-64.

Cripton, P. A., Reed, S. G. and Saari, A. (2006) 'Musculature Actuation and Biomechanics of the Spine', in Kurtz, S.M. & Edidin, A.A. (Eds.) *Spine Technology Handbook.* London, UK, Elsevier Academic Press, pp. 99-144.

Cunningham, B. W., Orbegoso, C. M., Dmitriev, A. E., Hallab, N. J., Sefter, J. C., Asdourian, P. and McAfee, P. C. (2003) 'The effect of spinal instrumentation particulate wear debris: an in vivo rabbit model and applied clinical study of retrieved instrumentation cases', *The Spine Journal,* 3(1), pp. 19-32.

Curtis, J. and Colas, A. (2013) 'Medical applications of silicones', in Ratner, B.D.;Hoffman, A.S.;Schoen, F.J. & Lemons, J.E. (Eds.) *Biomaterials Science: An Introduction to Materials in Medicine.* Third ed. Oxford, UK, Academic Press, pp. 1106-1116.

Davies, P. and Evrard, G. (2007) 'Accelerated ageing of polyurethanes for marine applications', *Polymer Degradation and Stability,* 92(8), pp. 1455-1464.

De Kleuver, M., Oner, F. and Jacobs, W. (2003) 'Total disc replacement for chronic low back pain: background and a systematic review of the literature', *European Spine Journal,* 12(2), pp. 108-116.

DeMerlis, C. C. and Schoneker, D. R. (2003) 'Review of the oral toxicity of polyvinyl alcohol (PVA)', *Food and chemical toxicology : an international journal published for the British Industrial Biological Research Association,* 41(3), pp. 319-326.

Derbyshire, B., Skorecki, J. and Wheble, V. H. (1980) 'Problems of encapsulation of total joint replacements', *Biomaterials,* 1(1), pp. 33-37.

Devin, C. J., Myers, T. G. and Kang, J. D. (2008) 'Chronic failure of a lumbar total disc replacement with osteolysis. Report of a case with nineteen-year follow up.', *Journal of Bone & Joint Surgery,* 90(10), pp. 2230-2234.

Dootz, E., Koran, A. r. and Craig, R. (1994) 'Physical properties of three maxillofacial materials as a function of accelerated aging', *The Journal of prosthetic dentistry,* 71(4), pp. 379-383.

Dunn, D. J. (2003) *Adhesives and Sealants: Technology, Applications and Markets*. Shropshire, UK: Rapra Technology Limited.

Dunn, D. J. (2004) *Engineering and Structural Adhesives*. Shropshire, UK: Rapra Technology Limited.

Ebnesajjad, S. and Ebnesajjad, C. (2006) *Surface Treatment of Materials for Adhesion Bonding*. New York, USA: Elsevier Science.

Edidin, A., Jewett, C., Kalinowski, A., Kwarteng, K. and Kurtz, S. (2000) 'Degradation of mechanical behavior in UHMWPE after natural and accelerated aging', *Biomaterials,* 21(14), pp. 1451-1460.

Enab, T. A. (2012) 'A comparative study of the performance of metallic and FGM tibia tray components in total knee replacement joints', *Computational Materials Science,* 53(1), pp. 94-100.

Eyre, D. R. and Muir, H. (1976) 'Types I and II collagens in intervertebral disc. Interchanging radial distributions in annulus fibrosus', *Biochemical Journal,* 157(1), pp. 267-270.

Faiz, O., Blackburn, S. and Moffat, D. (2011) *Anatomy at a Glance*. Sussex, UK: Wiley.

Fan, H., Wu, S., Wu, Z., Wang, Z. and Guo, Z. (2012) 'Implant Failure of Bryan Cervical Disc due to Broken Polyurethane Sheath: A Case Report', *Spine,* 37(13), pp. E814-E816.

Ferguson, S. J. and Steffen, T. (2005) 'Biomechanics of the aging spine', in Aebi, M.;Gunzburg, R. & Szpalski, M. (Eds.) *The Aging Spine.* Heidelberg, Germany, Springer, pp. 15-21.

Florence, A. T. (2010) *An Introduction to Clinical Pharmaceutics*. London, UK: Pharmaceutical Press.

Fong, S. Y., DuPlessis, S. J., Casha, S. and Hurlbert, R. J. (2006) 'Design limitations of Bryan disc arthroplasty', *The Spine Journal,* 6(3), pp. 233-241.

Fouad, H. (2011) 'In vitro evaluation of stiffness graded artificial hip joint femur head in terms of joint stresses distributions and dimensions: finite element study', *Journal of Materials Science: Materials in Medicine,* 22(6), pp. 1589-1598.

Fraser, R. D., Ross, E. R., Lowery, G. L., Freeman, B. J. and Dolan, M. (2004) 'AcroFlex design and results', *The spine journal : official journal of the North American Spine Society,* 4(6), pp. 245S-251S.

Furey, M. J. (2000) 'Joint Lubrication', in Bronzino, J.D. (Ed.) *The Biomedical Engineering Handbook 1.* Heidelberg, Germany, Springer Berlin Heidelberg, pp. 21-23.

Gadd, K. and Goddard, C. (2011) *TRIZ for Engineers: Enabling Inventive Problem Solving*. West Sussex, UK: Wiley.

Gajra, B., Pandya, S. S., Vidyasagar, G., Rabari, H., Dedania, R. R. and Rao, S. (2012) 'Poly vinyl alcohol Hydrogel and its Pharmaceutical and Biomedical Applications: A Review', *International Journal of Pharmaceutical Research,* 4(2), pp. 20-26.

Gent, A. (1958) 'On the relation between indentation hardness and Young's modulus', *Rubber Chemistry and Technology,* 31(4), pp. 896-906.

Gilad, I. and Nissan, M. (1986) 'A study of vertebra and disc geometric relations of the human cervical and lumbar spine', *Spine,* 11(2), pp. 154-157.

Gispert, M. P., Serro, A. P., Colaço, R. and Saramago, B. (2006) 'Friction and wear mechanisms in hip prosthesis: Comparison of joint materials behaviour in several lubricants', *Wear,* 260(1–2), pp. 149-158.

Goel, V. K., Dooris, A. P., McGowan, D. and Rengachary, S. (2003) 'Biomechanics of Artificial Discs', in Lewandrowski, K.U. (Ed.) *Advances in Spinal Fusion: Molecular Science, BioMechanics, and Clinical Management.* New York, USA, Taylor & Francis, pp. 191-216.

Goel, V. K., Sairyo, K., Vishnubhotla, S. L., Biyani, A. and Ebraheim, N. (2006) 'Spine Disorders: Implications for Bioengineering', in Kurtz, S.M. & Edidin, A.A. (Eds.) *Spine Technology Handbook.* London, UK, Elsevier Academic Press, pp. 145-182.

Gorna, K. and Gogolewski, S. (2003) 'The effect of gamma radiation on molecular stability and mechanical properties of biodegradable polyurethanes for medical applications', *Polymer Degradation and Stability,* 79(3), pp. 465-474.

Graham, J. (2006) 'Standard Test Methods for Spine Implants', in Kurtz, S.M. & Edidin, A.A. (Eds.) *Spine Technology Handbook.* London, UK, Elsevier Academic Press, pp. 397-442.

Grupp, T. M., Yue, J. J., Garcia, R., Basson, J., Schwiesau, J., Fritz, B. and Blömer, W. (2009) 'Biotribological evaluation of artificial disc arthroplasty devices: influence of loading and kinematic patterns during in vitro wear simulation', *European Spine Journal,* 18(1), pp. 98-108.

Guehring, T., Unglaub, F., Lorenz, H., Omlor, G., Wilke, H.-J. and Kroeber, M. W. (2006) 'Intradiscal pressure measurements in normal discs, compressed discs and compressed discs treated with axial posterior disc distraction: an experimental study on the rabbit lumbar spine model', *European Spine Journal,* 15(5), pp. 597-604.

Guerin, H. A. L. and Elliott, D. M. (2006) 'Structure and Properties of Soft Tissues in the Spine', in Kurtz, S.M. & Edidin, A.A. (Eds.) *Spine Technology Handbook.* London, UK, Elsevier Academic Press, pp. 35-62.

Hallab, N. J. (2009) 'A review of the biologic effects of spine implant debris: Fact from fiction', *Spine Arthroplasty Society,* 3(4), pp. 143-160.

Hallab, N. J., Cunningham, B. W. and Jacobs, J. J. (2003) 'Spinal implant debris-induced osteolysis', *Spine,* 28(20S), pp. S125-S138.

Hamrock, B. J., Schmid, S. R. and Jacobson, B. O. (2004) *Fundamentals of Fluid Film Lubrication*. New York, USA: Taylor & Francis.

Hassan, C. M., Trakarnpan, P. and Peppas, N. A. (2002) 'Water Solubility Characteristics of Poly(Vinyl Alcohol) and Gels Prepared by Freezing/Thawing Processes', in Amjad, Z. (Ed.) *Water Soluble Polymers: Solution Properties and Applications.* London, UK, Kluwer Academic Publishers, pp. 31-40.

Helal, B. and Karadi, B. (1968) 'Artificial lubrication of joints: use of silicone oil', *Rheumatology,* 9(8), pp. 334-340.

Herwig, B., Weyreuther, M., Heyde, C. E., Westphal, M., Zierski, J. and Weber, U. (2007) *MRI Atlas: Orthopedics and Neurosurgery, The Spine*. Berlin, Germany: Springer Berlin Heidelberg.

Hilibrand, A. S. and Robbins, M. (2004) 'Adjacent segment degeneration and adjacent segment disease: the consequences of spinal fusion?', *The Spine Journal,* 4(6), pp. S190-S194.

Hou, Y., Liu, Y., Yuan, W., Wang, X., Chen, H., Yang, L. and Zhang, Y. (2014) 'Cervical kinematics and radiological changes after Discover artificial disc replacement versus fusion', *The Spine Journal,* 14(6), pp. 867-877.

Hoy, D., March, L., Brooks, P., Blyth, F., Woolf, A., Bain, C., Williams, G., Smith, E., Vos, T., Barendregt, J., Murray, C., Burstein, R. and Buchbinder, R. (2014) 'The global burden of low back pain: estimates from the Global Burden of Disease 2010 study', *Annals of the rheumatic diseases,* 73(6), pp. 968-974.

Hua, X., Wroblewski, B. M., Jin, Z. and Wang, L. (2012) 'The effect of cup inclination and wear on the contact mechanics and cement fixation for ultra high molecular weight polyethylene total hip replacements', *Medical Engineering & Physics,* 34(3), pp. 318-325.

Hukins, D. W. L., Mahomed, A. and Kukureka, S. N. (2008) 'Accelerated aging for testing polymeric biomaterials and medical devices', *Medical Engineering & Physics,* 30(10), pp. 1270-1274.

Hutchinson, D., Savory, K. and Bachus, K. N. (1997) 'Crack‐growth properties of various elastomers with potential application in small joint prostheses', *Journal of biomedical materials research,* 37(1), pp. 94-99.

Hyde, P., Tipper, J., Fisher, J. and Hall, R. (2015) 'Wear and biological effects of a semi-constrained total disc replacement subject to modified ISO standard test conditions', *Journal of the mechanical behavior of biomedical materials,* 44, pp. 43-52.

Hyde, P. J. (2012) *Bio-tribology of Total Disc Replacements of the Lumbar Spine*. PHD, The University of Leeds.

Hyde, P. J., Fisher, J. and Hall, R. M. (2017) 'Wear characteristics of an unconstrained lumbar total disc replacement under a range of in vitro test conditions', *Journal of Biomedical Materials Research Part B: Applied Biomaterials,* 105(1), pp. 46-52.

Iatridis, J. C. and ap Gwynn, I. (2004) 'Mechanisms for mechanical damage in the intervertebral disc annulus fibrosus', *Journal of biomechanics,* 37(8), pp. 1165-1175.

Iatridis, J. C., Setton, L. A., Weidenbaum, M. and Mow, V. C. (1997) 'Alterations in the mechanical behavior of the human lumbar nucleus pulposus with degeneration and aging', *Journal of Orthopaedic Research,* 15(2), pp. 318-322.

Ingham, E. and Fisher, J. (2000) 'Biological reactions to wear debris in total joint replacement.', *Proceedings of the Institution of Mechanical Engineers, Part H: Journal of Engineering in Medicine,* 214(1), pp. 21-37.

Jiang, H., Campbell, G., Boughner, D., Wan, W.-K. and Quantz, M. (2004) 'Design and manufacture of a polyvinyl alcohol (PVA) cryogel tri-leaflet heart valve prosthesis', *Medical Engineering & Physics,* 26(4), pp. 269-277.

Jin, Z. (2002) 'Analysis of mixed lubrication mechanism in metal-on-metal hip joint replacements', *Proceedings of the Institution of Mechanical Engineers, Part H: Journal of Engineering in Medicine,* 216(1), pp. 85-89.

Jin, Z. M., Dowson, D. and Fisher, J. (1997) 'Analysis of fluid film lubrication in artificial hip joint replacements with surfaces of high elastic modulus', *Proceedings of the Institution of Mechanical Engineers. Part H, Journal of engineering in medicine,* 211(3), pp. 247-256.

Jin, Z. M., Fisher, J. and Ingham, E. (2006) 'Biotribology: Material Design, Lubrication, and Wear in Artificial Hip Joints', in Totten, G.E. (Ed.) *Handbook of Lubrication and Tribology: Volume I Application and Maintenance, Second Edition.* NW, USA, CRC Press, pp. (17-11)-(17-24).

Johannessen, W. and Elliott, D. M. (2005) 'Effects of degeneration on the biphasic material properties of human nucleus pulposus in confined compression', *Spine,* 30(24), pp. E724-E729.

John, K. R. S. (2014) 'The use of polyurethane materials in the surgery of the spine: a review', *The Spine Journal,* 14(12), pp. 3038-3047.

Johnson, W. G., Baldwin, M. L. and Butler, R. J. (1998) 'Back Pain and Work Disability: The Need for a New Paradigm', *Industrial Relations: A Journal of Economy and Society,* 37(1), pp. 9-34.

Jones, E., Scholes, S., Burgess, I., Ash, H. and Unsworth, A. (2009) 'Compliant layer bearings in artificial joints. Part 2: simulator and fatigue testing to assess the durability of the interface between an

elastomeric layer and a rigid substrate', *Proceedings of the Institution of Mechanical Engineers, Part H: Journal of Engineering in Medicine,* 223(1), pp. 1-13.

Katoozian, H., Davy, D. T., Arshi, A. and Saadati, U. (2001) 'Material optimization of femoral component of total hip prosthesis using fiber reinforced polymeric composites', *Medical Engineering & Physics,* 23(7), pp. 505-511.

Kita, M., Ogura, Y., Honda, Y., Hyon, S.-H., Cha, W., II and Ikada, Y. (1990) 'Evaluation of polyvinyl alcohol hydrogel as a soft contact lens material', *Graefe's Archive for Clinical and Experimental Ophthalmology,* 228(6), pp. 533-537.

Kobayashi, M., Koide, T. and Hyon, S. H. (2014) 'Tribological characteristics of polyethylene glycol (PEG) as a lubricant for wear resistance of ultra-high-molecular-weight polyethylene (UHMWPE) in artificial knee join', *Journal of the mechanical behavior of biomedical materials,* 38, pp. 33-38.

Konttinen, Y. T., Xu, J. W., Pätiälä, H., Imai, S., Waris, V., Li, T. F., Goodman, S. B., Nordsletten, L. and Santavirta, S. (1997) 'Cytokines in aseptic loosening of total hip replacement', *Current Orthopaedics,* 11(1), pp. 40-47.

Korhonen, R. K., Koistinen, A., Konttinen, Y. T., Santavirta, S. S. and Lappalainen, R. (2005) 'The effect of geometry and abduction angle on the stresses in cemented UHMWPE acetabular cups–finite element simulations and experimental tests', *Biomedical engineering online,* 4(1), pp. 32.

Krantz, W. B., Wasan, D. T. and Jain, R. K. (1986) *Thin liquid film phenomena*. New York, USA: American Institute of Chemical Engineers.

Kretzer, J. P. (2013) 'Chapter 1. Biotribology of Total Hip Replacement: the Metal-on-Metal Articulation 1', in Davim, J.P. (Ed.) *Biotribology.* London, UK, Wiley, pp. 1-49.

Kurtz, S. M. (2004) *The UHMWPE Handbook: Ultra-High Molecular Weight Polyethylene in Total Joint Replacement*. California, USA: Elsevier Science.

Kurtz, S. M. (2006) 'Total Disc Arthroplasty', in Kurtz, S.M. & Edidin, A.A. (Eds.) *Spine Technology Handbook.* London, UK, Elsevier Academic Press, pp. 303-370.

Kurtz, S. M. and Edidin, A. A. (2006) 'The Basic Tools and Terminology of Spine Treatment', in Kurtz, S.M. & Edidin, A.A. (Eds.) *Spine Technology Handbook.* London, UK, Elsevier Academic Press, pp. 1-10.

Kurtz, S. M., Steinbeck, M., Ianuzzi, A., van Ooij, A., Punt, I. M., Isaza, J. and Ross, E. (2009) 'Retrieval analysis of motion preserving spinal devices and periprosthetic tissues', *Spine Arthroplasty Society,* 3(4), pp. 161-177.

Lambert, B. J., Tang, F. W. and Rogers, W. J. (2001) *Polymers in Medical Applications*. Shropshire, UK: Rapra Technology Limited

Lauryssen, C., Coric, D., Dimmig, T., Musante, D., Ohnmeiss, D. D. and Stubbs, H. A. (2012) 'Cervical total disc replacement using a novel compressible prosthesis: Results from a prospective Food and Drug Administration–regulated feasibility study with 24-month follow-up', *The International Journal of Spine Surgery,* 6(1), pp. 71-77.

Leckie, F. A. and Bello, D. J. (2009) *Strength and Stiffness of Engineering Systems*. New York, USA: Springer US.

Lee, C. K. and Goel, V. K. (2004) 'Artificial disc prosthesis: design concepts and criteria', *The Spine Journal,* 4(6), pp. S209-S218.

Legorju-jago, K. and Bathias, C. (2002) 'Fatigue initiation and propagation in natural and synthetic rubbers', *International Journal of Fatigue,* 24(2–4), pp. 85-92.

Leslie, L., Jenkins, M., Shepherd, D. and Kukureka, S. (2008) 'The effect of the environment on the mechanical properties of medical grade silicones', *Journal of Biomedical Materials Research Part B: Applied Biomaterials,* 86(2), pp. 460-465.

Levitin, G., Reinhardt, K. and Hess, D. W. (2012) 'Plasma Cleaning for Electronic, Photonic, Biological, and Archeological Applications', in Kohli, R. & Mittal, K.L. (Eds.) *Developments in Surface Contamination and Cleaning: Contaminant Removal and Monitoring.* Oxford, UK, William Andrew, pp. 55-122.

Liao, Y.-S. and Hanes, M. (2006) 'The effects of load soak control on the wear of UHMWPE at various hydration levels in a joint simulation study', *Journal of ASTM International,* 3(9), pp. 1-5.

Lidgren, L. (2003) 'The bone and joint decade 2000-2010', *Bulletin of the World Health Organization,* 81(9), pp. 629-629.

Liuke, M., Solovieva, S., Lamminen, A., Luoma, K., Leino-Arjas, P., Luukkonen, R. and Riihimäki, H. (2005) 'Disc degeneration of the lumbar spine in relation to overweight', *International journal of obesity,* 29(8), pp. 903.

Logan, M. (2011) *Biostatistical Design and Analysis Using R: A Practical Guide*. Sussex, UK: Wiley.

Mackay, T. G., Wheatley, D. J., Bernacca, G. M., Fisher, A. C. and Hindle, C. S. (1996) 'New polyurethane heart valve prosthesis: design, manufacture and evaluation', *Biomaterials,* 17(19), pp. 1857-1863.

Mäkela, M., Heliövaara, M., Sievers, K., Impivaara, O., Knekt, P. and Aromaa, A. (1991) 'Prevalence, Determinants, and Consequences of Chronic Neck Pain in Finland', *American Journal of Epidemiology,* 134(11), pp. 1356-1367.

Maniadakis, N. and Gray, A. (2000) 'The economic burden of back pain in the UK', *Pain,* 84(1), pp. 95-103.

Marcolongo, M. S., Canella, M. and Massey, C. J. (2006) 'Nucleus Replacement of the Intervertebral Disc ', in Kurtz, S.M. & Edidin, A.A. (Eds.) *Spine Technology Handbook.* London, UK, Elsevier Academic Press, pp. 281-302.

Mars, W. and Fatemi, A. (2004) 'Factors that affect the fatigue life of rubber: a literature survey', *Rubber Chemistry and Technology,* 77(3), pp. 391-412.

Mars, W. V. and Fatemi, A. (2002) 'A literature survey on fatigue analysis approaches for rubber', *International Journal of Fatigue,* 24(9), pp. 949-961.

Mathews, H. H., LeHuec, J.-C., Friesem, T., Zdeblick, T. and Eisermann, L. (2004) 'Design rationale and biomechanics of Maverick Total Disc arthroplasty with early clinical results', *The Spine Journal,* 4(6), pp. S268-S275.

Matsui, H., Kanamori, M., Ishihara, H., Yudoh, K., Naruse, Y. and Tsuji, H. (1998) 'Familial Predisposition for Lumbar Degenerative Disc Disease: A Case‐Control Study', *Spine,* 23(9), pp. 1029-1034.

Mattei, L., Di Puccio, F., Piccigallo, B. and Ciulli, E. (2011) 'Lubrication and wear modelling of artificial hip joints: a review', *Tribology International,* 44(5), pp. 532-549.

Mazich, K. A., Morman, K., Oblinger, F., Fan, T. and Killgoar Jr, P. (1989) 'The effect of specimen thickness on the tearing energy of a gum vulcanizate', *Rubber Chemistry and Technology,* 62(5), pp. 850-862.

Mazzeo, F. (2015) *Introductory guide to using an AR series rheometer using rheology advantage software* [online].

http://www.bu.edu/becf/downloads/BioInterface%20Technologies/Guide%20to%20Set%20up%20Rheometer.pdf Boston University (Accessed 12 Jan 2015).

McCarberg, B., Stanos, S. and D'Arcy, Y. (2012) *Back and Neck Pain*. New York, USA: Oxford University Press.

McKay, B., Peckham, S. and Scifert, J. (2006) 'Biologics to Promote Spinal Fusion', in Kurtz, S.M. & Edidin, A.A. (Eds.) *Spine Technology Handbook.* London, UK, Elsevier Academic Press, pp. 241-280.

McKellop, H., Clarke, I., Markolf, K. and Amstutz, H. (1978) 'Wear characteristics of UHMW polyethylene: a method for accurately measuring extremely low wear rates', *Journal of Biomedical Materials Research Part A,* 12(6), pp. 895-927.

Mcmillin, C. R. (1987) 'Characterization of hexsyn, a polyolefin rubber', *Journal of biomaterials applications,* 2(1), pp. 3-99.

McNally, D., Naylor, J. and Johnson, S. (2012) 'An in vitro biomechanical comparison of Cadisc™-L with natural lumbar discs in axial compression and sagittal flexion', *European Spine Journal,* 21(5), pp. 612-617.

Medline Plus *Back Pain* [online]. http://www.nlm.nih.gov/medlineplus/backpain.html (Accessed 11 Jan 2014).

Middleditch, A. and Oliver, J. (2005) *Functional Anatomy of the Spine*. Pennsylvania, USA: Elsevier Butterworth-Heinemann.

Moghadas, P. (2012) *Tribology of ball-and-socket total disc arthroplasty*. PHD University of Birmingham.

Moghadas, P., Mahomed, A., Hukins, D. W. L. and Shepherd, D. E. T. (2012a) 'Friction in metal-on-metal total disc arthroplasty: Effect of ball radius', *Journal of biomechanics,* 45(3), pp. 504-509.

Moghadas, P., Mahomed, A., Shepherd, D. E. and Hukins, D. W. (2015) 'Wear of the Charité® lumbar intervertebral disc replacement investigated using an electro-mechanical spine simulator', *Proceedings of the Institution of Mechanical Engineers, Part H: Journal of Engineering in Medicine,* 229(3), pp. 264-268.

Moghadas, P. M., Shepherd, D. E., Hukins, D. W. and Mahomed, A. (2012b) 'Polymer-on-metal or metal-on-polymer total disc arthroplasty: does it make a difference?', *Spine,* 37(21), pp. 1834-1838.

Moon, S. M., Yoder, J. H., Wright, A. C., Smith, L. J., Vresilovic, E. J. and Elliott, D. M. (2013) 'Evaluation of intervertebral disc cartilaginous endplate structure using magnetic resonance imaging', *European Spine Journal,* 22(8), pp. 1820-1828.

Morishita, Y., Hida, S., Naito, M., Arimizu, J., Matsushima, U. and Nakamura, A. (2006) 'Measurement of the Local Pressure of the Intervertebral Foramen and the Electrophysiologic Values of the Spinal Nerve Roots in the Vertebral Foramen', *Spine,* 31(26), pp. 3076-3080.

Muratoglu, O. K. and Kurtz, S. M. (2002) 'Alternate Bearing Surfaces in Hip Replacement', in Sinha, R.K. (Ed.) *Hip Replacement: Current Trends and Controversies.* New Youk, USA, Marcel Dekker, Inc., pp. 1-46.

Naples, G. G., Mortimer, J. T., Scheiner, A. and Sweeney, J. D. (1988) 'A spiral nerve cuff electrode for peripheral nerve stimulation', *Institute of Electrical and Electronics Engineers transactions on biomedical engineering,* 35(11), pp. 905-916.

National Institute for Health and Clinical Excellence (2009) *Low back pain: Early management of persistent non-specific low back pain.* [online]. http://www.nice.org.uk/guidance/cg88 (Accessed 21 Jan 2014).

Noeske, M., Degenhardt, J., Strudthoff, S. and Lommatzsch, U. (2004) 'Plasma jet treatment of five polymers at atmospheric pressure: surface modifications and the relevance for adhesion', *International journal of adhesion and adhesives,* 24(2), pp. 171-177.

O'Leary, P., Nicolakis, M., Lorenz, M. A., Voronov, L. I., Zindrick, M. R., Ghanayem, A., Havey, R. M., Carandang, G., Sartori, M. and Gaitanis, I. N. (2005) 'Response of Charite total disc replacement under physiologic loads: prosthesis component motion patterns', *The Spine Journal,* 5(6), pp. 590-599.

Oka, M. (2001) 'Biomechanics and repair of articular cartilge', *Journal of Orthopaedic Science,* 6(5), pp. 448-456.

Pal, S. (2013) *Design of Artificial Human Joints & Organs*. New York, USA: Springer US.

Papageorgiou, I., Abberton, T., Fuller, M., Tipper, J. L., Fisher, J. and Ingham, E. (2014) 'Biological Effects of Clinically Relevant CoCr Nanoparticles in the Dura Mater: An Organ Culture Study', *Nanomaterials,* 4(2), pp. 485-504.

Park, P., Garton, H. J., Gala, V. C., Hoff, J. T. and McGillicuddy, J. E. (2004) 'Adjacent segment disease after lumbar or lumbosacral fusion: review of the literature', *Spine,* 29(17), pp. 1938-1944.

Pinchuk, L. (1994) 'A review of the biostability and carcinogenicity of polyurethanes in medicine and the new generation of 'biostable' polyurethanes', *Journal of biomaterials science. Polymer edition,* 6(3), pp. 225-267.

Pruitt, L. A. (2003) 'The Effects of Radiation on the Structural and Mechanical Properties of Medical Polymers', in Anjum, N.;Kausch, H.;Chevolot, Y.;Gupta, B.;Leonard, D.;Mathieu, H.J.;Pruitt, L.A.;Ruiz-Taylor, L. & Scholz, M. (Eds.) *Radiation Effects on Polymers for Biological Use.* Heidelberg, Germany, Springer Berlin Heidelberg, pp. 63-94.

Pugh, S. (1991) *Total Design: Integrated Methods for Successful Product Engineering*. London, UK: Addison-Wesley Publishing Company.

Punt, I., Baxter, R., Van Ooij, A., Willems, P., Van Rhijn, L., Kurtz, S. and Steinbeck, M. (2011) 'Submicron sized ultra-high molecular weight polyethylene wear particle analysis from revised SB Charite III total disc replacements', *Acta biomaterialia,* 7(9), pp. 3404-3411.

Punt, I. M., Cleutjens, J. P., de Bruin, T., Willems, P. C., Kurtz, S. M., Van Rhijn, L. W., Schurink, G. W. H. and van Ooij, A. (2009) 'Periprosthetic tissue reactions observed at revision of total intervertebral disc arthroplasty', *Biomaterials,* 30(11), pp. 2079-2084.

Pye, S. R., Reid, D. M., Adams, J. E., Silman, A. J. and O'neill, T. W. (2007) 'Influence of weight, body mass index and lifestyle factors on radiographic features of lumbar disc degeneration', *Annals of the rheumatic diseases,* 66(3), pp. 426-427.

Reyes-Sa´nchez, A. A., Patwardhan, A. G. and Block, J. E. (2008) 'The M6 Artificial Cervical Disc', in Yue, J.J.;Bertagnoli, R.;McAfee, P.C. & An, H.S. (Eds.) *Motion Preservation Surgery of the Spine: Advanced Techniques and Controversies.* Pennsylvania, USA, Saunders/Elsevier, pp. 272-276.

Reyes-Sanchez, A., Miramontes, V., Olivarez, L. M. R., Aquirre, A. A., Quiroz, A. O. and Zarate-Kalfopulos, B. (2010) 'Initial clinical experience with a next-generation artificial disc for the treatment of symptomatic degenerative cervical radiculopathy', *Spine Arthroplasty Society,* 4(1), pp. 9-15.

Roberts, B. J. (1982) *The lubrication of natural and artificial hip joints*. PHD, Durham University.

Roberts, B. J., Unsworth, A. and Mian, N. (1982) 'Modes of lubrication in human hip joints', *Annals of the rheumatic diseases,* 41(3), pp. 217-224.

Salvo, S. G. (2015) *Massage Therapy - E-Book: Principles and Practice*. Missouri, USA: Elsevier Health Sciences.

Sambrook, P., MacGregor, A. and Spector, T. (1999) 'Genetic influences on cervical and lumbar disc degeneration', *Arthritis and Rheumatism,* 42(2), pp. 366–372.

Sasso, R. C., Smucker, J. D., Hacker, R. J. and Heller, J. G. (2007) 'Artificial disc versus fusion: a prospective, randomized study with 2-year follow-up on 99 patients', *Spine,* 32(26), pp. 2933-2940.

Schmalzried, T. P., Peters, P. C., Maurer, B. T., Bragdon, C. R. and Harris, W. H. (1996) 'Long-duration metal-on-metal total hip arthroplasties with low wear of the articulating surfaces', *The Journal of arthroplasty,* 11(3), pp. 322-331.

Scholes, S. C. and Unsworth, A. (2006) 'The effects of proteins on the friction and lubrication of artificial joints', *Proceedings of the Institution of Mechanical Engineers. Part H, Journal of engineering in medicine,* 220(6), pp. 687-693.

Seroussi, R. E., Krag, M. H., Muller, D. L. and Pope, M. H. (1989) 'Internal deformations of intact and denucleated human lumbar discs subjected to compression, flexion, and extension loads', *Journal of Orthopaedic Research,* 7(1), pp. 122-131.

Shaheen, A. and Shepherd, D. E. (2007) 'Lubrication regimes in lumbar total disc arthroplasty', *Proceedings of the Institution of Mechanical Engineers, Part H: Journal of Engineering in Medicine,* 221(6), pp. 621-627.

Sharon, W. and Fernando, T. (2012) 'Chapter 27 : Patient Selection for Spine Surgery', in Benzel, E.C. (Ed.) *Spine Surgery : Techniques, Complication Avoidance, and Management* Pennsylvania, USA, Elsevier Health Sciences, pp. 235-240.

Simon, S. R., Paul, I., Rose, R. and Radin, E. (1975) '" Stiction-friction" of total hip prostheses and its relationship to loosening', *Journal of Bone and Joint Surgery,* 57(2), pp. 226-230.

Su, S. H., Hua, Z. K. and Zhang, J. H. (2006) 'Design and Mechanics Simulation of Bionic Lubrication System of Artificial Joints', *Journal of Bionic Engineering,* 3(3), pp. 155-160.

Swanson, A. (1969) 'Finger joint replacement by silicone rubber implants and the concept of implant fixation by encapsulation', *Annals of the rheumatic diseases,* 28(5), pp. 47.

Thong, D., Hutchinson, P., Wincierz, C. and Schimmel, T. (2014) 'Viscosity Modifiers', in Mang, T. (Ed.) *Encyclopedia of Lubricants and Lubrication.* Springer Berlin Heidelberg, pp. 2292-2316.

Toyoshima, K. (1973) 'General properties of Polyvinyl Alcohol in Relation to its Applications', in Finch, C.A. (Ed.) *Polyvinyl Alcohol: Properties and Applications.* Bristol, UK, John Wiley & Sons Ltd., pp. 1-16.

Tsukamoto, M., Ohnishi, H., Mori, T., Kawasaki, M., Uchida, S. and Sakai, A. (2017) 'Fifteen-Year Comparison of Wear and Osteolysis Analysis for Cross-Linked or Conventional Polyethylene in Cementless Total Hip Arthroplasty for Hip Dysplasia—A Retrospective Cohort Study', *The Journal of arthroplasty,* 32(1), pp. 161-165. e161.

U.S. Food and Drug Administration (2009) "BRYAN® Cervical Disc - P060023 SUMMARY OF SAFETY AND EFFECTIVENESS DATA (SSED) ".

Unal, H. and Mimaroglu, A. (2003) 'Friction and wear behaviour of unfilled engineering thermoplastics', *Materials & design,* 24(3), pp. 183-187.

Vaccaro, A., Beutler, W., Peppelman, W., Marzluff, J. M., Highsmith, J., Mugglin, A., DeMuth, G., Gudipally, M. and Baker, K. J. (2013) 'Clinical outcomes with selectively constrained SECURE-C cervical disc arthroplasty: two-year results from a prospective, randomized, controlled, multicenter investigational device exemption study', *Spine,* 38(26), pp. 2227-2239.

van Ooij, A., Kurtz, S. M., Stessels, F., Noten, H. and van Rhijn, L. (2007) 'Polyethylene wear debris and long-term clinical failure of the Charite disc prosthesis: a study of 4 patients', *Spine,* 32(2), pp. 223-229.

Van Ooij, A., Oner, F. C. and Verbout, A. J. (2003) 'Complications of artificial disc replacement: a report of 27 patients with the SB Charite disc', *Spine,* 28, pp. 369-383.

Vicars, R., Hyde, P., Brown, T. D., Tipper, J., Ingham, E., Fisher, J. and Hall, R. (2010) 'The effect of anterior–posterior shear load on the wear of ProDisc-L TDR', *European Spine Journal,* 19(8), pp. 1356-1362.

Vicars, R., Prokopovich, P., Brown, T. D., Tipper, J. L., Ingham, E., Fisher, J. and Hall, R. M. (2012) 'The effect of anterior-posterior shear on the wear of Charité TDR', *Spine,* 37(9), pp. E528.

Wang, A., Lin, R., Polineni, V. K., Essner, A., Stark, C. and Dumbleton, J. H. (1998) 'Carbon fiber reinforced polyether ether ketone composite as a bearing surface for total hip replacement', *Tribology International,* 31(11), pp. 661-667.

Wang, B. C. and Turndorf, H. (1983) 'Packaging as a medical device: labeling the product for clinical users', in Caceres, C.A. (Ed.) *Medical Devices-measurement, Quality Assurance, and Standards.* Michigan, USA, American Society for Testing and Materials, pp. 216-224.

Wang, Q., Ge, S. and Zhang, D. (2005) 'Nano-mechanical properties and biotribological behaviors of nanosized HA/partially-stabilized zirconia composites', *Wear,* 259(7–12), pp. 952-957.

Wasikiewicz, J. M., Roohpour, N. and Vadgama, P. (2013) 'Packaging and coating materials for implantable device', in Inmann, A. & Hodgins, D. (Eds.) *Implantable Sensor Systems for Medical Applications.* Oxford, UK, woodhead publishing limited, pp. 68-107.

Wathier, M., Lakin, B. A., Bansal, P. N., Stoddart, S. S., Snyder, B. D. and Grinstaff, M. W. (2013) 'A Large-Molecular-Weight Polyanion, Synthesized via Ring-Opening Metathesis Polymerization, as a Lubricant for Human Articular Cartilage', *Journal of the American Chemical Society,* 135(13), pp. 4930-4933.

Wells, M. R. (2010) 'Biomechanics', in Chila, A.G. (Ed.) *Foundations of Osteopathic Medicine.* Pennsylvania, USA, Wolters Kluwer Health/Lippincott Williams & Wilkins, pp. 93-117.

West, M. D. M., Boston, B., East, M. D. M. and San Jose, B. (2000) 'Thermoplastic silicone-urethane copolymers: A new class of biomedical elastomers', 22(4), pp. 68-77.

White, A. A. and Panjabi, M. M. (1990) *Clinical Biomechanics of the Spine*. Pennsylvania, USA: Lippincott.

Wilke, H.-J., Kettler, A. and Claes, L. E. (1997) 'Are sheep spines a valid biomechanical model for human spines?', *Spine,* 22(20), pp. 2365-2374.

Wilke, H.-J., Wenger, K. and Claes, L. (1998) 'Testing criteria for spinal implants: recommendations for the standardization of in vitro stability testing of spinal implants', *European Spine Journal,* 7(2), pp. 148-154.

Wilke, H. J., Neef, P., Caimi, M., Hoogland, T. and Claes, L. E. (1999) 'New in vivo measurements of pressures in the intervertebral disc in daily life', *Spine,* 24(8), pp. 755-762.

Williams, J. A. and Kauzlarich, J. J. (2004) 'Peeling shear and cleavage failure due to tape prestrain', *The journal of Adhesion,* 80(5), pp. 433-458.

Wolf, A., Shoham, M., Michael, S. and Moshe, R. (2001) 'Morphometric study of the human lumbar spine for operation-workspace specifications', *Spine,* 26(22), pp. 2472-2477.

Wong, D. A., Transfeldt, E. and Macnab, I. (2007) *Macnab's Backache*. Philadelphia, USA: Lippincott Williams & Wilkins.

Xin, H., Shepherd, D. E. T. and Dearn, K. D. (2013) 'A tribological assessment of a PEEK based self-mating total cervical disc replacement', *Wear,* 303(1), pp. 473-479.

Yanbin, Z., Yilong, Z., Yu, S., Feifei, Z. and Zhongjun, L. (2015) 'Application of Cervical Arthroplasty With Bryan Cervical Disc: 10 Years Follow-Up Results in China', *Spine,* 41(2), pp. 111-115.

Yao, J. Q., Laurent, M. P., Johnson, T. S., Blanchard, C. R. and Crowninshield, R. D. (2003) 'The influences of lubricant and material on polymer/CoCr sliding friction', *Wear,* 255(1–6), pp. 780-784.

Yao, Z. X. and Skorecki, J. (1985) 'Artificial encapsulation of joint prostheses', *Biomaterials,* 6(3), pp. 208-212.

Yoda, R. (1998) 'Elastomers for biomedical applications', *Journal of biomaterials science. Polymer edition,* 9(6), pp. 561-626.

Young, T.-H., Yao, N.-K., Chang, R.-F. and Chen, L.-W. (1996) 'Evaluation of asymmetric poly(vinyl alcohol) membranes for use in artificial islets', *Biomaterials,* 17(22), pp. 2139-2145.

Zhang, J., Hua, Z. and Su, S. (2009) 'A bionic artificial joint system and investigation of tribological performance', *Chinese Science Bulletin,* 54(4), pp. 599-607.

Zhang, Z., Zhu, W., Zhu, L. and Du, Y. (2014) 'Midterm outcomes of total cervical total disc replacement with Bryan prosthesis', *European Journal of Orthopaedic Surgery & Traumatology,* 24(1), pp. 275-281.